

Title	ポリプロピレン修飾ナノシリカによるナノコンポジットの特性改良
Author(s)	豊永, 匡仁
Citation	
Issue Date	2014-09
Type	Thesis or Dissertation
Text version	ETD
URL	http://hdl.handle.net/10119/12303
Rights	
Description	Supervisor: 寺野 稔, マテリアルサイエンス研究科, 博士

Characteristic Improvements of Nanocomposites using
Polypropylene-grafted Nanosilica

MASAHITO TOYONAGA

Japan Advanced Institute of Science and Technology

Characteristic Improvements of Nanocomposites using
Polypropylene-grafted Nanosilica

by

Masahito Toyonaga

Submitted to

Japan Advanced Institute of Science and Technology

In partial fulfillment of the requirements

For the degree of

Doctor of Philosophy

Supervisor: Professor Dr. Minoru Terano

School of Material Science Japan Advanced Institute of Science and Technology

September 2014

Referee-in-chief: **Professor** Dr. Minoru Terano

Japan Advanced Institute of Science and Technology

Referees: **Associate professor** Dr. Kazuaki Matsumura

Japan Advanced Institute of Science and Technology

Associate professor Dr. Toshiaki Taniike

Japan Advanced Institute of Science and Technology

Associate professor Dr. Tatsuo Kaneko

Japan Advanced Institute of Science and Technology

Professor Dr. Hisayuki Nakatani

KITAMI Institute of Technology

Preface

The present dissertation is the result of studies under the direction of Professor Dr. Minoru Terano during 2011-2014. The purpose of this dissertation is the investigations of both the mechanism and the application of polypropylene (PP)-based nanocomposites using PP-grafted nanosilica (SiO₂).

First of all, **Chapter 1** is a general introduction according to the object of this research. **Chapter 2** and **3** describe effects of among chain length, grafted amount, and filler content of the PP-grafted SiO₂ on the mechanical properties of PP-based nanocomposites. **Chapter 4** and **5** describe applications of the grafting technology. **Chapter 4** reports the “Influences of mechanical properties on polyethylene (PE)-based nanocomposites using PE-grafted SiO₂”. **Chapter 5** reports the “Development of high-performance and practical nanocomposites using *in-situ* polypropylene grafting reaction”. **Chapter 6** describes the general summary and conclusion of this dissertation.

Masahito Toyonaga

Terano Laboratory,
School of Materials Science,
Japan Advanced Institute of Technology

September 2014

Contents

Chapter 1. General Introduction	
1.1. Polymer materials	2
1.2. Polypropylene	4
1.3. Combination of materials	7
1.4. Objective	15
Chapter 2. The Influence of Mechanical Properties for Grafted Chain Length on Polypropylene/Polypropylene-grafted SiO ₂ Nanocomposites	
2.1. Introduction	22
2.2. Experimental	27
2.3. Results and Discussion	31
2.4. Conclusion	46
Chapter 3. The Influences of Mechanical Properties for Grafted Chain Number on Polypropylene-grafted SiO ₂ of Polypropylene-based Nanocomposites	
3.1. Introduction	52
3.2. Experimental	55
3.3. Results and Discussion	58
3.4. Conclusion	68

Chapter 4.	Influences of Mechanical Properties on Polyethylene-based Nanocomposites using Polyethylene-grafted Nanosilica Nanoparticles	
4.1.	Introduction	71
4.2.	Experimental	74
4.3.	Results and Discussion	78
4.4.	Conclusion	87
Chapter 5.	The Development of High-Performance and Practical Nanocomposites using In-Situ Polypropylene Grafting Reaction	
5.1.	Introduction	90
5.2.	Experimental	94
5.3.	Results and Discussion	99
5.4.	Conclusion	109
Chapter 6.	General Conclusion	
6.1.	General Summary	112
6.2.	General Conclusion	114
	Achievements	118
	Acknowledgements	122
	Minor Research Theme	123-136

Chapter 1.

General Introduction

1.1. Polymer materials

In general, polymer materials are a kind of macromolecule, which is constructed by continuous structure of monomer. Most polymer materials overtop the molding processability, lightness, productive capacity and cost compared with wood, metal, and so on. Therefore, these polymer materials are so important for people's lives and rapid industrial expansion. In particular, five general plastics (in **Figure 1**) predominate the majority of the polymer production volume because of the good balance between the cost and properties, which are polypropylene (PP), low- and high-density polyethylene (LDPE, HDPE), polystyrene (PS), and polyvinylchloride (PVC). {If LDPE and HDPE unionize PE, last one is the acrylonitrile-butadiene-styrene (ABS) resin or the polyethylene-terephthalate (PET).} Among them PP is gathering attention because of having various superior characteristics. Therefore, the production amount of PP is the highest in other versatile plastics, which is shown in **Figure 2** [1].

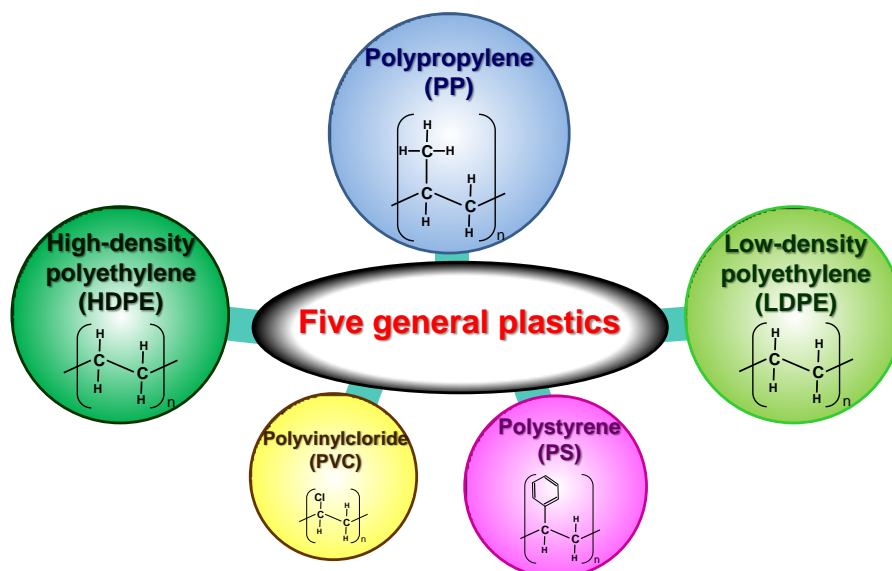


Figure 1. Five general plastics

The national production of versatile plastics is shown in **Figure 2 (Left)**. Each plastic decreased the production due to the global financial crisis in 2008. In particular, great decline of PVC suggests that it is gently alternated by Cl free materials. In the production amount of PP is temporarily restored in 2010 but, it also decrease after 2010.

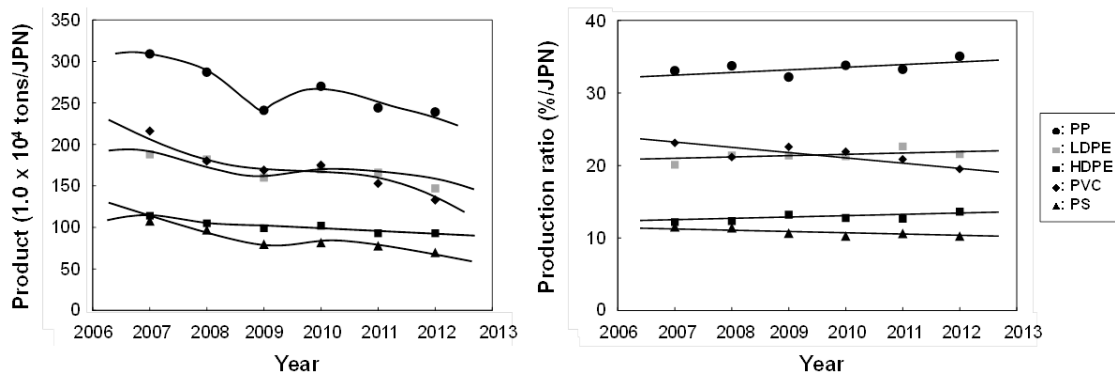


Figure 2. National production of major versatile plastics: Left figure is production amount, right figure is production ratio.

However, PP indicates increase of production ratio compared with other general plastics in **Figure 2 (Right)**. In addition, annual worldwide productions of PP and PEs are shown in **Figure 3**.

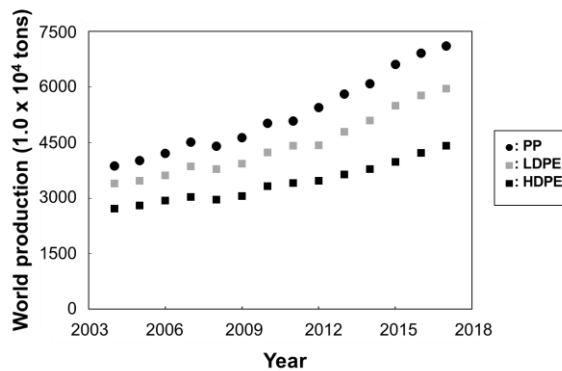


Figure 3. Annual worldwide productions of major polyolefin materials

In terms of world scale of polyolefin products, PP and PEs greatly improve the production amount. In general, this reason was significantly expanded by demand of polymer materials from the advancing countries. In specific, the progress rate of PP is so strong compared with PEs.

1.2. Polypropylene (PP)

The versatile plastic of PP has many superior properties, for instance well-balanced mechanical properties between the PE and PS, light weight (around 0.9 g/cm^3), low cost/low price, high chemical resistance, easy processability, high melting point in polyolefin materials (around 165°C), low environmental load (only straight alkyl chain from carbon and hydrogen atoms), and so on [1,2]. These advantages were given by the expansion of use application via the evolution of catalyst characteristic and combined techniques, which pride production amount of over 60 million tons/year in **Figure 3**. The supply and demand of PP rise year by year, and this state will be maintained for long years in the future. Therefore, the performance upgrade of PP is important research assignment. To achieve reinforcement of the PP, knowledge of structure and reinforcement method is necessary.

This short section explains a summary of the PP briefly. Before 1950, PP was oily polymer, which does not have the mechanical properties due to not only the low molecular weight but also the totally-amorphous phase. In 1954, Natta, et al succeeded in composition of the isotactic PP semicrystalline polymer via Ziegler-Natta catalyst [3]. This catalyst name was formed by Karl **Ziegler** (1898-1973) and Giulio

Natta (1903-1979). PP was strengthened with the improvement of the Ziegler-Natta catalyst since the discovery of isotactic PP.

The PP has three kinds of structure via among isotactic-PP (iPP), syndiotactic-PP (sPP), and atactic-PP (aPP). The 3 kinds of PP are shown in **Figure 4**.

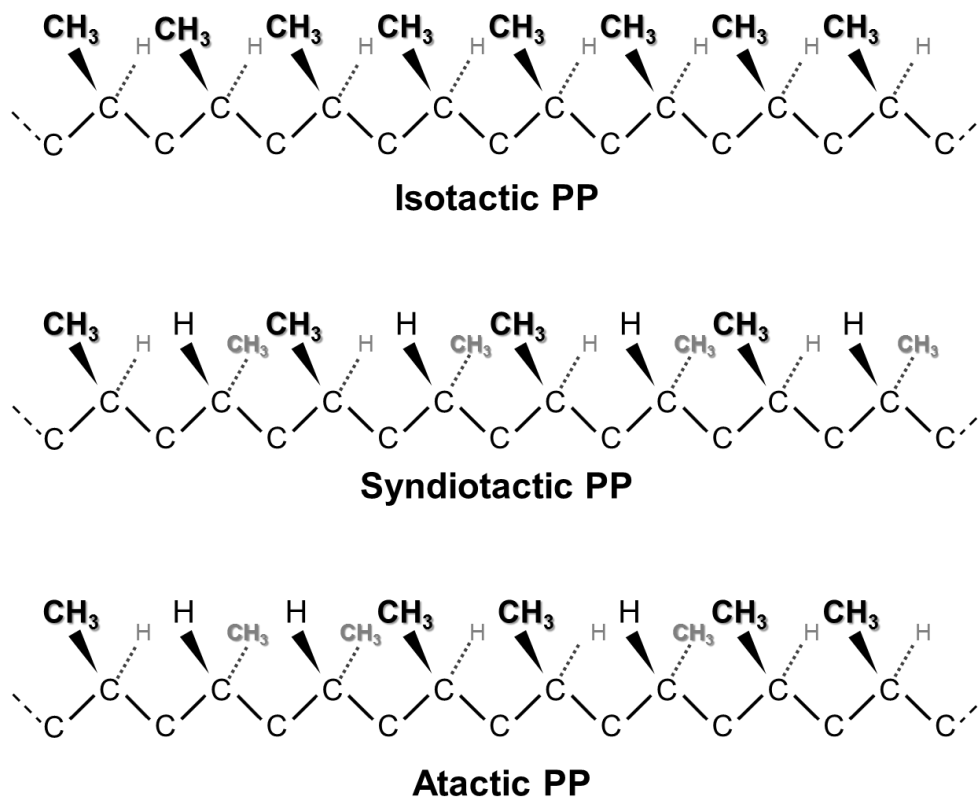


Figure 4. Various tacticity of PP

Various PPs were separated by the orientation pattern of methyl groups from side chain of molecular structure. aPP show the random orientation pattern, which is oily polymer when low molecular weights. sPP show almost alternateness orientation pattern. iPP show the almost trim orientation pattern [2]. However, methyl group of PPs does not turn to the same direction. Practically, PP chain form the gyro structure

of right-handed or left-handed [4]. The molecular weight distribution (MWD) of chain length depends on the catalytic, which is 5-7 of Ziegler-Natta catalyst and 2-3 of metallocene catalyst. The iPP and sPP can form the crystalline structure. Each crystalline structure is folded at constant distance (size is about $20 \times 7 \times 7 \text{ m}^{-10}$), which makes the alternate layer that is not a crystal and a crystal. This hierarchical structure is called a lamella, which scale size is about 100-300 m^{-10} . {In addition, crystalline structures are different by iPP (a_1, a_2, β, γ forms) or sPP.} Lamellar structure make the spherical shape structure of 1-50 μm . Finally, many spherical form the visible skin-core morphology [5-7].

1.3. Combination of materials

1.3.1. Definition of the composite

Composite materials define that it is constructed by more than two kinds of material, which shown as follows by (1) ~ (3) [8].

(1) ***Material A + Material B = Material A + B***

(2) ***Material A + Material B = Material A x B***

(3) ***Material A + Material B = Material C***

The (1) has both advantage factors by ***Material A*** and ***Material B***. The (2) so significantly improves both or one advantage factors by ***Material A*** and ***Material B***. This effect is called synergy effect. Moreover, (2) is included by broad sense in the (1). Finally, (3) indicates that ***Material A*** and ***Material B*** generate new (or different) advantage factor as a ***Material C***. In addition, these three definitions (1)-(3) presuppose the assuagement of disadvantage factors of the extent possible.

1.3.2. *Kinds of composite*

The polymer combined techniques exist for the three kinds of polymer alloy, polymer blend, and polymer composite. In addition, new method is called polymer hybrid, but is included in any one of three methods.

• Polymer Alloy

The polymer alloy is constructed by the two types or more than two types of different polymer, which is combined materials of new function-owning. The research of polymer alloy investigated enterprisingly via monomer blend and/or copolymer blend [9,10]. The biggest success and prominence in polymer alloy are ABS resin. In 1954, ABS resin was developed via the addition of butadiene rubber as a third monomer to styrene-acrylonitrile (AS) resin plastic resulted in development of a new range of widely used thermoplastics called ABS resin [11]. In addition, ABS is used as a combination with other materials well in **Table 1**.

Table 1. The list of major polymer alloy resins

Sample	1st material	2nd material	3rd material
ABS resin	Acrylonitrile	Butadiene	Styrene
dPPE alloy	PPE	PS	
PC/ABS alloy	PC	ABS	
PBT/ABS alloy	PBT	ABS	
PA/ABS alloy	PA	ABS	
PC/PS alloy	PC	PS	

dPPE: denaturated polyphenylether; PPE: Polyphenylether; PC: Polycarbonate;

PBT: Polybutyleneterephtalate; PA: Polyamide.

- **Polymer Blend**

The polymer blend indicates that it is mixed the two types or more than two types of different polymer by the physical method compared with polymer alloy. Therefore, polymer blend includes polymer alloy in the broad sense. This report also considers that polymer blend is included in a polymer alloy. By the way, for primitive technique, in 1846, Parkes reported that the first patent polymer blend was a mixture of natural rubber with gutta/cha patented [10]. In addition, AS resin is classified in a blend category (ABS resin used the blend and grafting technologies. AS resin used only blend technology).

- **Polymer Composite**

The polymer composites consist of the polymer matrix and numberless fillers. The choice of the filler is very important on polymer composites. The onset of functions and improvement of mechanical properties are greatly different with materials and the shape of the filler.

The mechanical properties of polymer composites using the microscale fillers can expect by Eq(1) [8]. (However, a lot of exceptions exist...)

$$E_c = E_m (1 - V_f) + E_f V_f \quad \text{Eq(1)}$$

E_c = Stiffness property of composites

E_m = Stiffness property of polymer matrix

E_f = Stiffness property of filler

V_f = Volume ratio of filler

In **Figure 5**, the polymer composites are superior to polymer alloy in the development of the properties of mechanical- and thermal-properties regions [8]. This fact is so important factor for the expansion of use application of PP.

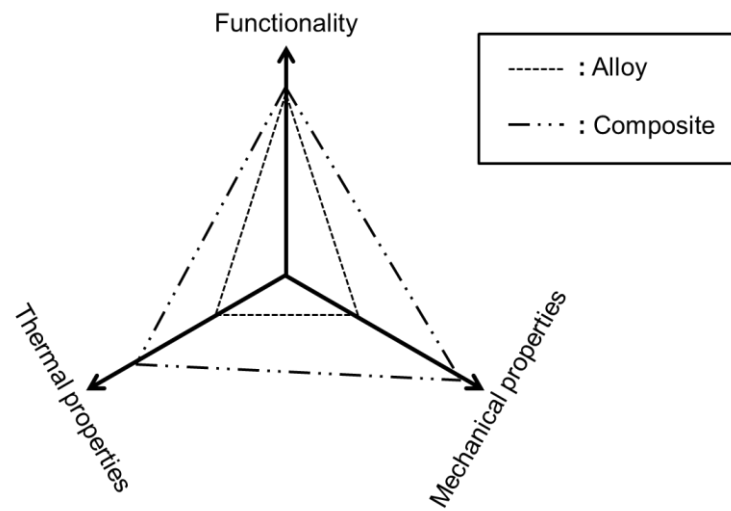


Figure 5. Comparison with polymer alloy and composites

1.3.4. Polymer-based nanocomposites

The polymer nanocomposite technique with nanoparticle is one of the most promising technologies for expansion of use application. The break through in the research of nanocomposites was reported by Usuki et al. They achieved excellent reinforcement in Nylon 6/montmorillonite nanocomposites, which showed twice the Young's modulus was twice and the heat distortion temperature about 80°C higher, compared with those of the matrix [12]. Thereafter various studies were conducted [13-17].

1.3.5. PP-based nanocomposites

However, PP-based nanocomposites have a problem concerning the compatibility between apolar matrix and polar nanofillers. In other words, pristine PP is immiscible for nanofillers, which is relation of the water and the oil nearly. The model by polymer matrix and unmodified fillers is shown in **Figure 6**.

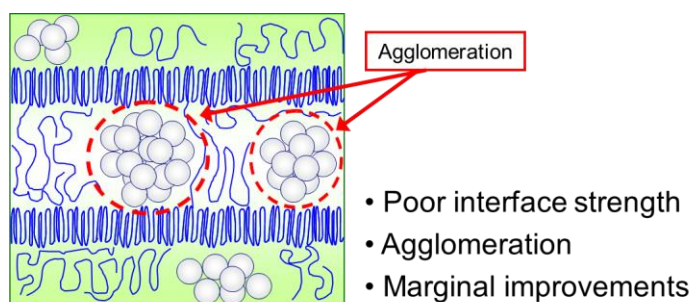


Figure 6. The model of PP with unmodified SiO₂

The fillers do not disperse well in PP matrix but form large agglomerates of micro size level via the high-surface energy of nano-sized filler. This filler agglomeration causes

the incomplete reinforcement, decrease of transparency, and low lifetime of material [18]. In detail, the adhesion and compatibility of PP matrix with fillers are very weak, and effective load transfer from the soft matrix to the rigid fillers is hardly achieved during the deformation. Various strategies by many laboratories were investigated for problem to resolve.

One of the most strategies was using PP side-chain-grafted maleic anhydride (MAPP) as compatibilizer [19,20]. The purpose of this strategy is the high dispersion of fillers via good compatibility.

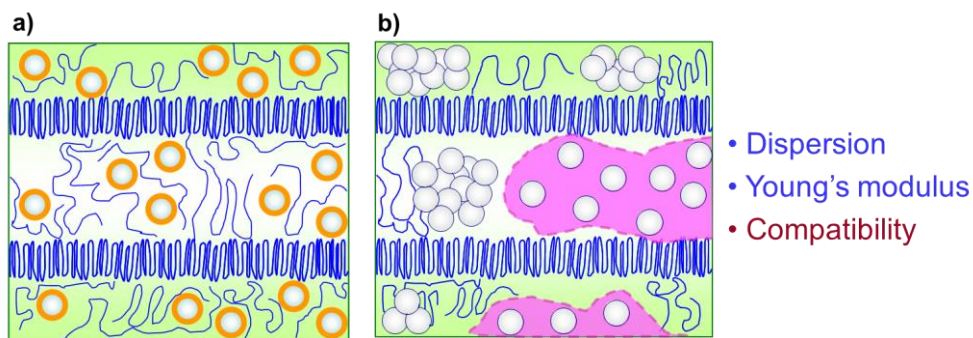


Figure 7. The models of high dispersion for a) PP with short alkyl chain modified SiO₂ and b) PP with MAPP (compatibilizer)

In **Figure 7 a)**, MAPP gives the high dispersion of fillers. However, this dispersion state is only confined to region of MAPP. Furthermore, nanocomposites with involvement of MAPP cannot improve the mechanical properties by the soft materials more than PP. On the other hand, the short alkyl chain-modified fillers give immensely-high dispersion state in **Figure 7 b)**. The surface-modified fillers improve the Young's modulus by blocking of flowing PP matrix for strain. However, these strategies do not improve the tensile strength. I consider that improvement of tensile

strength needs strong adhesion properties as a physical interaction between the PP matrix chain and filler.

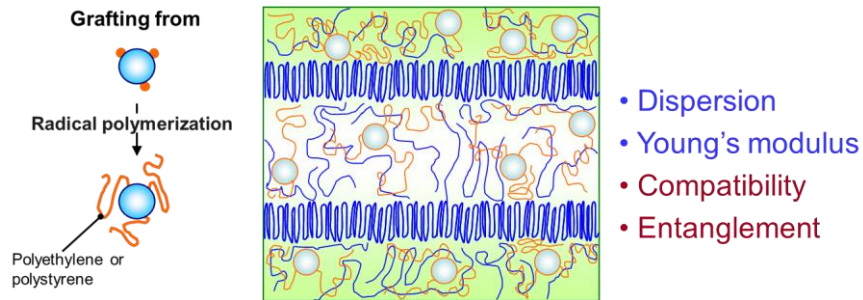


Figure 8. The model of PP with polymer-grafted SiO₂ via *Grafting from* method

In other major strategy, the polymer grafting method may achieve the ideal reinforcement via physical interaction between the matrix and filler. In **Figure 8**, the many grafting methods to nanoparticle use the radical polymerization, which synthesized grafted chain of PE or atactic PS [21-23]. Polymer-grafted fillers give not only the entanglements between matrix and filler but also the block of the filler aggregations by grafted chains.

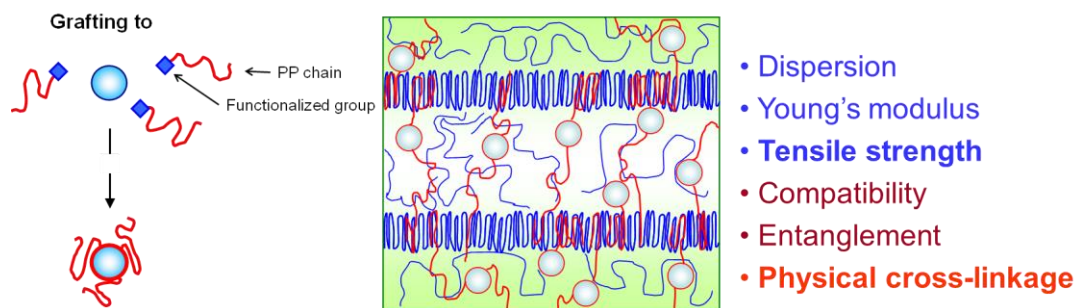


Figure 9. The model of PP with PP-g-SiO₂ via *Grafting to* method

I hope that that choice of grafted chain is PP chain, which is best strategy for PP matrix in **Figure 9**. Hence, grafted PP chains can reinforce the matrix/filler interface through an entanglement with PP chains in the amorphous phase. Therefore, the co-crystallization can occur between grafted and matrix PP chains in the crystallization process. This co-crystallizations form the structures of the physical-cross linkage via over two bonding between grafted chain and matrix. In this strategy, accurate interfacial design must be required, which indicated (1) and (2).

(1) It is necessary to maintain the basic characteristics of PP, though the reactive groups have to introduce. Therefore, the functionalization of grafted chain hopes only the terminal region.

(2) It is quite important to synthesize the homogeneous grafted chains to examine the effect of primary structure of grafted PP chains on the reinforcement. Therefore, we chose the isotactic specificity metallocene catalyst.

Therefore, this study is to establish the precise synthesis of the grafted PP chains with very narrow molecular weight distribution and the effective grafting method for the evaluations. And then, the effects and reinforce mechanism of the grafted PP chains on the mechanical properties of the nanocomposites were investigated. The detail of the purpose is a next section.

1.4. Objective

The abstract and purpose of research are as follows. PP-based nanocomposites have particularly attract great interest owing to the growing market, the improvement of mechanical properties, and the onset of functional properties such as gas barrier effect, flame resistance, transparency, and so on. The strong interfacial design between the matrix PP and nanoparticles is necessary to improvement of various performances of PP materials, which use the grafted PP chain. The grafted PP chain has highest compatibility with the matrix PP, which form the strong interaction between matrix and fillers when grafting to SiO₂. This interaction occurs by means of the physical cross-linkage between lamellae through co-crystallization between the matrix and grafted PP chains. However, the reinforcement mechanism by grafted PP chains on PP-*g*-SiO₂ is still the undissolved factor. Therefore, elucidation of this reinforcement matters for further improvement of characteristic, which links to expansion of the area of applications. For the further development of PP-based nanocomposites, three chapters of (i) ~ (iv) were explored in this dissertation.

(i) The influences to PP-based nanocomposites on the control of the grafted chain length on PP-g-SiO₂

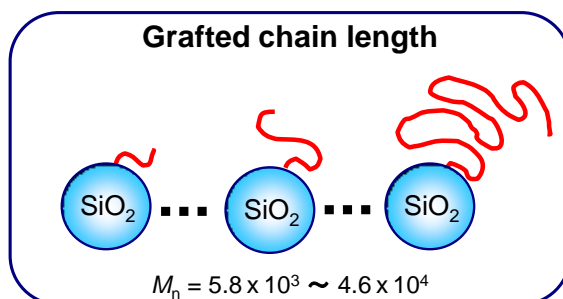


Figure 10. The model of various grafted chain length on PP-g-SiO₂

The length of grafted chain is most important factor in the structural development and the mechanism elucidation of the strong interfacial structure between the matrix and nanoparticle. Therefore, this factor was considered earliest within various factors such as grafted amount, filler content, filler diameter, tacticity, *mmmm*, filler types, and so on. In general, the critical molecular weight (M_c) of isotactic-PP is about 1.2×10^4 (g/mol) M_n . Incidentally, M_c value corresponds to double length of entanglement molecular weight (M_e) value. In the **Chapter 2**, grafted PP chains between the M_n of 5.8×10^3 and M_n of 4.6×10^4 (**Figure 10**) were prepared by TEA as a chain transfer agent in propylene polymerization and end functionalization reaction. This chain grafting to SiO₂ performed the grafting reaction via condensation reaction at 200°C between the PP-*t*-OH and SiO₂-OH, which can make the fillers of PP-g-SiO₂ nanoparticles. Grafted PP-g-SiO₂ nanoparticles and PP matrix make the PP/PP-g-SiO₂ nanocomposites from a melt-mixing process and hot press. Various PP-based nanocomposites investigated the filler the dispersion state by TEM observation, the morphology of freeze-fracture surface by SEM observation, the crystallization behaviors by DSC

measurement, the mechanical properties by tensile test, and the melt viscoelasticity of the rheometer instrument.

Additionally, the control and synthesis method of grafted chain length are described in Chapter 2. Moreover also, existence of grafted PP chains on PP-g-SiO₂ was confirmed by FT-IR measurement and TGA measurement.

(ii) The influences to PP-based nanocomposites on controls of the grafted amount and filler content on PP-g-SiO₂

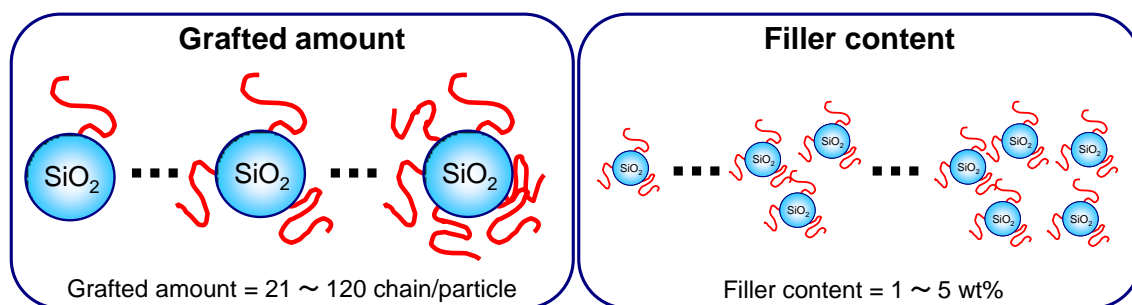


Figure 11. The models of various grafted amount and filler content on PP-g-SiO₂

In **Chapter 3**, we report the influence that grafted amount and filler content on PP-g-SiO₂ give the reinforce effect (**Figure 11**), which investigated by DSC measurement, TEM observation, and tensile test. The control of grafted amount was performed by the change of introduction amount of PP-*t*-OH.

(iii) Application to PE-based nanocomposites

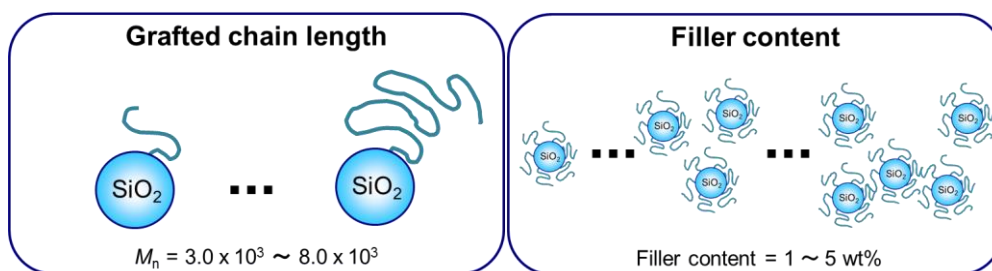


Figure 12. The model of PE-grafted SiO₂

In **Chapter 4**, grafting technologies employ the PE-based nanocomposites via PE-grafted SiO₂ (**Figure 12**).

(iv) Preparation and evaluation of PP-based nanocomposites based on the click chemistry

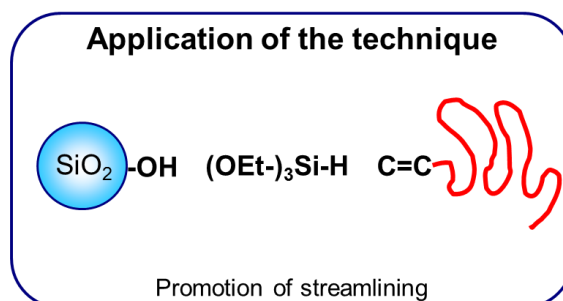


Figure 13. The model of PP-g-SiO₂ based on the click chemistry

In **Chapter 5**, PP-g-SiO₂ as a secondary application tries to establish a new cost- and time-efficient synthetic route for PP-grafted filler using hydrosilylation and microwave. (**Figure 13**)

The contents of this dissertation are constructed by six chapters via (i)-(iv), general introduction, and conclusions.

Reference:

- [1] Society of Polyolefin Science & Industry, Japan (Ed.), *next generation polyolefins* **2013**, 7.
- [2] Pasquini, N. (Ed.), *Polypropylene Handbook, 2nd Edition* **2012**.
- [3] Natta, G., Pasquon, I., Svab, J., Zambelli, A., *Chim. Ind.* **1962**, 44, 621-624.
- [4] Lieberman, R.B., Barbe, P.C., *Enc. Polym. Sci. Eng. John Wiley & Sons* **1988**.
- [5] Fujiyama, M., Awaya, H., Kimura, S., *J. Appl. Polym. Sci.* **1977**, 21, 3291.
- [6] Katti, S.S., Schultz, J.M., *Polym. Eng. Sci.* **1982**, 22, 1001.
- [7] Fujiyama, M., Wakino, T., Kawasaki, Y., *J. Appl. Polym. Sci.* **1988**, 35, 29.
- [8] Yui, H. (Ed.), *Polymer-based composites -Basic •Operational •Future-*, **2005**.
- [9] Utracki, L.A., Favis, B.D. (Eds), *Polymer alloys and blends*, **1989**, 4, 121-185.
- [10] Utracki, L.A., *Polym. Eng. Sci.* **1995**, 35, 2-17.
- [11] Plastics Technology (Ed.), *No.11 - ABS RESINS*, **2005**, 10.
- [12] Usuki, A., Kojima, Y., Kawasumi, M., Okada, A., Fukushima, Y., Kurauchi, T., Kamigaito, O., *J. Mater. Res.* **1993**, 8, 1185-1189.
- [13] Ray, S.S., Okamoto, M., *Prog. Polym. Sci.* **2003**, 28, 1539-1641.
- [14] Choudalok, G., Gotsis, A.D., *Eur. Polym. J.* **2009**, 45, 967-984.
- [15] Kashiwagi, T., Grulke, E., Hilding, J., Groth, K., Harris, R., Butler, K., Shields, J., Kharchenko, S., Douglas, J., *Polymer* **2004**, 45, 4227-4239.
- [16] Chan, C.M., Wu, J.S., Li, J.X., Cheung, Y.K., *Polymer* **2002**, 43, 2981-2992.
- [17] Manias, E., Touny, A., Wu, L., Strawhecker, K., Lu, B., Chung, T.C., *Chem. Mater.* **2001**, 13, 3516-3523.

- [18] Taniike, T., Umemori, M., Chiba, H., Terano, M., *J. Mater. Life Soc.* **2012**, *24*, 102.
- [19] Liu, Y., Kontopoulou, M., *J. Vinyl. Add. Tech.* **2007**, *13*, 147-150.
- [20] Pavlidou, E., Bikiaris, D., Vassiliou, A., Chiotelli, M., Karayannidis, G., *J. Phys.* **2005**, *10*, 190-193.
- [21] Zhou, H.J., Rong, M.Z., Zhang, M.Q., Ruan, W.H., Friedrich, K., *Polym. Eng. Sci.* **2007**, *47*, 499-509.
- [22] Wu, C.L., Zhang, M.Q., Rong, M.Z., Friedrich, K., *Compos. Sci. Technol.* **2002**, *62*, 1327-1340.
- [23] Rong, M.Z., Zhang, M.Q., Pan, S.L., Lehmann, B., Friedrich, K., *Polym. Int.* **2004**, *53*, 176-183.

Chapter 2.

The Influence of Mechanical Properties for Grafted Chain

Length on Polypropylene/

Polypropylene-grafted SiO₂ Nanocomposites

2.1. Introduction

Polymer nanocomposites are promising materials, in which a small fraction of nanoparticles dispersed in polymer matrices not only induces drastic reinforcements but also enhances functionalities such as conductivity and gas barrier properties [1-14]. Compared with micro-sized particles, nanoparticles dispersed in polymer give much larger interfacial areas to enable effective load transfer from a matrix to hard particles, and also have much greater particle number densities (i.e. short particle-particle distances) sufficient to interfere with polymer relaxation and to greatly diminish a percolation threshold. Moreover, as the sizes of nanoparticles are comparable or even smaller than those of higher-order structures of semi-crystalline polymer, nanoparticles can modulate the structures, especially at spherulitic and lamellar levels [15,16].

Polypropylene (PP) is one of the most widely used plastics, characterized by a wide range of advantages such as low cost, light weight, high melting temperature, good processability, balanced mechanical properties, low environmental load and so on. PP-based nanocomposites have attracted great attention in order to further expand its versatility and to explore a new specialty. However, fabrication of industrially valuable PP-based nanocomposites is extremely challenging owing to the extreme inertness of PP against inorganic nanoparticles, compared with other polymers containing polar functional groups that more or less interact with nanoparticles. In most cases, nanoparticles do not disperse well in PP but make large and compact aggregates, significantly diminishing reinforcement and even negatively affecting transparency and ductility [17,18]. The most versatile strategies to remedy the poor dispersion of nanoparticles are to add a compatibilizer, typically side-functionalized PP

such as maleic anhydride-grafted PP (MAPP) and to chemically modify particle surfaces by short aliphatic alkyl chains, for example, using ternary ammonium salts or silane coupling agents [19-21]. In recent years, more sophisticated routes have been developed to facilitate not only good dispersion of nanoparticles but also either polymer-filler interaction or filler-filler networking. For example, an in-situ method enables complete exfoliation of layered fillers through the polymer growth/formation inside gallery spaces [22-24]. In a sol-gel approach, metal alkoxide precursor blended or impregnated in molten or solid PP is subjected to the sol-gel reaction to generate nano-sized inorganic oxide particles [25,26]. Nanocomposites prepared with this method are featured with low percolation thresholds at the level of a few to several wt% [27,28]. Polymer grafting is a potentially versatile and scalable approach due to the direct applicability to the conventional melt mixing process, which aims at not only improved dispersion through organic modification and steric prevention of filler agglomeration but also better interfacial connection through interdiffusion and entanglement between grafted and matrix polymer chains [22,29-32]. Though all of these approaches have greatly refined the design of PP-based nanocomposites, further advances are essential to realize practically acceptable improvements over existing PP-based materials.

Spherical SiO₂ nanoparticles are one of the most representative nanofillers that have been used to prepare PP-based nanocomposites. This is not only because of their relative cheapness compared with most of other nanofillers, but also because of their characteristics to be regarded as a model nanofiller such as the absence of anisotropy, the ease of post chemical modifications, and diversities in size and dispersibility. A wide variety of strategies have been postulated to prepare PP/SiO₂ nanocomposites with

improved dispersion and/or physical properties [15,16,33]. Table 1 summarizes selected efforts from literature with special attention on tensile reinforcement achieved by the addition of SiO₂ nanoparticles. The maximum reinforcement reported for the Young's modulus is about +30%, which was attained by various strategies including polymer grafting [34], compatibilizer (MAPP) [20] and even unmodified colloidal SiO₂ [35]. On the contrary, reinforcement of tensile strength is rather difficult for spherical (i.e. minimal aspect ratio) nanofillers, and reinforcement over +10% was realized only by the polymer grafting [31,34,36]. It is interesting that both grafted polymer and compatibilizer form compatibilizing interfaces between the PP matrix and SiO₂ nanoparticles, but they exhibit quite different behaviors upon structural deformation at a lamellar scale [16]. Wang et al. attributed this difference to the fact that compatibilizer with polar functional groups at side chains wraps nanoparticles to form better compatibilized but less entangled interfaces, while grafted polymer chains with brush morphology on filler surfaces to entangle and interdiffuse with matrices [37,38]. In this way, it is apparent that an optimum strategy to enhance the tensile strength with SiO₂ nanoparticles is the polymer grafting. However, most of the previous works [20,30-32,34] were conducted for polymer which can be grafted onto SiO₂ by radical polymerization, while there have been few reports on the usage of PP-grafted SiO₂ (PP-*g*-SiO₂) nanoparticles, which must maximize the efficacy of the grafting.

In this article, a series of PP-*g*-SiO₂ nanoparticles were synthesized by reacting SiO₂ with terminally-hydroxylated PP (PP-*t*-OH) having different chain lengths ($M_n = 5.8 \times 10^3 \sim 4.6 \times 10^4$), and influences of the chain length on physical properties of PP/PP-*g*-SiO₂ nanocomposites were systematically examined. It was found that PP/PP-*g*-SiO₂ nanocomposites exhibited several prominent advantages over the pristine

PP and PP/SiO₂ nanocomposite: uniform dispersed at 5.0 wt%, highly accelerated crystallization of PP, and +30% improvements in both the Young's modulus and tensile strength without sacrificing the original melt viscosity of PP. I concluded that the immense reinforcement of the tensile strength results from physical cross-linking between lamellae through co-crystallization between the PP matrix and grafted PP chains.

Table 1. Reinforcements of PP-based nanocomposites in previous studies

Sample ^a	Filler content (wt%)	Young's modulus ^b (%)	Tensile strength ^b (%)
PP/SiO ₂ [15]	5.0	+7	+4
PP/MAPP/mSiO ₂ [15]	5.3	+7	0
PP/MAPP/SiO ₂ [20]	5.0	+31	+5
PP/colloidal SiO ₂ [35]	4.5	+33	-5
PP/PVP- <i>g</i> -SiO ₂ [49]	0.5	+8	+6
PP/PP-NH ₂ /PGMA- <i>g</i> -SiO ₂ [34]	1.6	+30	+13
PP/PS- <i>g</i> -SiO ₂ [31]	2.1	+18	+18
PP/PS- <i>g</i> -SiO ₂ [32]	1.4	+15	+4
PP/PBA- <i>g</i> -SiO ₂ [50]	1.1	+9	+7
PP/HBP- <i>g</i> -SiO ₂ [36]	5.0	-	+11
PP/PMMA- <i>g</i> -SiO ₂ [30]	0.2	-	+6

^a mSiO₂: SiO₂ modified with short alkyl chains, PVP: poly(*p*-vinylphenylsulfonylhydrazide), PP-NH₂: PP with terminal amine, PGMA: poly(glycidylmethacrylate), PS: polystyrene, PBA: poly(butylacrylate), HBP: octadecyl isocyanate-grafted hyperbranched polyester (BoltornTM H20), PMMA: poly(methylmethacrylate).

^b Reinforcement from pristine PP.

2.2. Experimental

2.2.1. Materials

PP pellet for the matrix polymer ($M_n = 4.6 \times 10^4$, MWD = 5.65, *mmmm* = 98 mol%) was donated by Japan Polypropylene Corporation. Propylene gas of research grade (Japan Polypropylene Co.) was used as delivered. Both modified methylaluminoxane (MMAO) as an activator and triethylaluminum (TEA) as a chain transfer agent were donated by Tosoh Finechem Corporation. *rac*-Ethylenebis(1-indenyl)zirconium dichloride (EBIZrCl₂) was purchased from Kanto Chemical Co., Inc. Anhydrous toluene and tetradecane (Wako Pure Chemicals Industries, Ltd.) were used after being dried over molecular sieve 4A. Nano SiO₂ (average diameter = 26 nm, surface area = 110 m²/g) was purchased from Kanto Chemical Co., Inc.

2.2.2. Synthesis of PP-*t*-OH

15 mmol of MMAO was introduced in a 500 ml glass flask containing 300 ml of dry toluene under N₂ at 0°C. After adding 5 μmol of EBIZrCl₂ and a specified amount of TEA into the flask, propylene was continuously flown at 1 atm at 0°C with vigorous stirring. The amount of TEA as a chain transfer agent was varied from 2.5 to 120 mmol in order to control the molecular weight of PP. The end hydroxylation of PP was conducted based on literature [39-44]. Followed by polymerization for 1 h, propylene supply was cut off and O₂ was bubbled for 1 h. Thereafter, 25 ml of 35% aqueous H₂O₂ was added under O₂ bubbling, which causes the insertion of O-O into Al-R bonds (R = PP or Et). Finally, 500 ml of methanol was added to hydrolyze Al-O-O-R bonds. Thus obtained PP-*t*-OH was filtered and then washed with distilled water, followed by

reprecipitation with xylene/methanol.

2.2.3. *Synthesis of PP-g-SiO₂*

500 mg of SiO₂ was dehydrated in a flask under N₂ flow at 160°C for 2 h. Then preliminary dehydrated PP-*t*-OH, whose amounts roughly corresponded to 50-100 mol% of surface hydroxyl groups of SiO₂, 0.1 mg of 2,6-di-*tert*-butyl-*p*-cresol (to prevent oxidative degradation of PP-*t*-OH), and 300 ml of tetradecane were added in the flask at room temperature. The mixture was heated to 200°C under stirring and reacted for 6 h. The resultant particles were washed with methanol, and dried in vacuo. Ungrafted PP-*t*-OH was completely removed by repetitive hot filtration with *o*-dichlorobenzene at 140°C, until the weights of grafted chains became constant.

2.2.4. *Preparation of PP/PP-g-SiO₂ nanocomposites*

Nanocomposites were prepared by melt mixing using a two-roll mixer at 20 rpm. PP pellets were kneaded at 185°C for 5 min and then 5.0 wt% of unmodified SiO₂, or PP-g-SiO₂ was added. The mixture was further kneaded at 185°C for additional 10 min. Thus produced nanocomposites were hot-pressed into sample films with the thickness of 200 μm at 230°C and 20 MPa, and then quenched at 100°C.

2.2.5. *Characterizations*

The M_n and molecular weight distribution (MWD) of PP-*t*-OH were measured by size-extrusion chromatography, using gel permeation chromatography (GPC, Viscotek, HT-GPC 350) equipped with a refractive index detector and a viscometer. Measurements were conducted at 140°C with polystyrene gel columns using

o-dichlorobenzene containing 0.03 wt% of 2,6-di-*tert*-butyl-*p*-cresol as an antioxidant.

¹³C-nuclear magnetic resonance (NMR) spectra were recorded with a Bruker 400 MHz NMR spectrometer operating at 100 MHz with proton decoupling at 120°C using hexachloro-1,3-butadiene as a diluent and 1,1,2,2-tetrachloroethane-*d*₂ as an internal lock and reference. The stereoregularity of PP-*t*-OH was obtained as the *mmmm* molar fraction. **Figure 1** shows a typical ¹³C-NMR spectrum of PP-*t*-OH. The percentage of end functionalization and *M_n* were respectively calculated based on **Eqs (1)** and **(2)**.

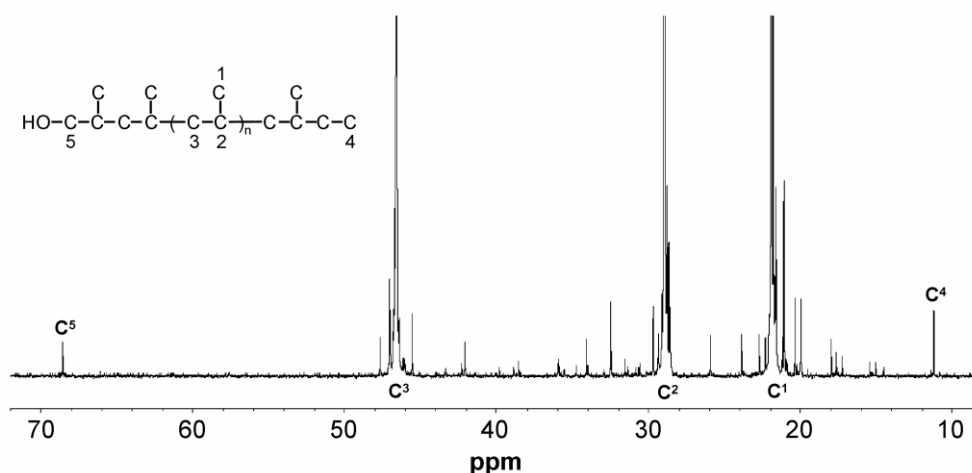


Figure 1. Typical ¹³C-NMR spectrum of PP-*t*-OH

$$\text{End Functionalization} = \frac{C^5}{1/2(C^4 + C^5)} \quad \text{Eq. (1),}$$

$$Mn = \frac{1/3(C^1 + C^2 + C^3)}{1/2(C^4 + C^5)} \times 42 \quad \text{Eq. (2).}$$

The presence of grafted chains on SiO₂ was confirmed by Fourier-transformed infrared spectroscopy (FT-IR 6100, JASCO) with resolution of 4 cm⁻¹ using the KBr method [45]. The weight of grafted chains was determined by thermogravimetric (TG, Mettler

Toledo TG50) analysis. The temperature was kept at 200°C for 30 min and then raised up to 650°C at 20 °C/min. The weight loss from 200 to 650°C for PP-*g*-SiO₂ with respect to that for neat SiO₂ corresponds to the grafted amount.

The dispersion of SiO₂ particles in nanocomposites was evaluated with transmission electron microscopy (TEM, Hitachi H-7100) operated at 100 kV, using microtomed specimens (Reichert Ultracut S with a FC-S cryoattachment). The freeze-fracture surfaces of nanocomposites were acquired with scanning electron microscopy (SEM, Hitachi S-4100), where sample films soaked in liquid N₂ were fractured. Differential scanning calorimeter (DSC) measurements were conducted under N₂ on a Mettler Toledo DSC 822 analyzer. The sample crystallinity was determined with the melting endotherm in the first heat cycle, where the samples were heated to 200°C at 20 °C/min. Isothermal crystallization experiments were also conducted. Samples were kept at 200°C for 5 min to erase a thermal history [46], and then cooled down to 128°C at a rate of 20 °C/min. A crystallization rate at 128°C was determined as an inverse of the half time of the crystallization (denoted as $t_{1/2}^{-1}$). To examine co-crystallization between the matrix PP and PP-*t*-OH or PP grafted to SiO₂ nanoparticles, 50 wt% or 10 wt% of the matrix PP respectively mixed with 50 wt% of PP-*t*-OH or 90 wt% of PP-*g*-SiO₂ was subjected to DSC measurements, where the samples with the thermal history erased at 200°C were cooled down to 40°C at 10 °C/min (first cooling) and then heated up to 200°C at 10 °C/min (second heating). The crystalline structure of a sample was evaluated by wide-angle X-ray diffraction (WAXD, Rigaku Rint-2000). The Cu-K α ($\lambda = 1.5418 \text{ \AA}$) radiation was used at 40 kV and 30 mA. Measurements were performed in the range of 10-40°. Tensile properties were determined with an Abe Dat-100 tensile tester using a dumbbell shaped specimen at a crosshead speed of 1 mm/min at

room temperature. At least 5 specimens were tested for each sample. The frequency dependence of oscillatory shear moduli in the molten state (G' , G'') was measured by a parallel-and-plate rheometer (AR2000ex TA) at 180°C with a frequency range from 100 to 0.01 rad/s under N₂ atmosphere. The diameter of the parallel plates was 25 mm. Each measurement was performed within a linear viscoelastic region. Samples were dried in vacuo 60°C for 1 h prior to the measurements.

2.3. Results and Discussion

2.3.1. Synthesis of PP-*t*-OH

PP-*t*-OH with different M_n was synthesized by varying the concentration of TEA ([TEA]) as a chain transfer agent in propylene polymerization using EBIZrCl₂ catalyst. The results of characterization for the synthesized PP-*t*-OH are summarized in **Table 2**. M_n determined by ¹³C-NMR coincided well with M_n determined by GPC, due to the single-site nature of the catalyst. It was found that M_n monotonically decreased as [TEA] increased, where $1/M_n$ was expressed as a linear function of [TEA]^{1/2} (**Figure 2**), indicating that monomeric TEA is responsible for the chain transfer reaction [47]. In addition, the positive x-intercept in Figure 2 indicates that the effective concentration of TEA became lower than the used concentration, plausibly due to a partial consumption of TEA for scavenging contaminants in the polymerization system. The stereoregularity of PP-*t*-OH was about 85-88 mol%, irrespective of [TEA]. The ratio of end functionalization was determined by ¹³C-NMR of PP-*t*-OH. Except the result for the lowest [TEA], 60-80 mol% of polymer chains were always functionalized with

hydroxyl groups relatively independently of [TEA], suggesting that the O₂ insertion into the Al-R bond might be responsible for incomplete functionalization [39,40].

Table 2. Polymerization^a and end-functionalization results

No.	[TEA] (mol/L)	M_n^b	M_n^c	$mmmm^b$ (mol%)	End functionalization ^b (mol%)
1	0	n.d.	9.0 x 10 ⁴	86	0
2	8	7.1 x 10 ⁴	n.d.	88	36
3	16	4.6 x 10 ⁴	n.d.	88	74
4	25	3.3 x 10 ⁴	n.d.	88	61
5	33	2.5 x 10 ⁴	n.d.	87	77
6	67	1.8 x 10 ⁴	n.d.	85	62
7	100	1.2 x 10 ⁴	1.2 x 10 ⁴	85	73
8	200	8.7 x 10 ³	8.7 x 10 ³	87	63
9	300	7.1 x 10 ³	5.4 x 10 ³	87	68
10	400	5.8 x 10 ³	4.9 x 10 ³	86	79

^a Total volume of toluene: 300 ml, propylene pressure: 1 atm, polymerization temperature: 0°C, polymerization time: 1 h, Zr concentration: 1.7 x 10⁻⁵ mol/L, Al concentration for MMAO: 5.0 x 10⁻¹ mol/L.

^b Determined with ¹³C-NMR.

^c Determined with GPC.

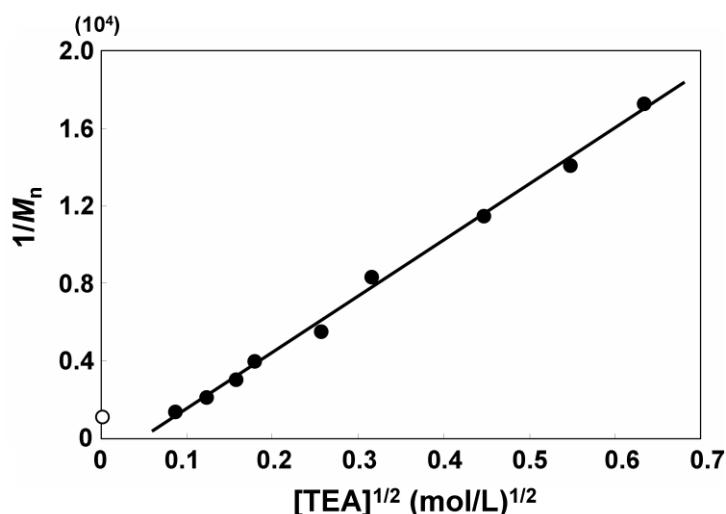


Figure 2. The inverse proportion of M_n to $[\text{TEA}]^{1/2}$.

(○) Determined with GPC and (●) determined with ^{13}C -NMR.

2.3.2. Synthesis of PP-g-SiO₂

A part of samples (Nos. 3, 4, 6, 7, 8, and 10 respectively designated as PP460-*t*-OH, PP330-*t*-OH, PP180-*t*-OH, PP120-*t*-OH, PP87-*t*-OH, and PP58-*t*-OH according to their M_n) were selected for grafting to SiO₂ nanoparticles. The amount of PP-*t*-OH to be used for the reaction was decided in order to fulfill 0.5-1.0 PP-*t*-OH chain added per OH groups of SiO₂ nanoparticles (ca. 3OH per nm²). The presence of the grafted chains was confirmed by the stretching vibration bands of -CH₂- and -CH₃ groups (**Figure 3**) [48] as well as TEM images of the nanoparticles (**Figure 4**). The amounts of grafted chains were determined by TG analysis (**Table 3**). The grafted amount was hardly dependent on M_n of PP-*t*-OH to be around 10-11 wt% except for PP58-g-SiO₂. This fact suggested that grafted chains restrict further migration of ungrafted chains to SiO₂ surfaces, thus converging into similar layer thicknesses. As a result, the number of grafted chains per particle decreased for higher M_n .

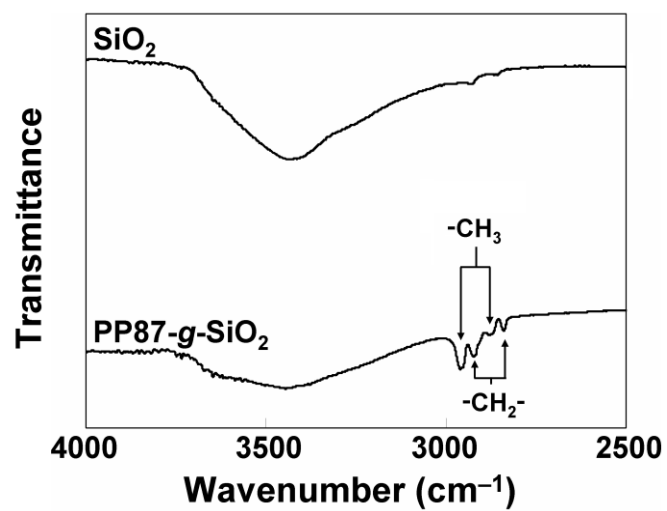


Figure 3. FT-IR spectra of neat SiO₂ and PP87-*g*-SiO₂

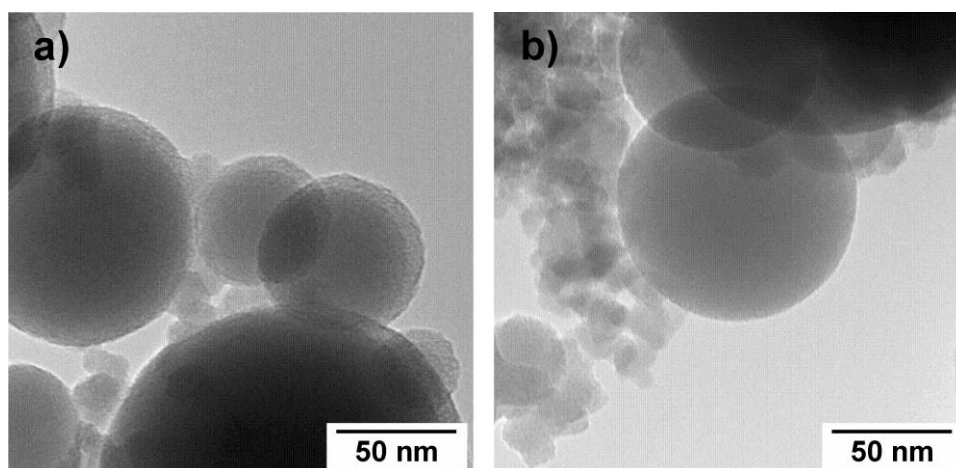


Figure 4. TEM images of a) as-synthesized PP87-*g*-SiO₂ and b) PP87-*g*-SiO₂ which was calcined at 650°C under air for 1 h.

Table 3. Results of grafted PP-*t*-OH to SiO₂ nanoparticles

Sample	Grafted amount ^a (wt%)	Grafted chain ^b (chain/particle)
PP58- <i>g</i> -SiO ₂	6.4	140
PP87- <i>g</i> -SiO ₂	10.7	160
PP120- <i>g</i> -SiO ₂	11.4	120
PP180- <i>g</i> -SiO ₂	9.6	70
PP330- <i>g</i> -SiO ₂	10.4	40
PP460- <i>g</i> -SiO ₂	10.9	30

^a Determined with TG.

^b The chain number per particle was estimated by using the specific surface area and diameter of SiO₂ nanoparticles (110 m²/g and 26 nm, respectively) and the M_n values given in Table 2.

3.3. Properties of PP/PP-*g*-SiO₂ nanocomposites

Figure 5 shows TEM images of PP/SiO₂ and PP/PP-*g*-SiO₂ nanocomposites, where the contents of unmodified SiO₂ and PP-*g*-SiO₂ were fixed at 5.0 wt%. In Figure 5a, unmodified SiO₂ nanoparticles formed huge and compact aggregates, whose sizes were around 1 μm, due to the poor compatibility with PP matrix. The grafted chains significantly improved the dispersion of the nanoparticles. PP58-*g*-SiO₂ with the shortest grafted chains partially formed a small size of aggregates plausibly due to both/either the slightly lower grafted amount and/or the chain length much shorter than the critical value for the entanglement. The other PP-*g*-SiO₂ showed similarly nice dispersion, irrespective of the length of the grafted chains. Even though

as-synthesized PP-*g*-SiO₂ nanoparticles were likely connected with each other through the entanglements among the grafted chains, the compatibility of PP-*g*-SiO₂ with the matrix was enough to disentangle the grafted chains under the applied shear force. Many of previous studies reported positive influences of polymer grafting on the dispersion of SiO₂ nanoparticles, where grafted chains not only improve the interfacial compatibility but also sterically hinder the agglomeration of nanoparticles [30-32,34,49,50]. In this study, the dispersion levels attained by using PP as grafted chains were excellent enough to keep similar dispersion up to 10 wt% of SiO₂ (not shown).

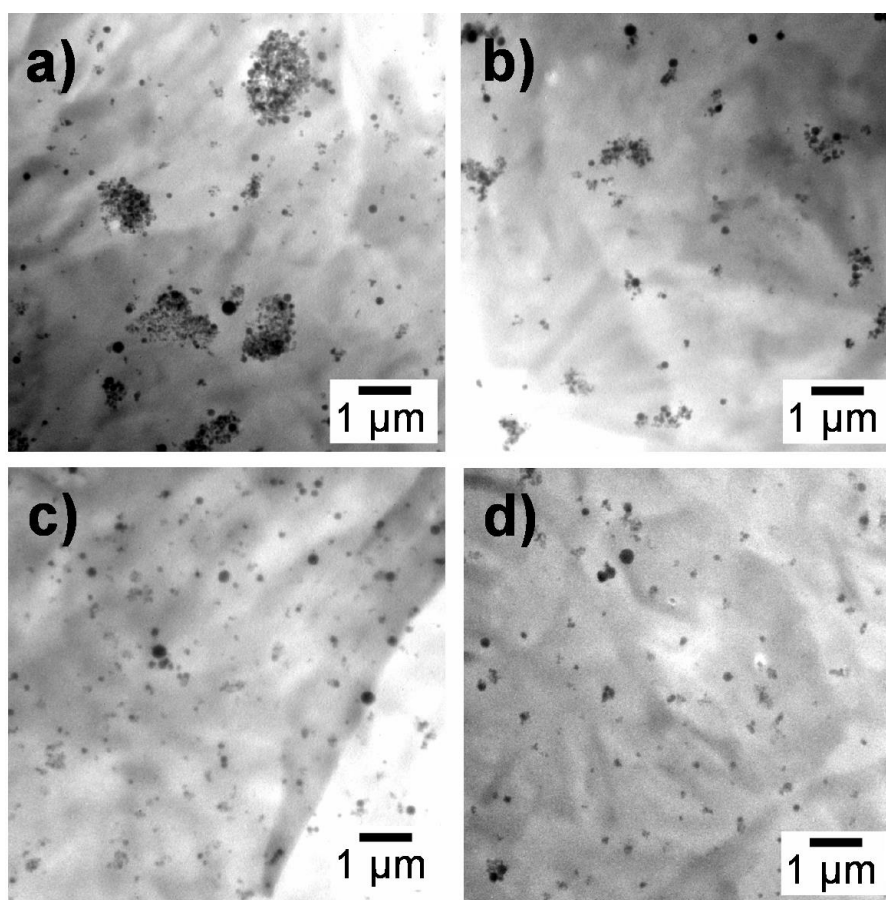


Figure 5. TEM images of a) PP/SiO₂, b) PP/PP58-*g*-SiO₂, c) PP/PP87-*g*-SiO₂, and d)

PP/PP460-*g*-SiO₂. The contents of SiO₂ and PP-*g*-SiO₂ were 5.0 wt%.

It is known that surface organic modifications endow the nucleating ability to SiO₂ nanoparticles [31], while unmodified SiO₂ nanoparticles do not act as a nucleating agent [15]. It was postulated in our previous study [51] that grafted PP chains whose one end is pinned to SiO₂ surfaces become nuclei of the crystallization and co-crystallize with the matrix chains (**Figure 6**). Table 4 collects the results of the melting behaviors and isothermal crystallization for pristine PP, PP/SiO₂ and PP/PP-*g*-SiO₂ nanocomposites. The crystallization rates ($t_{1/2}^{-1}$) were almost unchanged by the addition of neat SiO₂ nanoparticles at 5.0 wt%, while the addition of PP-*g*-SiO₂ greatly increased the crystallization rates. I have recently clarified that grafted PP chains forming a semi-dilute brush structure on SiO₂ not only enhance the nucleation of the matrix but also accelerate the spherulite growth as a plasticizer [29]. The enhancements of the crystallization rates were roughly proportional to the number of the grafted chains (**Figure 7**), supporting the idea that the grafted chains become the nuclei in the crystallization of the matrix. On the other hand, not only the melting temperature but also the crystallinity were hardly affected by the addition of SiO₂ or PP-*g*-SiO₂, based on which the effects of the sample crystallinity on the tensile properties results could be neglected. WAXD patterns for PP/SiO₂ and PP/PP-*g*-SiO₂ films (not shown) were identical to that for pristine PP, typical for the usual α form superimposed to the amorphous halo.

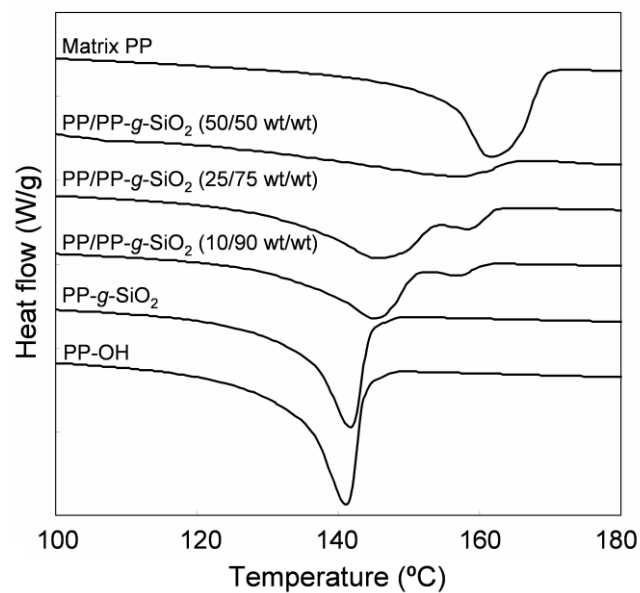


Figure 6. DSC exotherm for PP and PP120-*g*-SiO₂ blends

Table 4. Melting behaviors and isothermal crystallization results

Sample	T_m^a (°C)	X_c^b (%)	$t_{1/2}^{-1}{}^c$ (10 ² /s)
PP	163	50	0.46
PP/SiO ₂	162	47	0.51
PP/PP58- <i>g</i> -SiO ₂	159	50	2.1
PP/PP87- <i>g</i> -SiO ₂	162	51	1.8
PP/PP120- <i>g</i> -SiO ₂	160	51	1.7
PP/PP180- <i>g</i> -SiO ₂	163	48	1.1
PP/PP330- <i>g</i> -SiO ₂	162	51	1.4
PP/PP460- <i>g</i> -SiO ₂	161	53	1.2

^a T_m : peak melting temperature,

^b X_c : crystallinity of PP,

^c $t_{1/2}^{-1}$: half time of isothermal crystallization at 128°C.

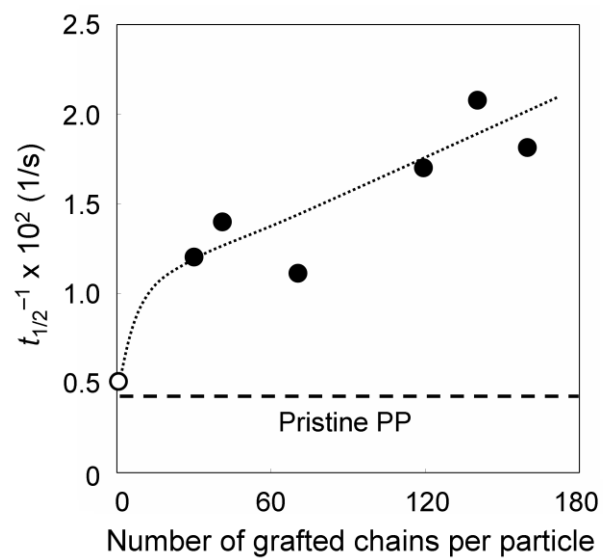


Figure 7. Half time of the crystallization ($t_{1/2}^{-1}$) at 128°C for PP/PP-*g*-SiO₂ nanocomposites plotted against the number of the grafted chain per particle

The uniaxial tensile test was performed for pristine PP, PP/SiO₂ and a series of PP/PP-*g*-SiO₂ samples. The obtained stress-strain curves (**Figure 8**) were compared with respect to M_n using a) Young's modulus, b) tensile strength, c) elongation at break, and d) toughness in **Figure 9**. In contrast to little reinforcement for unmodified SiO₂ nanoparticles, the addition of PP-*g*-SiO₂ greatly improved both the Young's modulus and tensile strength. The degrees of the reinforcement sharply increased along M_n below 1.2×10^4 . Above M_n of 1.2×10^4 , the Young's modulus nearly converged, while the tensile strength still kept increasing but much more slowly. Such a clear relationship between the chain length of grafted polymer and the degrees of reinforcement has been hardly established, which represents high controllability and reproducibility of our experiments.

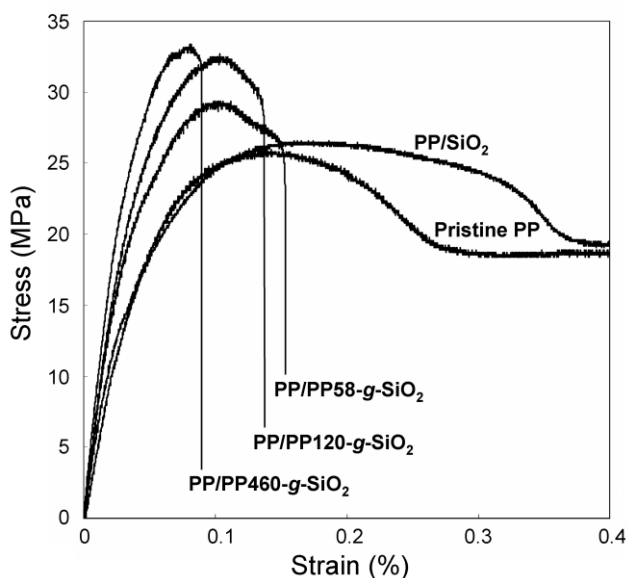


Figure 8. Stress-strain curves for PP/PP-*g*-SiO₂ nanocomposites

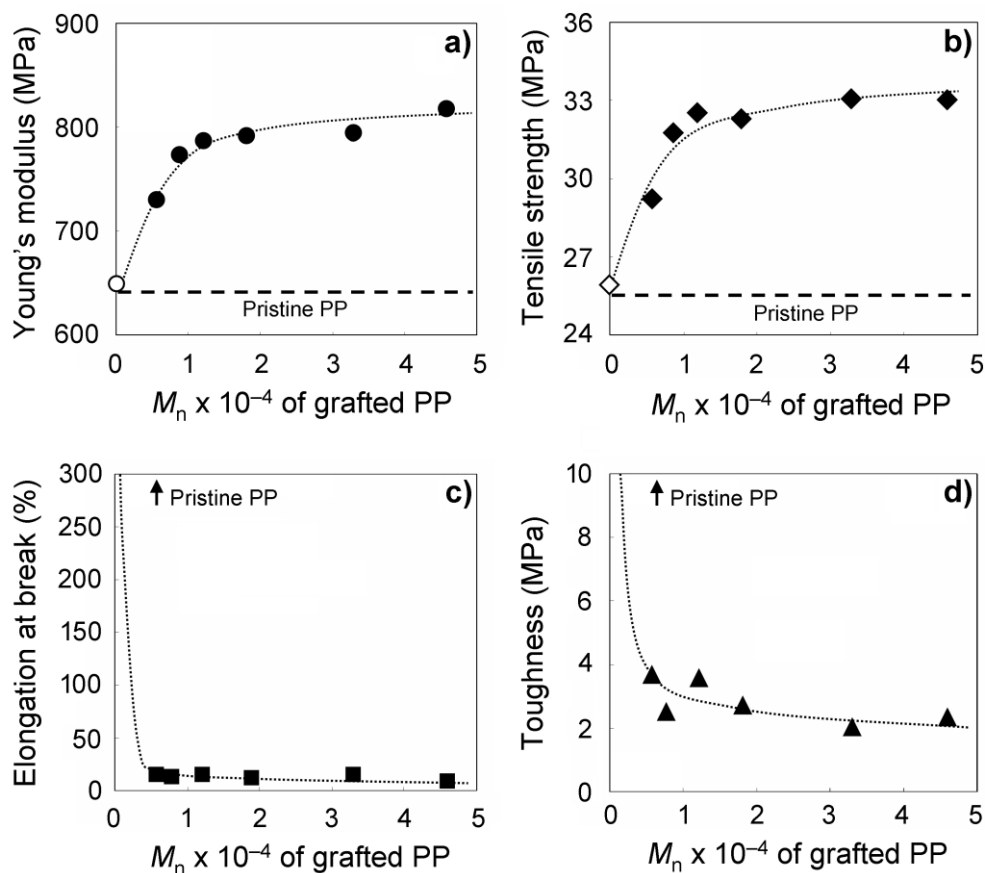


Figure 9. Results of tensile tests for PP/PP-g-SiO₂ nanocomposites: a) Young's modulus, b) tensile strength, c) elongation at break and d) toughness plotted against M_n of the grafted PP

The maximum reinforcement obtained in this study is about +30% for both the Young's modulus and tensile strength. In contrast, the addition of PP-g-SiO₂ at 5.0 wt% significantly reduced the elongation at break to 10-20% and the toughness to 2-4 MPa irrespective of the chain length of grafted PP, while the elongation at break for pristine PP and PP/SiO₂ was over 300%. It is somehow interesting that only a small fraction of the nanoparticles drastically affected these properties when highly dispersed. Generally speaking, the addition of nanoparticles tends to reduce the ductility of

original polymer. Grafted polymer more or less alleviates this reduction due to its flexibility. The opposite result for PP-g-SiO₂ is likely based on reduced flexibility of SiO₂ physically cross-linked with the matrix lamellae. SEM images of freeze-fracture surfaces for PP/PP-g-SiO₂ in Figure 10 supported good connectivity between the PP-g-SiO₂ nanoparticles and the matrix as evidenced by “elongated structures”, which were not observed for PP/SiO₂.

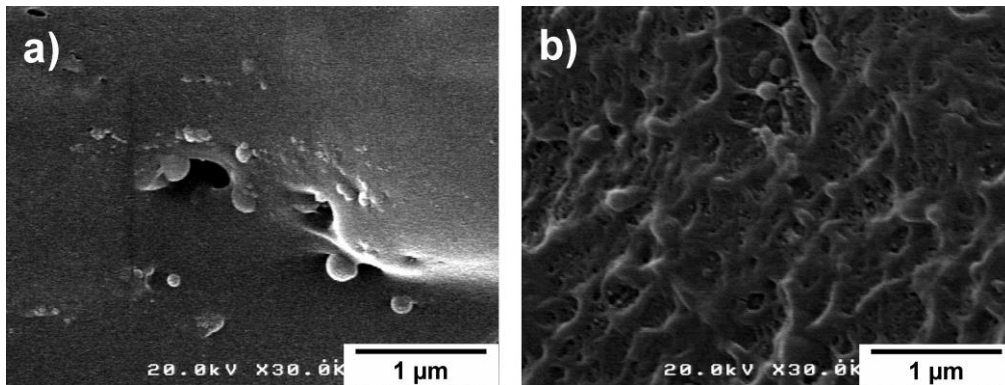


Figure 10. SEM images of freeze-fracture surfaces for a) PP/SiO₂ and b) PP/PP460-g-SiO₂. Sample films were fractured by soaking soaked in liquid N₂. The fracture surface for PP/SiO₂ exposed bare nanoparticles on a flat texture, while that for PP/PP460-g-SiO₂ showed the elongation of the matrix with the nanoparticles embedded under the surface, which is clear indication of strong interfacial connection.

In previous studies, it has been proposed that the reinforcement by the addition of unmodified SiO₂ arises from cohesive attraction among nanoparticles. On the other hand, reinforcement rendered by grafted polymer has been ascribed to efficient load transfer to nanoparticles through interdiffusion and/or entanglement between matrix and grafted chains, since the grafted polymer rather reduces the cohesive attraction among

nanoparticles. Returning to Table 1, the maximum reinforcement for the Young's modulus around +30% was reported in the cases of PP/MAPP/SiO₂ and PP/PP-*t*-NH₂/PGMA-*g*-SiO₂ [20,34]. It must be noted that a similar level of reinforcement (ca. +30%) was attained for unmodified colloidal SiO₂ as long as nanoparticles were uniformly dispersed at the nanolevel [35]. In the present case, ca. +30% of the reinforcement was also obtained except for PP58-*g*-SiO₂ that exhibited dispersion slightly worse than the others. In other words, the degree of the reinforcement was believed to be constant irrespective of the density and M_n of grafted PP as long as the uniform dispersion is achieved, indicating that the effective load transfer to hard SiO₂ nanoparticles plays the dominant role in improving the Young's modulus.

The enhancement in the tensile strength by +30% was much higher than the ever-reported values for spherical SiO₂ (i.e. filler with the smallest aspect ratio, see Table 1) and even greater than +24% reported for PP/MAPP/modified montmorillonite [52]. Such an anomalous enhancement must not be simply based on the effective load transfer to uniformly dispersed nanoparticles through interdiffusion and/or entanglement between matrix and grafted chains, but must arise from alternative reinforcing mechanism. As was already discussed for the accelerated crystallization in PP/PP-*g*-SiO₂ (also see Figure 6), grafted PP chains co-crystallize with the matrix chains as crystallization nuclei. Considering that 30-140 chains were grafted to one SiO₂ particle, the most plausible scenario is that PP-*g*-SiO₂ located in the amorphous phase of the matrix becomes a physical cross-linker between lamellae through grafted PP. Along the same scenario, the convergence of the reinforcement over M_n of 1.2×10^4 can be accounted by the fact that increasing probability of the cross-linkage for

longer grafted chains is compensated by the reduction in the graft density (Table 2).

The results of linear viscoelastic measurements at 200°C are shown in **Figure 11**. In general, the addition of nanoparticles tends to increase G' and η in melt either through cohesive attraction between nanoparticles for weak filler-matrix interaction or through polymer-mediated bridging connection between nanoparticles for strong interaction. PP/SiO₂ corresponds to the former case, exhibiting large increments in G' and η especially at a terminal region (Figure 11). Grafting PP chains to SiO₂ greatly suppressed the enlargement of G' and η especially at lower frequencies. This is because the grafted PP chains form a polymer overlayer on SiO₂ surfaces to inhibit the cohesive attraction between nanoparticles, and also because chemically inert PP chains do not bridge between nanoparticles. On the other hand, we have postulated that the reinforcement for the tensile strength is based on the physical cross-linkage via PP-*g*-SiO₂. In a PP-based thermoplastic elastomer, the G' value of the amorphous phase as the main component is reinforced by the physical cross-linkage between dispersed crystallites, while it converges to the original value for the amorphous phase once the crystallites dissolve over their melting temperature [53]. The PP/PP-*g*-SiO₂ nanocomposites represented similar behaviors between the solid and melt states. The increment in η over pristine PP was much lower compared with PP/SiO₂, and almost independent of M_n of grafted PP. Considering that the addition of nanoparticles generally lowers the melt flowability of polymer, it is important that grafted PP reinforced tensile properties in solid without largely sacrificing the original flowability of PP in melt.

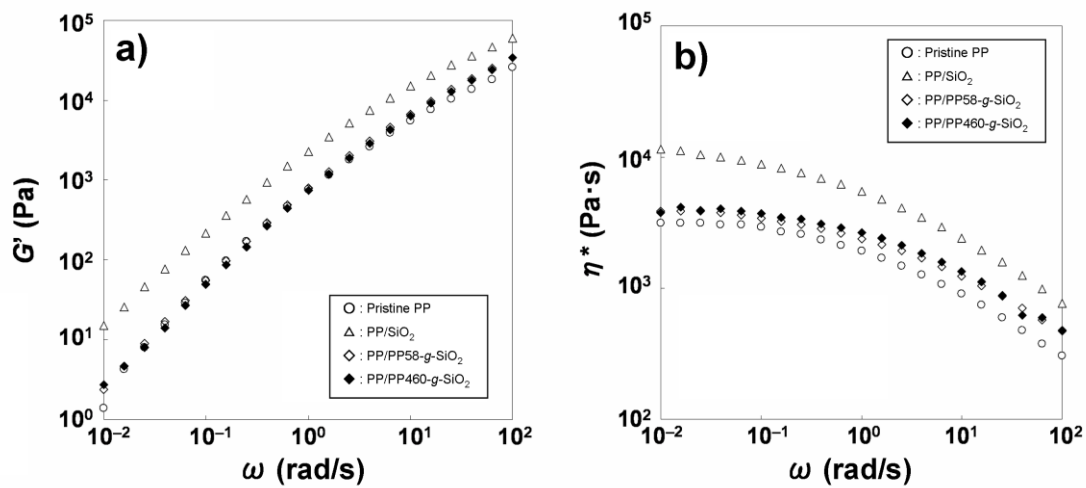


Figure 11. Linear viscoelastic behaviors of PP/PP-g-SiO₂ nanocomposites at 200°C: a) storage modulus and b) complex viscosity.

2.4. Conclusions

In this article, a series of PP/PP-*g*-SiO₂ nanocomposites having different chain lengths of grafted PP ($M_n = 5.8 \times 10^3$ - 4.6×10^4) were prepared by melt mixing. I found that the prepared nanocomposites exhibit profoundly improved physical properties compared not only with pristine PP & PP/neat SiO₂ but also with ever-reported PP/SiO₂-based nanocomposites. The PP-*g*-SiO₂ nanoparticles were highly dispersible in the matrix up to the filler content of 10 wt%, irrespective of the chain length of grafted PP, and exhibited pronounced nucleation effects in the crystallization of PP, where the enhancement of the crystallization rate over pristine PP was proportional to the number of grafted chains per nanoparticle. The inclusion of PP-*g*-SiO₂ nanoparticles at 5.0 wt% achieved +30% reinforcement for the Young's modulus irrespective of the chain length of grafted PP, as a result of the effective load transfer to uniformly dispersed hard particles. The most important finding was the +30% reinforcement for the tensile strength, which is unexpectedly high for spherical nanoparticles. On the contrary to these reinforcements in the solid state, increments in G' and η for PP-*g*-SiO₂ were much lower than those observed for unmodified SiO₂. All these facts let us propose that the reinforcement for the tensile strength is due to physical cross-linking through co-crystallization between the matrix and grafted PP. Thus, we have proved that PP-grafted nanoparticles are promising materials to greatly enhance the crystallization rate, Young's modulus, and tensile strength without sacrificing the melt flowability of PP [54].

References:

- [1] Usuki, A., Kojima, Y., Kawasumi, M., Okada, A., Fukushima, Y., Kurauchi, T., Kamigaito, O., *J. Mater. Res.* **1993**, *8*, 1185-1189.
- [2] Ray, S.S., Okamoto, M., *Prog. Polym. Sci.* **2003**, *28*, 1539-1641.
- [3] Kashiwagi, T., Grulke, E., Hilding, J., Groth, K., Harris, R., Butler, K., Shields, J., Kharchenko, S., Douglas, J., *Polymer* **2004**, *45*, 4227-4239.
- [4] Chan, C.M., Wu, J.S., Li, J.X., Cheung, Y.K., *Polymer* **2002**, *43*, 2981-2992.
- [5] Manias, E., Touny, A., Wu, L., Strawhecker, K., Lu, B., Chung, T.C., *Chem. Mater.* **2001**, *13*, 3516-3523.
- [6] Gilman, J.W., Jackson, C.L., Morgan, A.B., Harris, Jr. R., *Chem. Mater.* **2000**, *12*, 1866-1873.
- [7] Fina, A., Tabuani, D., Frache, A., Camino, G., *Polymer* **2005**, *46*, 7855-7866.
- [8] Zanetti, M., Camino, G., Canavese, D., Morgan, A.B., Lamelas, F.J., Wilkie, C.A., *Chem. Mater.* **2002**, *14*, 189-193.
- [9] Sun, T., Garces, J.M., *Adv. Mater.* **2002**, *14*, 128-130.
- [10] Ellis, T.S., D'Angelo, J.S., *J. Appl. Polym. Sci.* **2003**, *90*, 1639-1647.
- [11] Hood, M.A., Gold, C.S., Beyer, F.L., Sands, J.M., Li, C.Y., *Polymer* **2013**, *54*, 6510-6515.
- [12] Wen, Y., Hui, Z., Heyi, H., Shen, W., Gregory, L.B., *ACS Appl. Mater. Interfaces* **2013**, *5*, 4155-4161.
- [13] Qian, J., Cheng, G., Zhang, H., Xu, Y., *J. Polym. Res.* **2011**, *18*, 409-417.
- [14] Diego, B., Vivianne, N.D., Humberto, P., Raúl, Q., *J. Nanomater.* **2012**, DOI:10.1155/2012/263915.

- [15] Liu, Y., Kontopoulou, M., *J. Vinyl. Add. Tech.* **2007**, *13*, 147-150.
- [16] Nitta, K., Asuka, K., Liu, B., Terano, M., *Polymer* **2006**, *47*, 6457-6463.
- [17] Bikiaris, D., Papageorgiou, G., Pavlidou, E., Vouroutzis, N., Palatzoglou, P., Karayannidis, G., *J. Appl. Polym. Sci.* **2006**, *100*, 2684-2696.
- [18] Hieda, J., Shirafuji, T., Noguchi, Y., Saito, N., Takai, O., *J. Japan Inst. Metals* **2009**, *73*, 938- 942.
- [19] Kawasumi, M., Hasegawa, N., Kato, M., Usuki, A., Okada, A., *Macromolecules* **1997**, *30*, 6333-6338.
- [20] Pavlidou, E., Bikiaris, D., Vassiliou, A., Chiotelli, M., Karayannidis, G., *J. Phys.* **2005**, *10*, 190-193.
- [21] Lin, O.H., Akil, H.M., Ishak, Z.A.M., *Polym. Compos.* **2011**, *32*, 1568-1583.
- [22] Wang, Z.M., Nakajima, H., Manias, E., Chung, T.C., *Macromolecules* **2003**, *36*, 8919-8922.
- [23] Brune, D.A., Bicerano, J., *Polymer* **2002**, *43*, 369-387.
- [24] He, H., Riedl, T., Lerf, A., Klinowski, J., *J. Phys. Chem.* **1996**, *100*, 19954-19958.
- [25] Bahloul, W., Mélis, F., Bounor-Legeré, V., Cassagnau, P., *Mater. Chem. Phys.* **2012**, *134*, 399- 406.
- [26] Sun, D.H., Zhang, R., Liu, Z.M., Huang, Y., Wang, Y., He, J., Han, B.X., Yang, G.Y., *Macromolecules* **2005**, *38*, 5617-5624.
- [27] Ji-Eun, A., Jeon, G.W., Jeong, Y.G., *Fib. Polym.* **2012**, *13*, 507-514.
- [28] Bahloul, W., Bounor-Legaré, V., David, L., Cassagnau, P., *J. Polym. Sci. Part B: Polym. Phys.* **2010**, *48*, 1213-1222.
- [29] Fukuyama, Y., Kawai, T., Kuroda, S., Toyonaga, M., Taniike, T., Terano, M., *J. Therm. Anal. Calorim.* **2013**, *113*, 1511-1519.

- [30] Rong, M.Z., Zhang, M.Q., Pan, S.L., Lehmann, B., Friedrich, K., *Polym. Int.* **2004**, *53*, 176- 183.
- [31] Rong, M.Z., Zhang, M.Q., Zheng, Y.X., Zeng, H.M., Walter, R., Friedrich, K., *Polymer* **2001**, *42*, 167-183.
- [32] Wu, C.L., Zhang, M.Q., Rong, M.Z., Friedrich, K., *Compos. Sci. Technol.* **2002**, *62*, 1327-1340.
- [33] Sumino, K., Taniike, T., Terano, M., George, G.A., *Macromol. React. Eng.* **2008**, *2*, 135-141.
- [34] Zhou, H.J., Rong, M.Z., Zhang, M.Q., Ruan, W.H., Friedrich, K., *Polym. Eng. Sci.* **2007**, *47*, 499-509.
- [35] García, M., van Vliet, G., Jain, B., Schrauwen, B.A.G., Sarkissov, A., van Zyl, W.E., Boukamp, B., *Rev. Adv. Mater. Sci.* **2004**, *6*, 169-175.
- [36] Xu, N., Zhou, W., Shi, W., *Polym. Adv. Technol.* **2004**, *15*, 654-661.
- [37] Wang, Z.M., Hong, H., Chung, T.C., *Macromolecules* **2005**, *38*, 8966-8970.
- [38] Chung, T.C., *J. Org. Chem.* **2005**, *690*, 6292-6299.
- [39] Han, C.J., Lee, H.S., Byun, D.J., Kim, S.Y., *Macromolecules* **2002**, *35*, 8923-8925.
- [40] Kuo, J.C., Lin, W.F., Yu, C.H., Tsai, J.C., Wang, T.C., Chung, T.M., Ho, R.M., *Macromolecules* **2008**, *41*, 7967-7977.
- [41] Collins, S., Gauthier, W.J., Holden, D.A., Kuntz, B.A., Taylor, N.J., Ward, D.G., *Organometallics* **1991**, *10*, 2061-2068.
- [42] Shiono, T., Soga, K., *Macromol. Chem. Rapid. Commun.* **1992**, *13*, 371-376.
- [43] Duschek, T., Mullhaupt, R., *Polym. Prepr.* **1992**, *33*, 170-171.
- [44] Yanjarappa, M.J., Sivaram, S., *Prog. Polym. Sci.* **2002**, *27*, 1347-1398.
- [45] Antonow, D., Graebin, C.S., Eifler-Lima, V.L., *Chem. Soc.* **2004**, *15*, 782-785.

- [46] Shijie, S., Peiyi, W., Jiachun, F., Mingxin, Y., Yuliang, Y., *Polymer* **2009**, *50*, 286-295.
- [47] Natta, G., Pasquon, I., Svab, J., Zambelli, A., *Chim. Ind.* **1962**, *44*, 621-624.
- [48] Abdel-Hamid, H.M., *Solid-State Electron.* **2005**, *49*, 1163-1167.
- [49] Cai, L.F., Huang, X.B., Rong, M.Z., Ruan, W.H., Zhang, M.Q., *Polymer* **2006**, *47*, 7043-7050.
- [50] Ruan, W.H., Huang, X.B., Wang, X.H., Rong, M.Z., Zhang, M.Q., *Macromol. Rapid. Commun.* **2006**, *27*, 581-585.
- [51] Umemori, M., Taniike, T., Terano, M., *Polym. Bull.* **2013**, *68*, 1093-1108.
- [52] Hasegawa, N., Okamoto, H., Kato, M., Usuki, A., *Appl. Polym. Sci.* **2000**, *78*, 1918-1922.
- [53] McNally, T., McShane, P., Nally, G.M., Murphy, W.R., Cook, M., Miller, A., *Polymer* **2002**, *43*, 3785-3793.
- [54] Taniike, T., Toyonaga, M., Terano, M., *Polymer* **2014**, *55*, 1012-1019.

Chapter 3.

The Influences of Mechanical Properties for Grafted Chain Number on Polypropylene-grafted SiO₂ of Polypropylene-based Nanocomposites

3.1. Introduction

The application of polymer materials has increasingly expanded in recent years, in which a variety of compounding techniques have played an important role. In particular, polymer nanocomposites are one of the most promising materials, where the inclusion of nanosized fillers in polymer matrices can improve not only mechanical but also other properties such as thermal stability, transparency, gas barrier properties, and so on [1-6]. While a number of nanocomposites have been investigated by changing the combination between polymer and nanofillers, polypropylene (PP)-based nanocomposites have attracted particular attention, owing to the huge market of PP and a multitude of potential applications [7]. However, the development of practically useful PP nanocomposites is highly challenging, since the apolar nature of PP prevents the dispersion and interfacial bonding of nanofillers. In most of cases, nanofillers lead to macroscopic agglomeration in the PP matrix, which result in marginal reinforcement as well as other problems like embrittlement, enhanced degradation, and so on.

In order to overcome the compatibility problem, a variety of strategies have been proposed. The most popular strategy is the addition of a compatibilizer, which is often combined with surface organic modification [8,9]. The strategy has been successful in terms of the dispersion, but not in terms of the reinforcement, where the compatibilizer forms a soft interfacial layer between PP and nanofillers without bonding. As a consequence, the load transfer to the nanofillers is not effectively achieved during the deformation. Polymer grafting is a way to attain both of the dispersion and the effective load transfer [10-11]: Polymer chains grafted onto filler surfaces not only suppress cohesive attraction among nanofillers but also entangle/inter-diffuse with the

matrix polymer so as to create strong interfacial bonding. While many kinds of polymer have been grafted to nanofillers for the fabrication of PP nanocomposites, our recent efforts are one of a few examples that successfully applied PP-grafted nanofillers [12-13]: Terminally hydroxylated isotactic PP (PP-*t*-OH) chains were grafted to SiO₂ nanoparticles and the resultant PP-*g*-SiO₂ nanoparticles were melt mixed with PP. I found a variety of positive consequences of the PP grafting such as extremely nice dispersion up to 10 wt%, four times faster crystallization, *ca.* +30% improvement in both the Young's modulus and tensile strength, and no viscoelastic penalty by the addition of SiO₂ nanoparticles. It was concluded that the key feature of our PP/PP-*g*-SiO₂ nanocomposites is at a physical cross-linkage structure made by co-crystallization between the matrix and grafted chains, where SiO₂ nanoparticles bridge neighboring lamellae through the grafted chains (**Figure 1**).

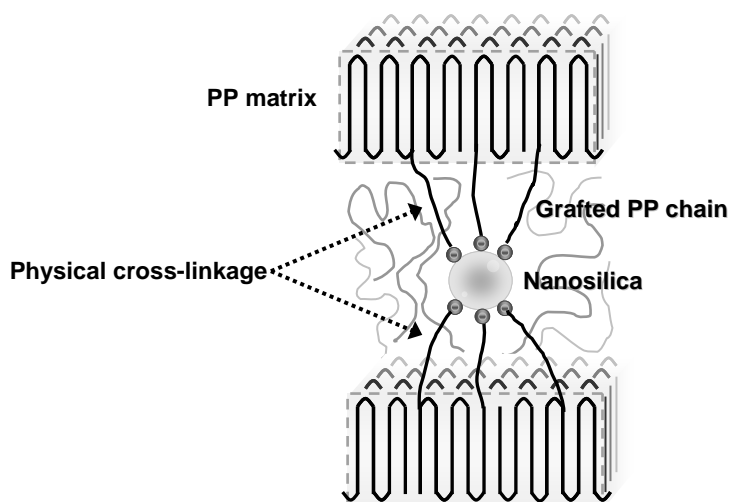


Figure 1. Structure model of physical cross-linkage

In this **Chapter 3**, we have investigated influences of the number of grafted chains per particle as well as the amount of PP-*g*-SiO₂ nanoparticles on the properties of resultant PP/PP-*g*-SiO₂ nanocomposites. The different grafted chains per particle (21-120 chain/particle) on PP-*g*-SiO₂ nanoparticles were controlled by the amount of PP-*t*-OH before the grafting reaction. In the same way, filler content (0-5 wt%) on PP/PP-*g*-SiO₂ nanocomposites was controlled by the introduction amount of PP-*g*-SiO₂ nanoparticles in the melt mixing process. As a result, the grafted chains on PP-*g*-SiO₂ significantly improved the dispersion of the filler compared with unmodified SiO₂. The other PP/PP-*g*-SiO₂ nanocomposites showed similarly nice dispersion, irrespective of not only grafted amount but also filler content. It was found that the difference of not only filler content but also grafted amount greatly affects the crystallization behavior and mechanical properties. In dependence on grafted amount, increases of the chain number directly improve the tensile strength and crystallization rate, which indicated reinforcements of the around 30% and 400% respectively. On the other hand, predominant factor of Young's modulus related to the dispersion state of filler regardless of grafted amount. In dependence on filler content, various characteristics greatly depended on the filler content by high dispersion.

3.2. Experimental

3.2.1. Materials

PP pellets ($M_n = 4.6 \times 10^4$, MWD = 5.65, *mmmm* = 98 mol%) were donated from Japan Polypropylene Corporation. Propylene gas of research grade (Japan Polypropylene Corporation) was used as delivered. *rac*-Ethylenebis(1-indenyl)-zirconium dichloride (EBIZrCl₂) was purchased from Kanto Chemical Co., Inc. Triethylaluminum (TEA) and modified methylaluminoxane (MMAO) were kindly donated by Tosoh Finechem Corporation. Toluene and *n*-tetradecane were dried over molecular sieve 4A followed by N₂ bubbling. SiO₂ nanoparticles with an average diameter of 26 nm and a surface area of 110 m²/g were purchased from Kanto Chemical Co., Inc.

3.2.2 Synthesis of PP-*t*-OH

PP-*t*-OH was prepared according to **Chapter 2**. Briefly, 300 ml of dry toluene (as solvent), 4.5 mmol of MMAO (as an activator), 1.5 μmol of EBIZrCl₂ (as a catalyst) and 9.0 mmol of TEA (as a chain transfer agent) were charged in a stirred flask maintained at 0°C. The propylene polymerization was conducted at 0°C by supplying 1 atm of propylene for 1 h. Thereafter, the obtained product was reacted with hydrogen peroxide under oxygen atmosphere at the same temperature for 1 h. Thus obtained PP-*t*-OH was purified by repetitive washing with acidic ethanol and subsequent vacuum drying. The M_n , *mmmm*, and end functionalization rate of PP-*t*-OH determined by ¹³C-NMR (100 MHz, Bruker) and GPC (Viscotek, HT-GPC 350) were 1.2×10^4 , 85 mol% and 73 mol%, respectively.

3.2.3. *Synthesis of PP-g-SiO₂*

PP-*t*-OH was grafted onto SiO₂ nanoparticles via dehydration between the terminal hydroxyl groups and surface silanol groups of SiO₂. A specified amount of PP-*t*-OH (4.0-0.1 g) and 0.5 g of SiO₂ nanoparticles (dried at 160°C prior to the grafting) were reacted in tetradecane containing 0.1 mol/L of 6-di-*tert*-butyl-*p*-cresol (BHT) at 200°C for 6 h. The resultant particles were washed with methanol, and dried in vacuo at 60°C for 6 h. Unreacted polymer was carefully removed with repetitive hot filtration in *o*-dichlorobenzene at 140°C. The grafted chain number per SiO₂ particle was controlled from 21-120 chain/particle by changing the amount of PP-*t*-OH to be reacted with SiO₂.

3.2.4. *Compounding of PP/PP-g-SiO₂ nanocomposites*

PP-based nanocomposites were prepared by a two-roll mixer at 20 rpm. 10 g of the PP pellets was preliminarily kneaded at 185°C for 5 min, followed by the addition of a specified amount of unmodified SiO₂ or PP-*g*-SiO₂ nanoparticles (0, 1, 3, 5 wt%). The mixture was further kneaded at 185°C for additional 10 min. The sample sheets with the thickness of 200 μm were prepared by hot press at 230°C and 20 MPa, followed by quenching at 100°C for 5 min.

3.2.5. Analyses

Thermogravimetric analysis (TGA, METTLER TOLEDO TG50) was employed to measure the grafted polymer amounts. The temperature was kept at 200°C for 30 min to remove physisorbed water, and then increased up to 650°C at 20 °C/min. The grafted amount was estimated from the difference in the weight loss between PP-g-SiO₂ to unmodified SiO₂ in the range of 200-650°C. The dispersion of the SiO₂ nanoparticles was observed by a transmission electron microscope (TEM, Hitachi H-7100), using specimens with the thickness of 100 nm which were prepared by an ultramicrotome (Reichert Ultracut S with a FC-S cryoattachment). The crystallization behavior of the nanocomposites was examined using a differential scanning calorimeter (DSC, METTLER TOLEDO DSC 822). A sample in an aluminum pan was heated from room temperature to 200°C at 20 °C/min, then kept at 200°C for 5 min to eliminate the thermal history, and finally cooled down to 128°C at 20 °C/min for the isothermal crystallization experiment. The melting point (T_m) and the crystallinity (X_c) of the sample were respectively determined as the peak-top temperature and the peak area of the endotherm during the first heat cycle. Sample crystallinity was determined from the endothermic peak area of melting curves using Equation of Hoffman-Weeks extrapolation methods. The isothermal crystallization rate (denoted as $t_{1/2}^{-1}$) was defined as an inverse of the half time of the crystallization at 128°C. Tensile properties of the nanocomposites were measured by a tensile tester (Abe Dat-100). A stress-strain curve was acquired at room temperature and at a crosshead speed of 1.0 mm/min. At least 5 specimens were tested for each sample.

3.3. Results and Discussion

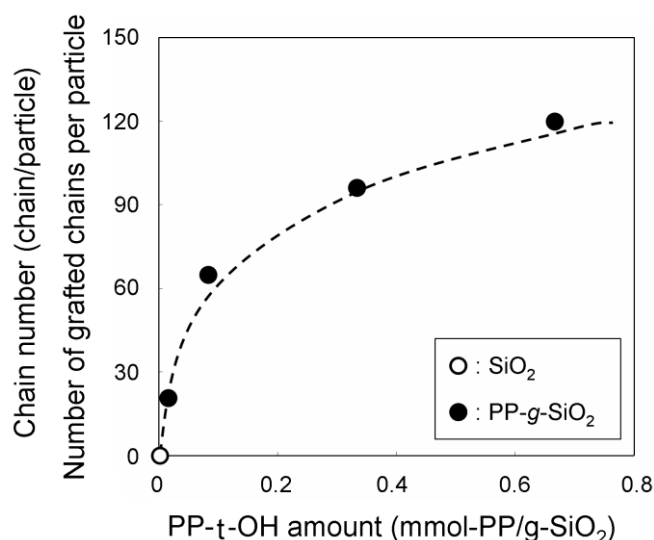
3.3.1. Synthesis of PP-g-SiO₂

Control of grafted amount on PP-g-SiO₂ was determined by the introduction amount of PP-*t*-OH before the grafting reaction. Relations of PP-*t*-OH amount and grafted amount are shown in **Table 1** and **Figure 2**. As indicated in the **Chapter 2, Chapter 3** suggested that grafted PP chains on SiO₂ restrict migration of unmodified PP chains to SiO₂ surfaces. Thus, grafted amount was hardly dependent on M_n of PP chain when using excess amount of PP-*t*-OH. This result on Figure 2 supports the **Chapter 2**. Grafted amount converged according to the increase of PP-*t*-OH introduction amount even if grafted chain number is less than the silanol group on SiO₂ surface. The convergence value of the grafted amount becomes approximately 10 wt%, and this corresponding to 120 chain/particle. In any case, the grafting reaction successfully controlled the grafted amount on PP-g-SiO₂ nanoparticles, which denominated the sample name to 21PP-g-SiO₂, 65PP-g-SiO₂, 96PP-g-SiO₂, and 120PP-g-SiO₂ in response to the number of the grafted chains.

Table 1. Synthesized PP-*g*-SiO₂ nanoparticles with different grafted chain densities

Sample	PP- <i>t</i> -OH amount x 10 ² (mmol-PP/g-SiO ₂)	Grafted amount (wt%) [a]	Grafted chain (chain/particle) [b]
21PP- <i>g</i> -SiO ₂	1.67	2.2	21
65PP- <i>g</i> -SiO ₂	8.33	6.3	65
96PP- <i>g</i> -SiO ₂	33.3	9.1	96
120PP- <i>g</i> -SiO ₂	66.7	11.4	120

[a] Determined with TGA; [b] The chain number per particle was estimated by using the specific surface area and the diameter of SiO₂ nanoparticles (110 m²/g and 26 nm, respectively) as well as M_n of grafted PP chains (1.2×10^4 g/mol).

**Figure 2.** Result of grafting reaction from different PP-*t*-OH amount

Additionally, TEM images for PP-*g*-SiO₂ are shown in **Table 2** together with that for unmodified SiO₂. Various PP-*g*-SiO₂ can observe the polymer layer of several nanometers of the different permeation rate compared with unmodified SiO₂ nanoparticles in Figure 3 a). Moreover the layer thickness enlarged with an increase of the number of grafted chains. Grafted amount by the TGA measurement don't

correspond with thickness of the polymer layer by the TEA observation, because there are possibility and reason for "decrease of the density by the gap in the layer" and "thickness of the layer don't depend on the SiO₂ diameter". In addition, the observation of 21PP-g-SiO₂ was extraordinarily-difficult, because the polymer layer is the thinnest of the PP-g-SiO₂ samples.

Table 2. Thickness of grafted PP layer on SiO₂ surface

Sample	Thickness of PP layer (nm)[a]
Dried SiO ₂	0
21PP-g-SiO ₂	< 2
65PP-g-SiO ₂	4-8
120PP-g-SiO ₂	8-10

[a] Determined with TEM observation

3.3.2. Properties of PP/PP-g-SiO₂ nanocomposites

Figure 3 shows the TEM micrographs of the prepared nanocomposites to evaluate the dispersion state of the nanoparticles in matrix. Nanocomposite samples denominated the sample name to a) PP/SiO₂_1w, b) PP/SiO₂_5w, c) PP/120PP-g-SiO₂_1w, d) PP/120PP-g-SiO₂_5w, e) PP/65PP-g-SiO₂_5w, and f) PP/21PP-g-SiO₂_5w in response to the filler content. In Figure 3 a,b), PP/SiO₂ nanocomposites using unmodified nanoparticles formed the large aggregation according to increasing fillers. In contrast to PP/SiO₂ nanocomposites, PP/120PP-g-SiO₂ nanocomposites of Figure 3 c,d) can maintain the high dispersion state while PP-g-SiO₂ with the high miscibility increases introduction amount. Furthermore, various PP/PP-g-SiO₂_5w nanocomposites using fillers with different grafted amounts show the

observation result in Figure 3 d-f). The dispersion states of various PP/PP-g-SiO₂_5w definitely improved not only 120PP-g-SiO₂_5w nanoparticles of d) but also 21PP-g-SiO₂_5w nanoparticles of f), which indicate that the huge aggregation of SiO₂ can dramatically scatter SiO₂ with low grafted amount compared with existing amount in the **Chapter 2**. Moreover, PP/PP-g-SiO₂ nanocomposites of c-f) cannot judge the differences of the dispersion state and the cluster size by TEM images due to regional nanoparticles which are smaller than resolution. Therefore, these results conclude that excess amount of grafted chains don't change the filler dispersibility.

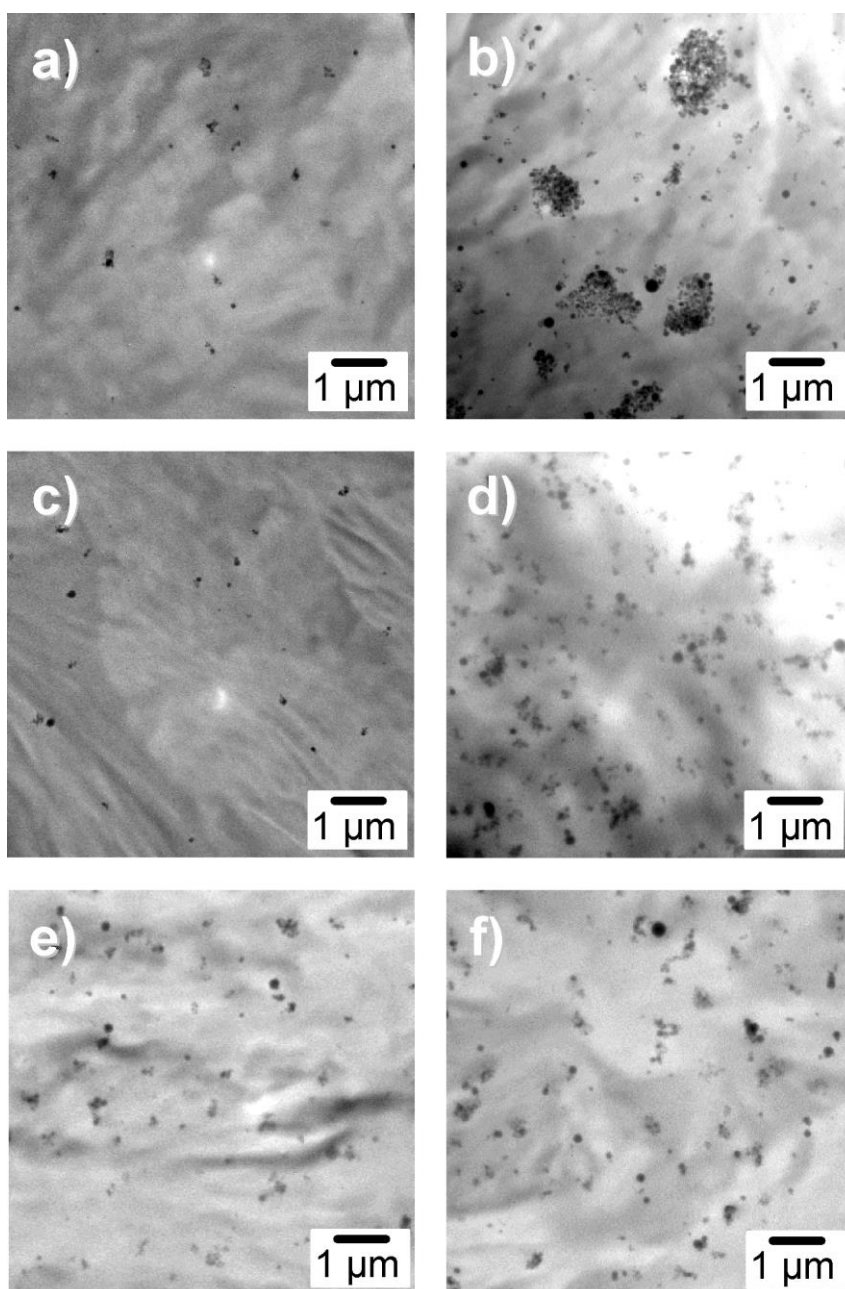


Figure 3. TEM images of a) PP/SiO₂ 1wt%, b) PP/SiO₂ 5w, c) PP/120PP-g-SiO₂ 1w, d) PP/120PP-g-SiO₂ 5w, e) PP/65PP-g-SiO₂ 5w, and f) PP/21PP-g-SiO₂ 5w.

The crystallization behaviors of pristine PP and various nanocomposites were assessed using the DSC instrument, which were summarized in **Table 3** and **Figure 4**.

The melting point and crystallinity of nanocomposites showed the same results nearly, which indicate that lamella thickness is same. Crystallization rate by the dependence of grafted amount is shown in Figure 4 a). Various PP/PP-*g*-SiO₂ nanocomposites improved crystallization rate compared with PP/SiO₂ nanocomposites, which conclude that grafted chain has the nuclei effects. Furthermore, in the range of PP/SiO₂ from PP/21PP-*g*-SiO₂, the curve produces a large shift. It shows clearly that grafted PP chains of 21 chain/particle exert the nuclei effect enough. On the other hand, in the range of PP/21PP-*g*-SiO₂ from PP/120PP-*g*-SiO₂, the curve produces a minute change. The data would seem to suggest that minimal improvement of crystallization rate is a thing by the increase in filler surface area of increasing grafted chain number.

Table 3. Melting behaviors and isothermal crystallization results

Sample	Filler content (wt%)	Chain number (chain/particle)	T_m (°C) [a]	X_c (%) [b]	$t_{1/2}^{-1}$ (10 ² /s) [c]
Pristine PP	0	0	163	50	0.46
PP/SiO ₂ 1w	1	0	160	49	0.48
PP/SiO ₂ 3w	3	0	161	49	0.52
PP/SiO ₂ 5w	5	0	162	47	0.51
PP/120PP- <i>g</i> -SiO ₂ 1w	1	120	161	50	0.90
PP/120PP- <i>g</i> -SiO ₂ 3w	3	120	162	49	1.4
PP/120PP- <i>g</i> -SiO ₂ 5w	5	120	160	51	1.7
PP/96PP- <i>g</i> -SiO ₂ 5w	5	96	161	52	1.4
PP/65PP- <i>g</i> -SiO ₂ 5w	5	65	162	51	1.5
PP/21PP- <i>g</i> -SiO ₂ 5w	5	21	163	51	1.3

[a] T_m : peak top of endotherm peak; [b] X_c : crystallinity; [c] $1/2t$: half time of isothermal crystallization at 128°C.

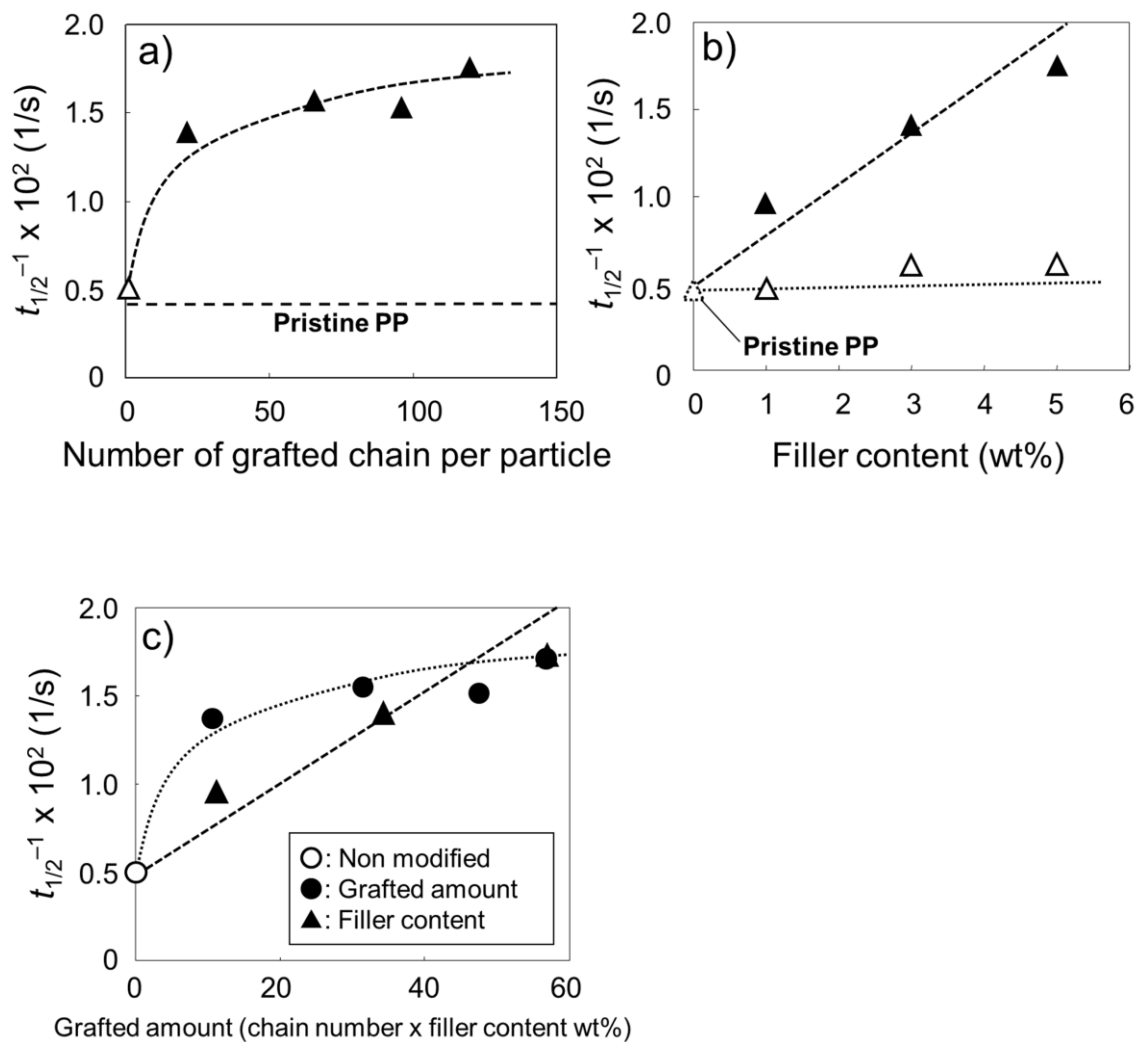


Figure 4. Crystallization rates of a) grafted amount, b) filler content, and c) total grafted amount

After that the dependence of filler content is shown in Figure 4 b). The crystallization rate of PP/SiO₂ curve indicated approximately-same value from 1 wt% to 5 wt% of SiO₂ content by the low compatibility between the matrix and fillers. On the other hand, crystallization rate of PP/120PP-g-SiO₂ indicates the linear improvement

from pristine PP to 5 wt% of sample. It pertains to not only the same grafted amount compared with other PP/120PP-*g*-SiO₂ samples but also the high dispersion state of fillers.

Furthermore, Figure 4 c) shows crystallization rate as against the total grafted amount in defiance of the particles. The lines of grafted amount and filler content dependence clearly indicate different behavior. PP/21PP-*g*-SiO₂ and PP120-*g*-SiO₂_1w of similar total-grafted amount greatly differ in a value of crystallization rate. PP/21PP-*g*-SiO₂ already presents the expression of nuclei effect, which is superior to PP/120PP-*g*-SiO₂_1w of almost same total grafted amount. Thus, this result is caused by the number of functional nanoparticles having nuclei effect. Furthermore, this results suggest that grafted amount of 120PP-*g*-SiO₂ is excess amount for crystallization rate. However, this idea doesn't correspond to the characterization of mechanical properties.

To analyze the mechanical properties of samples, tensile test is investigated using dumbbell specimen. As a result, stress-strain curves in **Figure 5** were compared with respect to Young's modulus and tensile strength in **Figure 6**. PP-based nanocomposites with PP-*g*-SiO₂ indicated the short elongation at break via structure of the physical cross-linkage. Toughness also looked the decrease. However, in actuality the toughness before the yield stress is higher than pristine PP and PP with unmodified SiO₂. This result indicate the strong interfacial structure via physical cross-linkage between the grafted chain and matrix chain. In Figure 6 a,d), the maximum improvements of Young's modulus and tensile strength were obtained by PP/120PP-*g*-SiO₂_5w, which is the most grafted sample of all samples. In Figure 6 a), the curve of Young's modulus shows a plateau at the level of PP/21PP-*g*-SiO₂_5w.

This curve consider that the reinforcer of Young's modulus differ from grafted chain number, which correlate significantly with dispersion states of fillers.

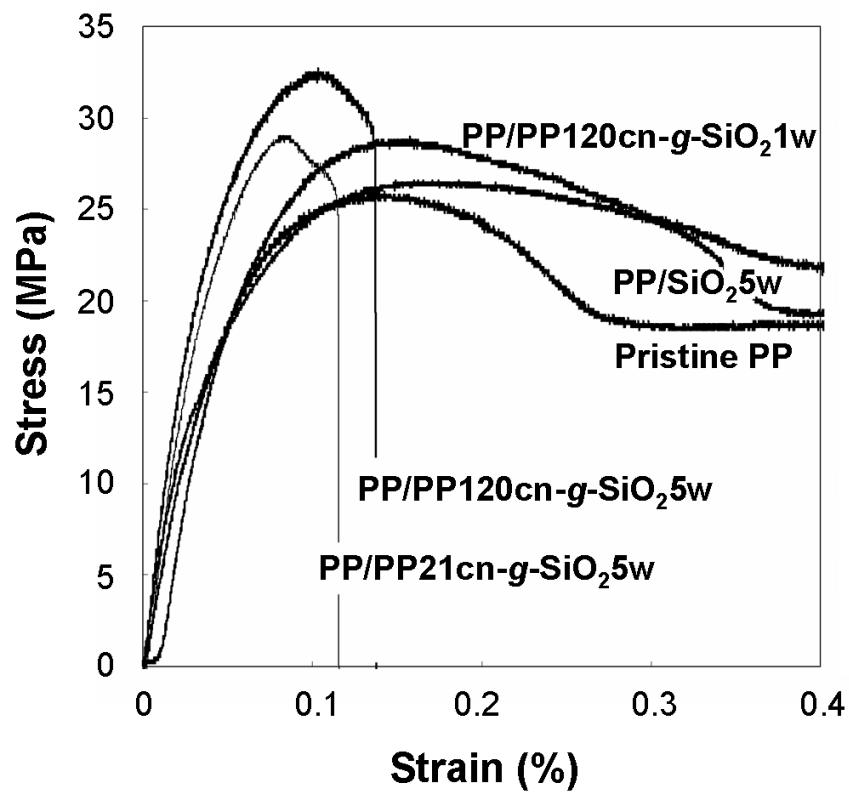


Figure 5. Raw data of tensile test

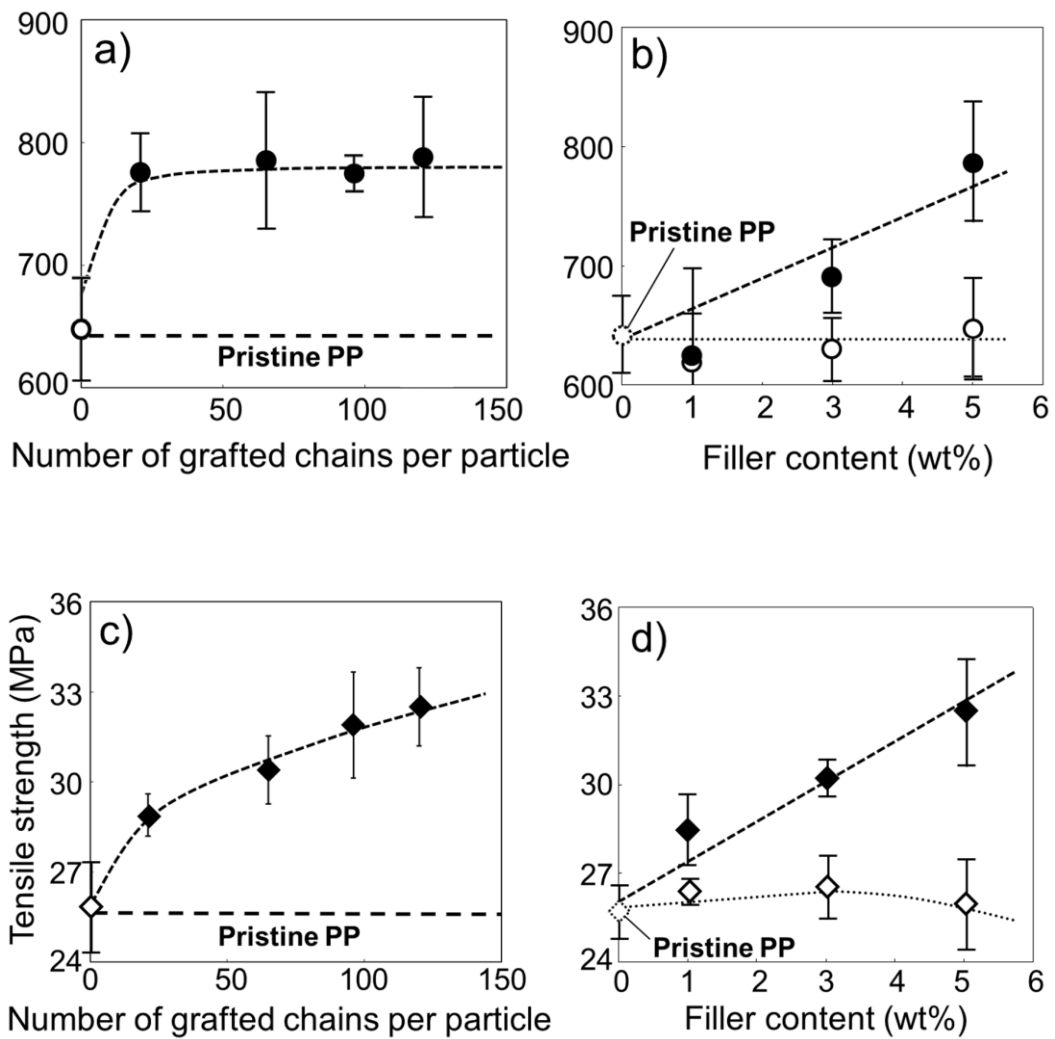


Figure 6. Tensile properties of nanocomposites for a,b) Young's modulus and c,d) tensile strength.

In Figure 6 c,d), tensile strength linearly improves both condition by grafted amount and filler content via simply increase of grafted chain number. This result show that the improvement of tensile strength depend on the density of physical cross-linkage.

3.4. Conclusion

Preparations of various PP-*g*-SiO₂ and PP/PP-*g*-SiO₂ nanocomposites succeeded. PP-*g*-SiO₂ with different grafted amount was prepared by varying the amount of PP-*t*-OH in grafting reaction, which is between the 21-120 chain/particle. The characterizations for PP/PP-*g*-SiO₂ nanocomposites raise a number of intriguing results. In TEM observation, PP/PP-*g*-SiO₂ nanocomposites greatly improve the dispersion states compared with PP/SiO₂ regardless of grafted PP amount on PP-*g*-SiO₂. Various PP-*g*-SiO₂ enhanced the crystallization rate of pristine PP, whose extent was deeply correlated with the grafted PP amounts. The dependence on the graft amount was totally different between the Young's modulus and tensile strength. It was suggested that the dispersion of nanoparticles dominated the Young's modulus. The tensile strength was effectively-improved by increasing the number of grafted PP chains. In the dependence on the filler amount, the Young's modulus and tensile strength were partially linearly improved by increasing the PP-*g*-SiO₂ contents. These results consider that grafted chain number greatly important factor in reinforce of PP-*g*-SiO₂.

Reference:

- [1] Ray, S.S., Okamoto, M., *Prog. Polym. Sci.* **2003**, 28, 1539-1641.
- [2] Choudalak, G., Gotsis, A.D., *Eur. Polym. J.* **2009**, 45, 967-984.
- [3] Lange, L., Wyser, Y., *Package. Technol. Sci.* **2003**, 16, 149-158.
- [4] Ketan, K.M., *Polym. Nanocomp. A Rev.* **2004**, 43, 427-443.
- [5] Usuki, A., Kojima, Y., Kawasumi, M., Okada, A., Fukushima, Y., Kurauchi, T., Kamigaito, O., *J. Mater. Res.* **1993**, 8, 1185-1189.
- [6] Kashiwagi, T., Grulke, E., Hilding, J., Groth, K., Harris, R., Butler, K., Shields, J., Kharchenko, S., Douglas, J., *Polymer* **2004**, 45, 4227-4239.
- [7] Manias, E., Touny, A., Wu, L., Strawhecker, K., Lu, B., Chung, T.C., *Chem. Mater.* **2001**, 13, 3516-3523.
- [8] Liu, Y., Kontopoulou, M., *J. Vinyl. Add. Tech.* **2007**, 13, 147-150.
- [9] Pavlidou, E., Bikiaris, D., Vassiliou, A., Chiotelli, M., Karayannidis, G., *J. Phys.* **2005**, 10, 190-193.
- [10] Zhou, H.J., Rong, M.Z., Zhang, M.Q., Ruan, W.H., Friedrich, K., *Polym. Eng. Sci.* **2007**, 47, 499-509.
- [11] Wu, C.L., Zhang, M.Q., Rong, M.Z., Friedrich, K., *Compos. Sci. Technol.* **2002**, 62, 1327-1340.
- [12] Umemori, M., Taniike, T., Terano, M., *Polym. Bull.* **2013**, 68, 1093-1108.
- [13] Taniike, T., Toyonaga, M., Terano, M., *Polymer* **2014**, 55, 1012-1019.

Chapter 4.

Influences of Mechanical Properties on Polyethylene-based Nanocomposites using Polyethylene-grafted Nanosilica Nanoparticles

4.1. Introduction

Polymer nanocomposites are one of the most successful nanomaterials, where the inclusion of a small amount of nanoparticles in polymer matrices can dramatically improve a variety of properties of the original matrices, such as mechanical strength, thermal stability, gas barrier properties, and so on [1-4]. Moreover, the polymer matrices can equip novel functionalities of nanoparticles such as electric and thermal conductivities through the formation of percolation network [1,5,6]. Enormous efforts have been devoted to apply the great potentials of polymer nanocomposites to polyolefin as the most important synthetic plastic over the world, but these efforts exhibited a number of technical difficulties to design practically useful polyolefin-based nanocomposites. The most serious problem for the polyolefin-based nanocomposites is attributed to the chemical inertness of polyolefin. The apolar C-H and C-C bonds exhibit poor compatibility and interfacial bonding with most of nanoparticles (mainly inorganic), leading to macroscopic agglomeration of nanoparticles as well as scarcely connected boundaries. These problems caused the deterioration of mechanical properties and optical clarity. Moreover, the loosely connected boundaries accelerate the physical loss of stabilizers, thus shortening the lifetime of the polymer [7].

A variety of strategies have been postulated to alleviate these problems, and thus to develop improved nanocomposites. The most traditional strategy is the addition of a compatibilizer such as maleic anhydride-grafted polyolefin, where side functional groups wrap nanoparticles to improve the dispersion in a matrix [8,9]. It has been often combined with organic modification of filler surfaces, typically via short aliphatic alkyl groups, which further improved the compatibility between the matrix and filler

surfaces [10]. One of more recent strategies is *in-situ* formation of nanocomposites: Olefin polymerization is conducted using a catalytic component immobilized in/on a support material, where the generation of polyolefin inside the support material facilitates the disintegration of the material, eventually leading to the dispersion of nanosized building units in the formed matrix [11,12]. The *in-situ* formation of well-dispersed nanoparticles in a polyolefin matrix is also possible by chemically converting a metal oxide precursor (such as metal alkoxide) into metal oxide during melt-mixing with polyolefin. Recently, we [13] and other laboratories [14-16] have reported a strategy to synthesize novel polyolefin-based nanocomposites by combining impregnation of a precursor into a reactor powder of polyolefin and subsequently converting it into metal oxide or hydroxide during melt-mixing. These *in-situ* methods are generally suitable for the formation of percolation network at a small filler content. For improving the interfacial connection, the polymer grafting is the most promising strategy: Polymer chains that are grafted to nanoparticles entangle/inter-diffuse with a matrix, resulting in not only good dispersion but also strong interfacial bonding.

Recently, we have firstly reported the synthesis of polypropylene (PP)-grafted SiO₂ nanoparticles (PP-*g*-SiO₂) by reacting terminally hydroxylated PP (PP-*t*-OH) with surface silanol groups of SiO₂ and their application to PP-based nanocomposites [17,18]. The developed PP-based nanocomposites exhibited a wide variety of advantages not only over pristine PP and nanocomposites with unmodified SiO₂ nanoparticles but also over ever-reported PP/SiO₂ nanocomposites. In concrete, PP-*g*-SiO₂ was nicely dispersed in the PP matrix up to 10 wt%, and accelerated the crystallization rate by 300-400% as compared with pristine PP. Moreover, the tensile properties such as the Young's modulus and tensile strength were dramatically improved (*ca.* +30% over

pristine PP) at 5.0 wt% of PP-*g*-SiO₂. Such dramatic improvements had not been reported for PP-based nanocomposites with spherical SiO₂ nanoparticles. By changing the molecular weight and the amount of the grafted chains, we have concluded that the grafted PP chains co-crystallized with the matrix PP and reinforced the matrix as a physical cross-linker (**Figure 1**).

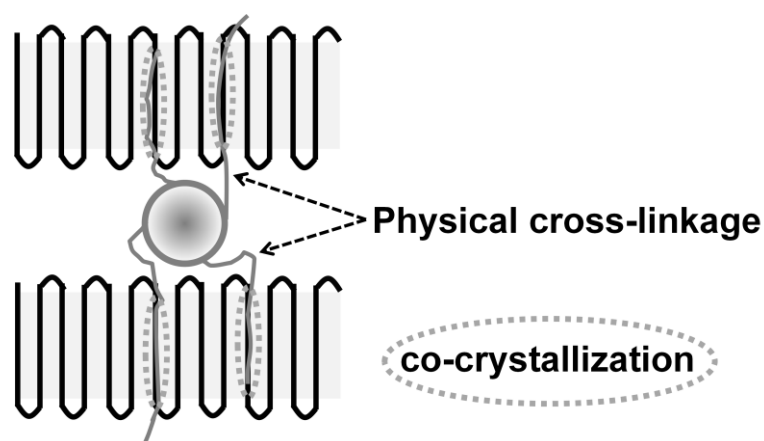


Figure 1. Schematic image of a physical cross-linkage structure for PP/PP-*g*-SiO₂

In the present contribution, the same strategy was applied to polyethylene (PE) nanocomposites with SiO₂ nanoparticles not only to develop improved PE-based nanocomposites but also to understand mechanistic aspects of reinforcements by the addition of PE-*g*-SiO₂ in a comparative way to the PP/PP-*g*-SiO₂ nanocomposites.

4.2. Experimental

4.2.1. Materials

High-density PE pellets with the following characteristics were employed as a matrix for nanocomposites: $M_n = 1.48 \times 10^4$, MWD = 3.98, MFR = 1.2 g/10 min, and $T_m = 137^\circ\text{C}$. Ethylene gas of research grade was donated by Asahi Kasei Chemicals Corporation and Sumitomo Chemical Co., Ltd. *rac*-Ethylenebis(1-indenyl)zirconium dichloride (EBIZrCl₂) was purchased from Kanto Chemical Co., Inc. Triethylaluminum (TEA) and modified methylaluminoxane (MMAO) were kindly donated by Tosoh Finechem Corporation. Toluene and *n*-tetradecane were dried over molecular sieve 4A followed by N₂ bubbling. SiO₂ nanoparticles with an average diameter of 26 nm and a surface area of 110 m²/g were purchased from Kanto Chemical Co., Inc.

4.2.2. Synthesis of PE-*t*-OH

Terminally hydroxylated PE (PE-*t*-OH) was prepared according to literature [18,19]. Briefly, 300 ml of dry toluene (as solvent), 5.0 mmol of MMAO (as an activator), 1.7 μmol of EBIZrCl₂ (as a catalyst) and a specified amount of TEA (as a chain transfer agent) were charged in a stirred flask maintained at 0°C. The ethylene polymerization was conducted at 0°C by supplying 1 atm of ethylene for 1 h. Thereafter, the obtained product was reacted with hydrogen peroxide under oxygen atmosphere at the same temperature for 1 h. Thus obtained PE-*t*-OH was purified by repetitive washing with acidic ethanol and subsequent vacuum drying.

4.2.3. Synthesis of PE-g-SiO₂

PE-*t*-OH was grafted onto SiO₂ nanoparticles via dehydration between the terminal hydroxyl groups of PE-*t*-OH and surface silanol groups of SiO₂. A specified amount of PE-*t*-OH (0.5 chain per surface silanol group) and 0.5 g of SiO₂ nanoparticles (dried at 160°C prior to the grafting) were reacted in tetradecane containing 0.1 mol/L of 6-di-*tert*-butyl-*p*-cresol at 200°C for 6 h. The resultant particles were washed with methanol, and dried in vacuo at 60°C for 6 h. Unreacted polymer was carefully removed with repetitive hot filtration in *o*-dichlorobenzene at 140°C.

4.2.4. Compounding of PE/PE-g-SiO₂ nanocomposites

PE-based nanocomposites were prepared using a two-roll mixer at 20 rpm. 10 g of the PE pellets was preliminarily kneaded at 157°C for 5 min, followed by the addition of a specified amount of unmodified SiO₂ or PE-g-SiO₂ nanoparticles (0-5 wt%). The mixture was further kneaded at 157°C for additional 10 min. The sample sheets with the thickness of 200 μm were prepared by hot press at 190°C and 20 MPa, followed by quenching at room temperature for 5 min. For the sake of comparison, pristine PP, PP/SiO₂ and PP/PP-g-SiO₂ nanocomposites were also prepared, where PP-*t*-OH with M_n of 1.2×10^4 was grafted at the chain density of 120 chain/particle. Details on the synthesis and characteristics can be found in our previous report [18].

4.2.5. Analyses

^{13}C -NMR spectra were recorded on a Bruker 400 MHz NMR spectrometer operating at 100 MHz with proton decoupling at 120°C using hexachloro-1,3-butadiene as a diluent and 1,1,2,2-tetrachloroethane- d_2 as an internal lock and reference [18].

Figure 2 shows a ^{13}C -NMR spectrum for a PE- t -OH sample. The M_n and the end functionalized mole fraction of PE- t -OH were respectively determined by the following equations according to literature [18],

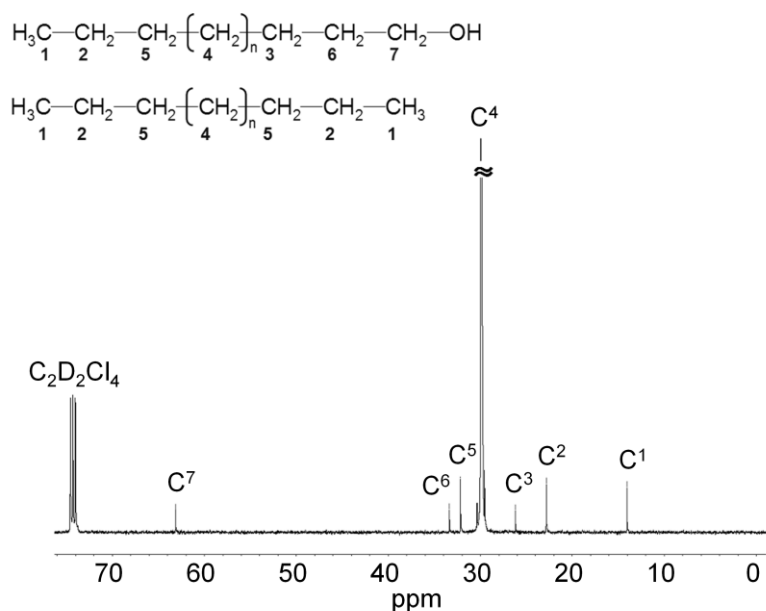


Figure 2. Typical ^{13}C -NMR spectrum of PE- t -OH

$$M_n = \frac{C^1 + C^2 + C^3 + C^4 + C^5 + C^6 + C^7}{C^1 + C^7} \times 28 \quad \text{Eq. (1),}$$

$$\text{End functionalization (mol\%)} = \frac{C^7}{1/2(C^1 + C^7)} \times 100 \quad \text{Eq. (2).}$$

Thermogravimetric analysis (TGA, METTLER TOLEDO TG50) was employed to measure the grafted polymer amounts, where the temperature was kept at 200°C for 30 min to remove physisorbed water, and then increased up to 650°C at 20 °C/min. The grafted amount was estimated from the difference in the weight loss between PE-*g*-SiO₂ and unmodified SiO₂ in the range of 200-650°C. The dispersion of nanoparticles in the matrix was evaluated with transmission electron microscopy (TEM, Hitachi H-7100) operated at 100 kV, using microtomed specimens (Reichert Ultracut S with a FC-S cryoattachment). The crystallization behavior of the nanocomposites was examined using a differential scanning calorimeter (DSC, METTLER TOLEDO DSC 822). A sample in an aluminum pan was heated from room temperature to 180°C at 20 °C/min, then kept at 180°C for 5 min to eliminate the thermal history, and finally cooled down to 124°C at 20 °C/min for the isothermal crystallization experiment [20]. The melting point (T_m) and the crystallinity (X_c) of a sample were determined as the peak-top temperature and the peak area of the endotherm during the first heat cycle, respectively. The sample crystallinity was determined from the endothermic peak area of melting curves using the Hoffman-Weeks extrapolation method. The isothermal crystallization rate (denoted as $t_{1/2}^{-1}$) was defined as an inverse of the half time of the crystallization at 124°C. Tensile properties of the nanocomposites were measured by a tensile tester (Abe Dat-100). A stress-strain curve was acquired at 20°C and at a crosshead speed of 1.0 mm/min. At least 5 specimens were tested for each sample.

4.3. Results and Discussion

4.3.1. Synthesis of PE-g-SiO₂

Table 1 summarizes the characteristics of PE-*t*-OH synthesized at two different concentrations of TEA as the chain transfer agent. As the TEA concentration increased, the molecular weight of PE-*t*-OH decreased due to enhanced chain transfer. On the other hand, the end functionalization degree was kept around 70 mol%, plausibly due to incomplete oxidation of PE-*t*-Al bonds by hydrogen peroxide [18,19]. The obtained two PE-*t*-OH samples with different M_n values were termed as PEM_n-*t*-OH and employed for grafting. Note that M_n of 8.0×10^3 for PE8000-*t*-OH and M_n of 1.2×10^4 for PP-*t*-OH have similar polymerization degrees.

Table 1. Characteristics of synthesized PE-*t*-OH

Sample	TEA concentration (mmol/L)	M_n [a]	End functionalization (mol%) [a]
PE3000- <i>t</i> -OH	200	3.0×10^3	73
PE8000- <i>t</i> -OH	50	8.0×10^3	71
PP- <i>t</i> -OH [b]	100	1.2×10^4	73

[a] Determined with ¹³C-NMR; [b] Taken from literature [18] or Chapter 2.

The results of the grafting are summarized in **Table 2**. Similarly to the grafting of PP-*t*-OH with different M_n [18], the grafted amount of PE-*t*-OH was rather insensitive to the M_n value, becoming 9-10 wt%. This is explained by the restricted diffusion of PE-*t*-OH, where the grafting of PE-*t*-OH made the diffusion of PE-*t*-OH onto the surfaces of nanoparticles more and more difficult. Consequently, the chain number per particle became almost anti-proportional to the M_n value.

Table 2. Amounts of PE-*t*-OH grafted to SiO₂ nanoparticles

Sample	Grafted amount	Grafted chain number
	(wt%) [a]	(chain/particle) [b]
PE3000- <i>g</i> -SiO ₂	9.1	390
PE8000- <i>g</i> -SiO ₂	10.0	160
PP- <i>g</i> -SiO ₂ [c]	11.4	120

[a] Determined with TGA; [b] The chain number per particle was estimated by using the specific surface area and the diameter of SiO₂ nanoparticles as well as M_n of grafted PE chains; [c] Taken from literature [18] or Chapter 2.

4.3.2. Properties of PE/PE-*g*-SiO₂ nanocomposites

Employing the synthesized PE-*g*-SiO₂ samples, PE-based nanocomposites were prepared at the filler content of 1-5 wt%. **Figure 3** compares the dispersion of SiO₂ nanoparticles with and without the grafted PE chains. As is usual for unmodified nanoparticles, SiO₂ nanoparticles formed micron-sized agglomerates due to poor chemical compatibility with the PE matrix. On the contrary, the grafted PE chains

dramatically improved the dispersion of SiO₂ nanoparticles, where most of nanoparticles were dispersed in an isolated manner. The grafted chains not only improved the compatibility with the matrix but also reduced the cohesive interaction among nanoparticles.

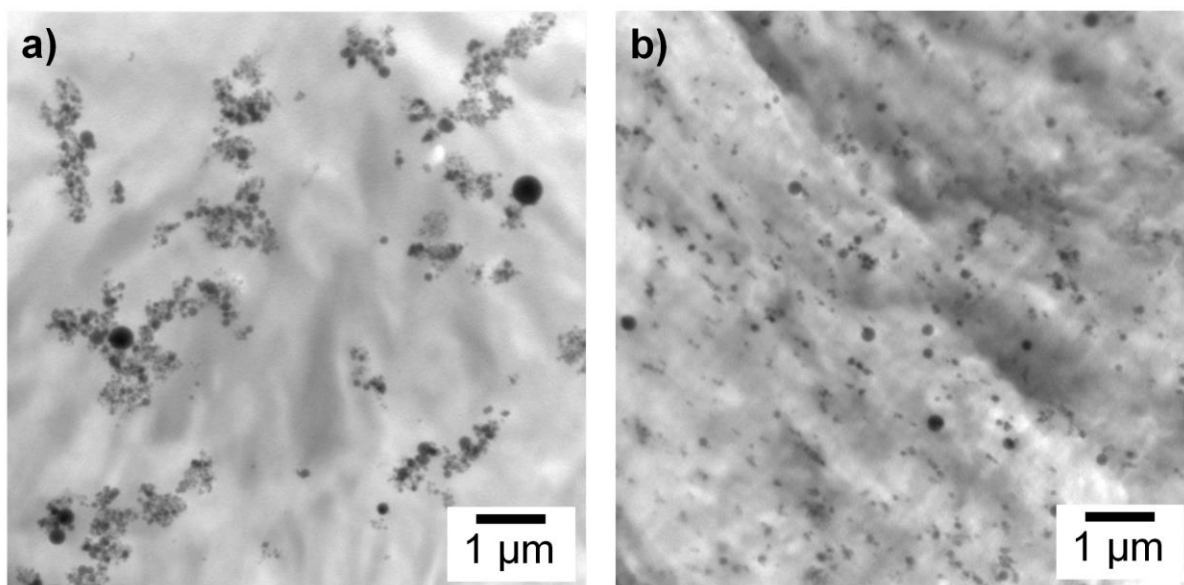


Figure 3. TEM images of a) PE/SiO₂ and b) PE/PE3000-*g*-SiO₂ nanocomposites at 5.0 wt% of the filler content

The melting point and the crystallinity of sample films as well as the isothermal crystallization rate are summarized in **Table 3** and **Figure 4**. Both the SiO₂ content and the polymer grafting hardly affected the melting point and the crystallinity. However, the isothermal crystallization was pronouncedly affected by these parameters. The addition of unmodified SiO₂ nanoparticles tended to accelerate the isothermal crystallization.

Table 3. DSC results

Sample	T_m (°C) [a]	X_c (%) [b]	$t_{1/2}^{-1}$ ($10^2/s$) [c]
Pristine PE	135	71	0.65
PE/SiO ₂ (1.0 wt%)	133	69	1.19
PE/SiO ₂ (3.0 wt%)	134	69	1.04
PE/SiO ₂ (5.0 wt%)	132	70	1.33
PE/PE3000- <i>g</i> -SiO ₂ (1.0 wt%)	135	73	1.41
PE/PE3000- <i>g</i> -SiO ₂ (3.0 wt%)	135	73	1.77
PE/PE3000- <i>g</i> -SiO ₂ (5.0 wt%)	134	70	2.08
PE/PE8000- <i>g</i> -SiO ₂ (1.0 wt%)	135	72	1.40
PE/PE8000- <i>g</i> -SiO ₂ (5.0 wt%)	134	73	1.97
Pristine PP [d]	163	50	0.46
PP/SiO ₂ (5.0 wt%) [d]	162	47	0.51
PP/PP- <i>g</i> -SiO ₂ (5.0 wt%) [d]	160	51	1.70

[a] T_m : peak melting temperature; [b] X_c : crystallinity; [c] $t_{1/2}^{-1}$: half time of isothermal crystallization at 124°C; [d] Taken from literature [18] or Chapter 2.

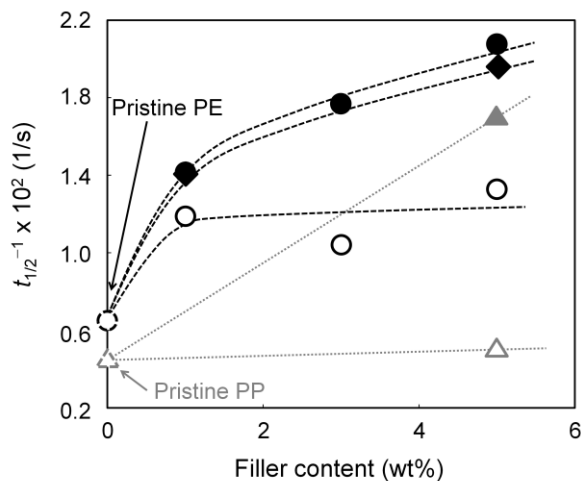


Figure 4. Isothermal crystallization rate at 124°C: (○) PE/SiO₂, (●) PE/PE3000-g-SiO₂, (◆)PE/PE8000-g-SiO₂, (△) PP/SiO₂, and (▲) PP/PP-g-SiO₂

It was reported that even unmodified SiO₂ nanoparticles can reduce the activation energy of the nucleation in the crystallization of PE, unlikely for PP [21]. The polymer grafting further enhanced the nucleation effect, where the observed crystallization rate reached at maximum *ca.* 300% compared with that of pristine PE. In our previous research for PP-g-SiO₂, the nucleation effect was found to increase in a convergent manner in terms of the chain density. In this sense, the marginal difference between PE3000-g-SiO₂ (390 chain/particle) and PE8000-g-SiO₂ (160 chain/particle) in the crystallization rate was attributed to the excess chain density, where the influence of the chain density was saturated.

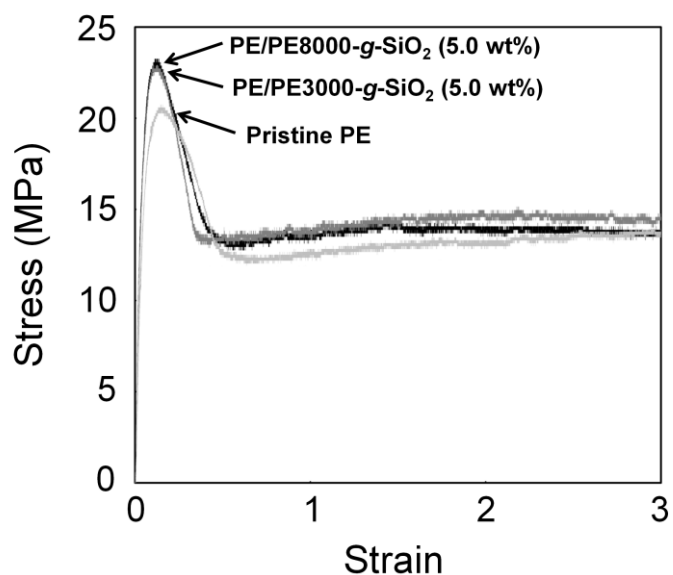


Figure 5. Stress-strain curves for PE/PE-*g*-SiO₂ nanocomposites

Uniaxial tensile measurements were performed for all the samples. **Figure 5** illustrates raw stress-strain curves for selected samples: Stress-strain curves for pristine PE and PE/PE-*g*-SiO₂ nanocomposites were basically similar but the stress at a given strain became always higher for the nanocomposites. Note that all the samples could be elongated over the machinery limitation of 300% strain. The average of five independent measurements for each sample is summarized in **Table 4** and **Figures 6,7**.

Table 4. Results of tensile tests

Sample	Young's modulus (MPa)	Tensile strength (MPa)
Pristine PE	464 ± 46	20.7 ± 1.1
PE/SiO ₂ (1.0 wt%)	450 ± 75	20.8 ± 1.4
PE/SiO ₂ (3.0 wt%)	467 ± 45	20.4 ± 1.2
PE/SiO ₂ (5.0 wt%)	496 ± 35	19.3 ± 1.4
PE/PE3000- <i>g</i> -SiO ₂ (1.0 wt%)	494 ± 12	21.9 ± 1.2
PE/PE3000- <i>g</i> -SiO ₂ (3.0 wt%)	510 ± 12	21.7 ± 1.0
PE/PE3000- <i>g</i> -SiO ₂ (5.0 wt%)	576 ± 26	22.7 ± 1.4
PE/PE8000- <i>g</i> -SiO ₂ (1.0 wt%)	562 ± 46	22.1 ± 0.8
PE/PE8000- <i>g</i> -SiO ₂ (5.0 wt%)	574 ± 57	23.0 ± 2.0
Pristine PP [a]	641 ± 31	25.6 ± 1.0
PP/SiO ₂ (5.0 wt%) [a]	648 ± 39	25.9 ± 1.2
PP/PP- <i>g</i> -SiO ₂ (5.0 wt%) [a]	787 ± 48	32.5 ± 1.3

[a] Taken from literature [18].

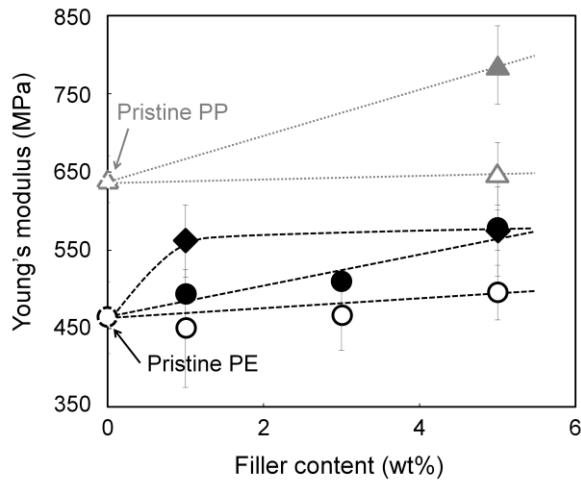


Figure 6. Reinforcement of the Young's modulus: (○) PE/SiO₂, (●) PE/PE3000-g-SiO₂, (◆) PE/PE8000-g-SiO₂, (△) PP/SiO₂, and (▲) PP/PP-g-SiO₂

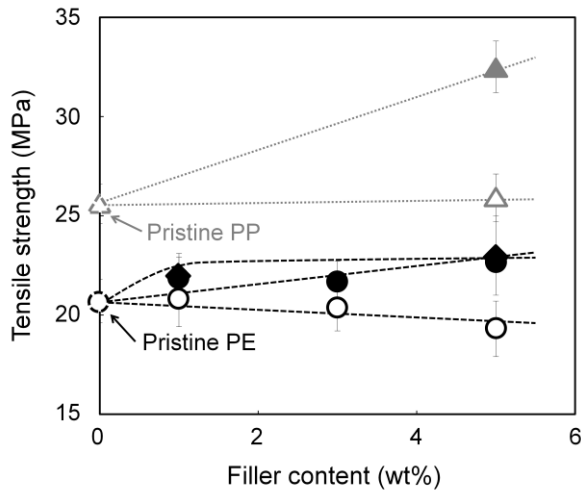


Figure 7. Reinforcement of the tensile strength: (○) PE/SiO₂, (●) PE/PE3000-g-SiO₂, (◆) PE/PE8000-g-SiO₂, (△) PP/SiO₂, and (▲) PP/PP-g-SiO₂

Similarly to the PP/SiO₂ nanocomposites [18], the addition of unmodified SiO₂ nanoparticles hardly improved or even reduced the Young's modulus and tensile strength, due to poor dispersion (Figure 3) and interfacial bonding. On the contrary,

the addition of PE-*g*-SiO₂ markedly improved the tensile properties. Especially, 5.0 wt% of PE8000-*t*-SiO₂ led to the reinforcements of 23% for the Young's modulus and 11% for the tensile strength as compared with pristine PE. These reinforcements were attributed to good dispersion of the nanoparticles and strong interfacial bonding through entanglement and/or co-crystallization. The influences of the molecular weight of the grafted chains were rather unclear: The tensile strength was not sensitive to the molecular weight, while the Young's modulus showed a positive influence of the molecular weight only at a small filler content. This result was somehow very different from that for PP/PP-*g*-SiO₂, where the molecular weight greatly affected the tensile strength through the extent of cross-linkage, while the Young's modulus was only dependent on the dispersion of the nanoparticles. These results suggest possible difference of the design concepts between PP- and PE-based nanocomposites, especially for reinforcements. For PP/PP-*g*-SiO₂ nanocomposites, it was previously concluded that the physical cross-linkage via co-crystallization between the grafted and matrix chains was the main source of the anomalous tensile reinforcement (*ca.* +30% over pristine PP), where longer grafted chains caused the increment in the cross-linkage degree and consequently resulted in greater tensile reinforcement. To be important, the tensile reinforcement always accompanied great reduction in the toughness and elongation at break, since the cross-linkage made the nanoparticles immobile along the deformation. As for PE/PE-*g*-SiO₂ nanocomposites, neither anomalous tensile reinforcements nor sacrificed toughness were observed. These considerations let us conclude that the cross-linkage through the grafted chains for PE/PE-*g*-SiO₂ was not as beneficial as that for PP/PP-*g*-SiO₂ nanocomposites. This fact is probably attributed to both/either much higher crystallinity and/or crystallization rate of PE compared with PP.

4.4. Conclusions

Polyethylene (PE)-based nanocomposites were developed by adding PE-grafted SiO₂ (PE-*g*-SiO₂) nanoparticles, which were prepared by grafting terminally hydroxylated PE (PE-*t*-OH). PE-*t*-OH samples with different molecular weights (3.0×10^3 and 8.0×10^3 in M_n) were prepared in metallocene-catalyzed ethylene polymerization using triethylaluminum as a chain transfer agent. The amount of PE-*t*-OH grafted to SiO₂ nanoparticles was insensitive to the M_n value, becoming around 9-11 wt%. PE/PE-*g*-SiO₂ nanocomposites were prepared by melt-mixing, where 1-5 wt% of PE-*g*-SiO₂ nanoparticles were added. The addition of PE-*g*-SiO₂ markedly improved the dispersion of the nanoparticles in the matrix and accelerated the crystallization. The addition of 5.0 wt% of PE-*g*-SiO₂ led to increments of the Young's modulus and tensile strength over pristine PE by 23% and 11%, respectively, while the addition of unmodified SiO₂ hardly improved these properties. The reinforcing mechanism in PE/PE-*g*-SiO₂ nanocomposites was discussed by comparing the obtained results with our previous results on PP/PP-*g*-SiO₂ nanocomposites. It was suggested that the physical cross-linkage effect on the tensile reinforcements was less pronounced for PE/PE-*g*-SiO₂ compared with PP/PP-*g*-SiO₂. Nonetheless, the PE grafting, which improved the dispersion, the crystallization and the tensile properties, is regarded as an effective strategy to design improved PE-based nanocomposites.

Reference:

- [1] Ray, S.S., Okamoto, M., *Prog. Polym. Sci.* **2003**, *28*, 1539-1641.
- [2] Choudalakk, G., Gotsis, A.D., *Eur. Polym. J.* **2009**, *45*, 967-984.
- [3] Kashiwagi, T., Grulke, E., Hilding, J., Groth, K., Harris, R., Butler, K., Shields, J., Kharchenko, S., Douglas, J., *Polymer* **2004**, *45*, 4227-4239.
- [4] Hussain, F., Hojjati, M., Okamoto, M., Gorga, R.E., *J. Comp. Mater.* **2006**, *40*, 1511.
- [5] Jang, B.Z., Zhamu A., *J. Mater. Sci.*, **2008**, *43*, 5092.
- [6] Biswas, M., Ray, S.S., *Adv. Polym. Sci.* **2001**, *155*, 167.
- [7] Taniike, T., Umemori, M., Chiba, H., Terano, M., *J. Mater. Life Soc.* **2012**, *24*, 102.
- [8] Pöllänen, M., Pelz, U., Suvanto, M., Pakkanen, T.T., *J. Appl. Polym. Sci.* **2010**, *116*, 1218.
- [9] Pavlidou, E., Bikiaris, D., Vassiliou, A., Chiotelli, M., Karayannidis, G., *J. Phys.* **2005**, *10*, 190.
- [10] Liu, Y., Kontopoulou, M., *J. Vinyl. Add. Tech.*, **2007**, *13*, 147.
- [11] Junfeng, R., Zhenhua, J., Hangquan, L., Miao, S., *Macromol. Rapid Comm.* **2001**, *22*, 329.
- [12] Scharlach, K., Kaminsky, W., *Macromol. Symp.* **2008**, *261*, 10.
- [13] Takeuchi, K., Terano, T., Taniike, T., *Polymer* **2014**, *55*, 1940-1947.
- [14] Fritz, H., Emerson, M.G., Roberto, M.T., Daniel, A.B., *J. Electro. Chem.*, **2002**, *536*, 37.
- [15] Karim, D., Celso, V.S., Sandra, H. P., *J. Phys. Chem. B* **1999**, *103*, 4937.
- [16] Wang, Z.M., Nakajima, H., Manias, E., Chung, T.C., *Macromolecules* **2003**, *36*, 8919.
- [17] Umemori, M., Taniike, T., Terano, M., *Polym. Bull.* **2013**, *68*, 1093.
- [18] Taniike, T., Toyonaga, M., Terano, M., *Polymer* **2014**, *55*, 1012-1019.
- [19] Chul, J.H., Mong, S.L., Doo-J.B., Sang, Y.K., *Macromolecules* **2002**, *35*, 8923
- [20] Krumme, A., Lehtinen, A., Viikna, A., *Eur. Polym. J.* **2004**, *40*, 359.
- [21] Qian, J., He, P., *J. Mater. Sci.* **2003**, *38*, 2299.

Chapter 5.

The Development of

High-Performance and Practical Nanocomposites using

***In-Situ* Polypropylene Grafting Reaction**

5.1. Introduction

Polymer nanocomposites are promising materials, in which a small fraction of nanoparticles dispersed in polymer matrices not only induces drastic reinforcements but also enhances functionalities such as conductivity and gas barrier properties. Compared with micro-sized particles, nanoparticles dispersed in polymer give much larger interfacial areas to enable effective load transfer from a matrix to hard particles, and also have much greater particle number densities (i.e. short particle-particle distances) sufficient to interfere with polymer relaxation and to greatly diminish a percolation threshold.

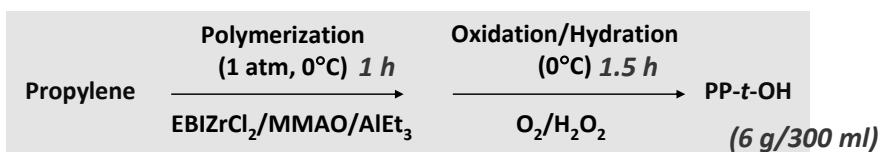
Polypropylene (PP) is one of the most widely used plastics, characterized by a wide range of advantages such as low cost, light weight, high melting temperature, good processability, balanced mechanical properties, low environmental load and so on. PP-based nanocomposites have attracted great attention in order to further expand its versatility and to explore a new specialty. However, fabrication of industrially valuable PP-based nanocomposites is extremely challenging owing to the extreme inertness of PP against inorganic nanoparticles, in contrast to other polymers containing polar functional groups. In most cases, nanoparticles do not disperse well in PP but make large and compact aggregates, significantly diminishing reinforcement and even negatively affecting transparency and ductility. The most versatile strategies to remedy the poor dispersion of nanoparticles are to add a compatibilizer, typically side-functionalized PP such as maleic anhydride-grafted PP (MAPP) and to chemically modify particle surfaces by short aliphatic alkyl chains, for example, using ternary ammonium salts or silane coupling agents. In recent years, more sophisticated routes

have been developed to facilitate not only good dispersion of nanoparticles but also either polymer-filler interaction or filler-filler networking. For example, an in-situ method enables complete exfoliation of layered fillers through the polymer growth / formation inside gallery spaces [1,2]. In a sol-gel approach, metal alkoxide precursor blended or impregnated in molten or solid PP is subjected to the sol-gel reaction to generate nano-sized inorganic oxide particles [3,4]. Polymer grafting is a potentially versatile and scalable approach due to the direct applicability to the conventional melt mixing process, which aims at not only improved dispersion through organic modification and steric prevention of filler agglomeration but also better interfacial connection through interdiffusion and entanglement between grafted and matrix polymer chains [5-7]. Though all of these approaches have greatly refined the design of PP-based nanocomposites, further advances are essential to realize practically acceptable improvements over existing PP-based materials.

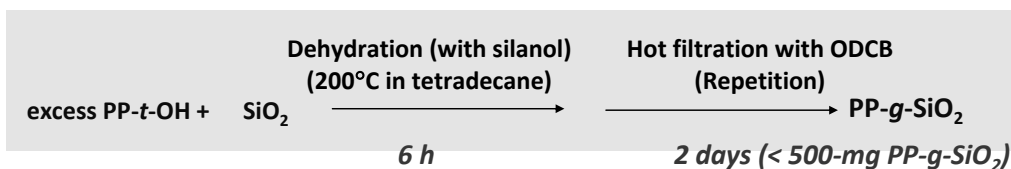
Recently, we have firstly synthesized PP-grafted SiO₂ nanoparticles (PP-*g*-SiO₂) using terminally hydroxylated PP (PP-*t*-OH), and clarified promising advantages of PP/PP-*g*-SiO₂ nanocomposites such as [8]: In tensile properties, dramatic improvement of tensile strength achieves the world-record reinforcements from the physical cross-linkage via grafted PP chains. In dispersion state, PP-*g*-SiO₂ nanoparticles provide high dispersion up to 5.0 wt% of filler content. The crystallization rate of PP/PP-*g*-SiO₂ nanocomposites improves up to 300-400% compared with pristine PP by the smaller mobility of grafted PP chain. The melt viscoelasticity of PP/PP-*g*-SiO₂ indicates good processability similar to pristine PP.

The purpose of **Chapter 5** tries to establish a new cost- and time-efficient synthetic route for PP-grafted filler, aiming at scalable manufacturing of PP-based nanocomposites. The original synthetic route (**Scheme 1**) involved i) metallocene-catalyzed polymerization at a low-yield condition to maintain a high end-functionalization ratio, ii) grafting poorly reactive PP-*t*-OH onto SiO₂ that required an excess amount of PP-*t*-OH, and iii) repetitive hot filtration for 2 days to remove ungrafted PP-*t*-OH, where the inclusion of metallocene-catalyzed PP was expected to deteriorate the physical properties of the nanocomposites.

1. OH-terminated isotactic PP (PP-*t*-OH)



2. PP-grafted SiO₂



3. Melt-mixing with matrix

Scheme 1. Synthetic route for PP/PP-*g*-SiO₂ nanocomposites

The best synthetic route consider to the start from Ziegler-Natta-catalyzed PP with terminal double bonds (PP-*t*-DB) introduced via a visbreaking process. The usage of the Ziegler-Natta-catalyzed PP is expected to eliminate the necessity of the most demanding hot filtration process, while it is necessary to convert less reactive DBs to highly reactive one. The connecting method from PP-terminal vinylidene group (*t*-VD) to SiO₂ selects to the silane coupling agent using hydrosilylation reaction.

Integrated PP-*t*-Si(OEt)₃ can expect the easy grafting to SiO₂ in the reactive matrix polymer blending.

5.2. Experimental

5.2.1. Materials

PP pellet for the matrix polymer ($M_n = 4.6 \times 10^4$, MWD = 5.65, *mmmm* = 98 mol%) was donated by Japan Polypropylene Corporation. Nano SiO₂ (average diameter = 26 nm, surface area = 110 m²/g) was purchased from Kanto Chemical Co., Inc. Two kinds of PP-*t*-DB samples (PPV1 and PPV2) were prepared by visbreaking process from pristine PP. Triethoxysilane (TES) and Platinum(0)-1,3-divinyl-1,1,3,3-tetramethyldisiloxane, known as the Karstedt catalyst for hydrosilylation, were used as delivered under nitrogen atmosphere.

5.2.2. Hydrosilylation reaction

In order to rapidly screen plausible post-modification reactions for PP-*t*-DB, we employed a high-throughput (HTP) microwave system, which can automatically execute at maximum 72 reactions according to a pre-defined protocol with the aid of a robotic arm for sample handling (**Figure 1**). The microwave-assisted heating can greatly enhance reaction rates through the acceleration of molecular motion and vibration, thus enabling much shorter reaction time.

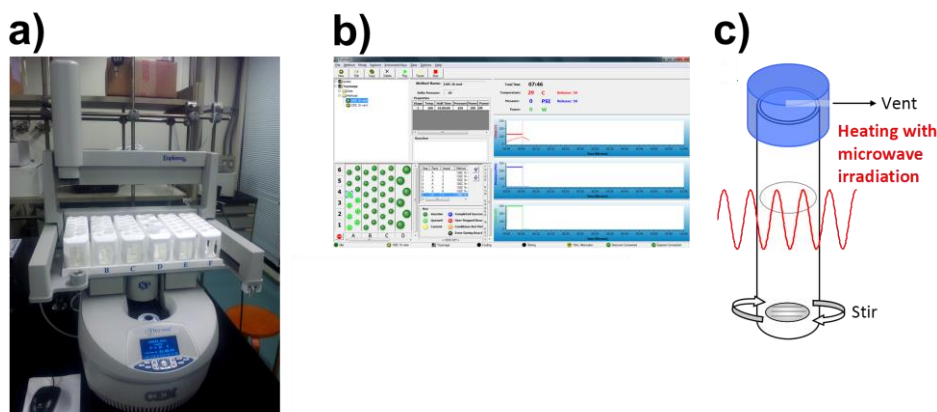


Figure 1. HTP microwave instrument of a) photograph, b) control monitors by personal computer, and c) synthesis image of microwave irradiation

Hydrosilylation reactions were conducted as follows:

- i) 1.25 g of PP-*t*-DB, 12 ml of dehydrated solvent, specified amounts of TES and the Karstedt catalyst were charged in a 10 ml vial and sealed with a septum cap under nitrogen atmosphere. In some cases, 500 mg of SiO₂ was also added to examine the possibility of one-pot “modification and grafting” (these samples are hereafter termed as PP-*g*-inSiO₂)
- ii) The mixture was heated under microwave irradiation to desired temperature and kept for 1 or 3 h.
- iii) Thus obtained product was repeatedly washed with dehydrated toluene, dried in vacuo at 50°C, and stored in an ambient condition to minimize the hydration of silicon alkoxide groups before melt mixing.

5.2.3. Preparation of nanocomposites

Nanocomposites were prepared by melt-mixing using a two-roll mixer at 20 rpm. 10 g of the PP pellet was kneaded at 185°C for 5 min in the presence of 0.3 wt% of AO-50 (a hindered phenol stabilizer), and subsequently melt mixed with 5.0 wt% of unmodified SiO₂ and a specified amount of PP-*t*-Si(OEt)₃ for additional 10 min. Otherwise, PP-*g*-inSiO₂ (which originally contained 12 wt% of PP-*t*-DB and 5.0 wt% of SiO₂) was melt mixed instead of SiO₂ and PP-*t*-Si(OEt)₃. Thus prepared nanocomposites (PP/PP-*g*-(in)SiO₂) were hot-pressed into sample films with the thickness of 200 μm at 230°C and 20 MPa, and then quenched at 100°C.

As references, the PP pellet was also melt mixed either with the corresponding amount of PP-*t*-DB, with 5.0 wt% of unmodified SiO₂, or with 5.0 wt% of mPP-*g*-SiO₂ consisting of 4.5 wt% of SiO₂ and 0.5 wt% of grafted metallocene-catalyzed PP.

5.2.4. Characterizations

¹H-NMR spectra were recorded on a Bruker 400 MHz NMR spectrometer operating at 400 MHz at 120°C using 1,1,2,2-tetrachloroethane-*d*₂ as an internal lock and reference. **Figure 2** shows the ¹H-NMR spectrum of PP-*t*-DB (PPV1), where both of vinyl and vinylidene groups are visible at similar intensities.

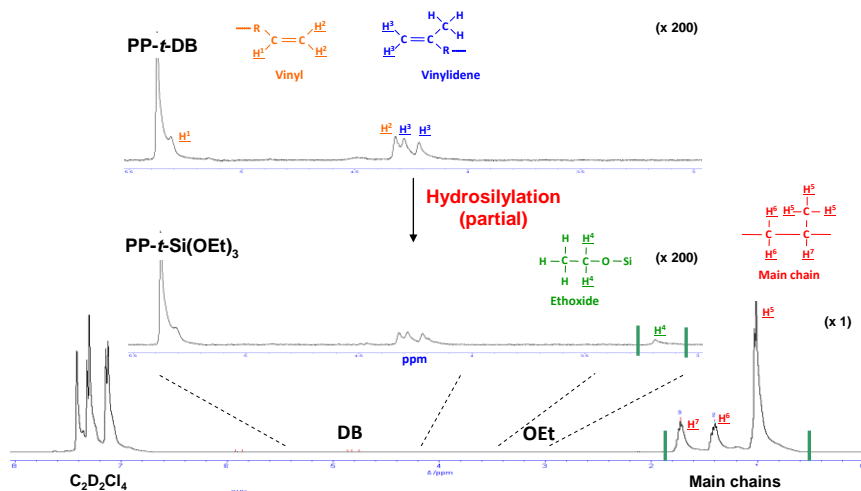


Figure 2. $^1\text{H-NMR}$ spectra of PP-*t*-DB (PPV1) before and after Hydrosilylation

The terminal DB content, estimated according to **Eq. (1)**, was 3.7×10^{-3} mol/mol for PPV1 and 2.2×10^{-3} mol/mol for PPV2.

$$\text{DB content} = \frac{(\underline{\text{H}}^2/2 + \underline{\text{H}}^3/2)}{(\underline{\text{H}}^5/3 + \underline{\text{H}}^6/2 + \underline{\text{H}}^7)/3} \quad \text{Eq. (1).}$$

The presence of the DBs was also detectable by IR spectroscopy in ATR mode, but the absorption intensity was not strong enough for quantitative measurements. The degree of the hydrosilylation was also estimated based on $^1\text{H-NMR}$ (Figure 2) in terms of the reduction in the DB content and the increase in the OEt content defined as,

$$\text{OEt content} = \frac{(\underline{\text{H}}^4/2)/3}{(\underline{\text{H}}^5/3 + \underline{\text{H}}^6/2 + \underline{\text{H}}^7)/3} \quad \text{Eq. (2).}$$

In general, high-temperature NMR measurements have risks for the isomerization of the DBs and the hydration/condensation of the silicone alkoxide groups. Consequently, these contents must be regarded as semi-quantitative or even qualitative values.

The dispersion of SiO₂ nanoparticles in PP was evaluated with transmission electron microscopy (TEM, Hitachi H-7100) operated at 100 kV, using microtomed specimens (Reichert Ultracut S with a FC-S cryoattachment). Differential scanning calorimeter (DSC) measurements were conducted under nitrogen on a Mettler Toledo DSC 822 analyzer. The sample crystallinity was determined with the melting endotherm in the first heat cycle, where the samples were heated to 200°C at 20 °C/min. Isothermal crystallization experiments were also conducted. Samples were kept at 200°C for 5 min to erase a thermal history, and then cooled down to 128°C at a rate of 20 °C/min. A crystallization rate at 128°C was determined as an inverse of the half time of the crystallization (denoted as $t_{1/2}^{-1}$). Tensile properties were determined with an Abe Dat-100 tensile tester using a dumbbell shaped specimen at a crosshead speed of 1 mm/min at room temperature. At least 5 specimens were tested for each sample.

5.3. Results and Discussion

5.3.1. Microwave-assisted hydrosilylation

Screening of hydrosilylation conditions for PP-*t*-DB was conducted using the HTP microwave instrument. The obtained polymer was subsequently analyzed by ¹H-NMR after the purification. The results summarized in **Table 1** uncovered the following items.

- Microwave treatment of PP-*t*-DB in the absence of TES slightly reduced the DB content (Nos. 1,2) probably due to the isomerization into internal DBs during both/either the microwave heating and/or the NMR measurement.
- Further reduction in the DB content occurred when it was reacted with TES, and accompanied an increase in the OEt content. However, the OEt content became much smaller than the reduction in the DB content, suggesting a non-negligible contribution of the above-mentioned isomerization or the sol-gel reaction in the NMR measurement.
- The hydrosilylation slightly progressed even in the absence of the catalyst (Nos. 3,15).
- Neither the increase in the TES amount nor the elongation of the reaction time improved the hydrosilylation degree (Nos. 3-6). It seems that the amount of accessible DBs was limited, even though the vinyl and vinylidene groups were similarly consumed.

- The impact of the catalyst addition on the hydrosilylation degree is significant: it increased the hydrosilylation degree 2-3 times (Nos. 6,7, Nos. 10,11, Nos. 15,16, Nos. 18,19, and Nos. 20,21).
- There was no clear tendency between the hydrosilylation degree and the kind of solvent employed (Nos. 7,11 and Nos. 19,21), while the increase in the reaction temperature appeared to improve the hydrosilylation degree (Nos. 11-13, Nos. 16,17,21). The reaction temperature beyond 180°C produced wax materials, indicative of degradation.
- The hydrosilylation occurred even in the presence of SiO₂ (Nos. 8,9).

In summary, it was concluded that the increase in the reaction temperature and the addition of the catalyst are effective to promote the hydrosilylation of PP-*t*-DB. However, the applicable temperature was restricted due to the degradation. Since the condition of “180°C under nitrogen” is never harsh for usual PP, the main cause is attributed to oxidative species formed on PP-*t*-DB during the visbreaking process.

Hereafter, we have employed samples Nos. 6-9,22 (all hydrosilylated at 130°C) for the preparation of the nanocomposites.

Table 1. Results of microwave-assisted hydrosilylation

No.	PP- <i>t</i> -DB	Solvent ^d	TES (mmol)	Catalyst ^b (μ mol)	SiO ₂ (mg)	Temp. (°C)	Time (h)	DB cont. ^c (mol/mol)	OEt cont. ^c (mol/mol)
1		n/a	n/a	n/a	n/a	n/a	n/a	3.7×10^{-3}	0.0
2		ODCB	n/a	n/a	n/a	130	3	3.4×10^{-3}	0.0
3		ODCB	13.5	n/a	n/a	130	1	3.2×10^{-3}	1.1×10^{-4}
4		ODCB	67.5	n/a	n/a	130	1	3.1×10^{-3}	9.7×10^{-5}
5		ODCB	67.5	n/a	n/a	130	3	3.1×10^{-3}	1.1×10^{-4}
6		ODCB	67.5	n/a	n/a	130	3	3.1×10^{-3}	1.0×10^{-4}
7	PPV1	ODCB	67.5	1.0	n/a	130	3	2.4×10^{-3}	3.4×10^{-4}
8		ODCB	67.5	n/a	500	130	3	2.9×10^{-3}	1.4×10^{-4}
9		ODCB	67.5	1.0	500	130	3	2.5×10^{-3}	2.6×10^{-4}
10		TCB	67.5	n/a	n/a	130	3	2.8×10^{-3}	8.0×10^{-5}
11		TCB	67.5	1.0	n/a	130	3	2.8×10^{-3}	1.3×10^{-4}
12		TCB	67.5	1.0	n/a	180	1	1.8×10^{-3}	2.4×10^{-4}
13		TCB	67.5	1.0	n/a	180	3	2.7×10^{-3}	2.2×10^{-4}
14		n/a	n/a	n/a	n/a	n/a	n/a	2.2×10^{-3}	0.0
15		XL	13.5	n/a	n/a	100	1	2.0×10^{-3}	3.5×10^{-5}
16		XL	13.5	1.0	n/a	100	1	1.6×10^{-3}	5.8×10^{-5}
17		TD	13.5	1.0	n/a	100	1	1.5×10^{-3}	9.6×10^{-5}
18	PPV2	ODCB	13.5	n/a	n/a	130	1	2.1×10^{-3}	6.3×10^{-5}
19		ODCB	13.5	1.0	n/a	130	1	1.6×10^{-3}	1.1×10^{-4}
20		TCB	13.5	n/a	n/a	130	1	1.8×10^{-3}	7.0×10^{-5}
21		TCB	13.5	1.0	n/a	130	1	1.4×10^{-3}	1.9×10^{-4}

22		TCB	67.5	1.0	n/a	130	3	1.6×10^{-3}	1.6×10^{-4}
----	--	-----	------	-----	-----	-----	---	----------------------	----------------------

^a ODCB: *o*-dichlorobenzene, TCB: trichlorobenzene, XL: xylene, TD: tetradecane.

^b The Karstedt catalyst.

^c Determined by ¹H-NMR based on **Eqs. (1,2)**.

5.4.2. Preparation and evaluation of nanocomposites

Table 2 summarizes the information of the prepared samples. Eight nanocomposites (Nos. 1-8) were prepared by melt mixing the PP pellet either with SiO₂ and hydrosilylated PP-*t*-DB or with PP-*g*-inSiO₂ (*i.e.* SiO₂ added in the hydrosilylation). In parallel, six reference samples (Nos. R1-R6) were prepared. In particular, best result of sample from **Chapter 2** (PP/mPP-*g*-SiO₂) is nominated as reference sample of No. R5. The SiO₂ content was always fixed at 5.0 wt% except for No. R5 that consisted of 95 wt% of the PP pellet and 4.5 wt% of SiO₂ grafted to the remaining 0.5 wt% of metallocene-catalyzed PP. It must be noted that we failed to melt mix hydrosilylated PP-*t*-DB with SiO₂ in the absence of the main PP pellet (for preparing a master batch), where severe degradation was identified irrespective of the mixing conditions.

Table 2. The list of sample prepared in this study and their physical properties^a

No. ^b	Name	PP- <i>t</i> -DB (wt%)	X _c (wt%)	T _m (°C)	$t^{-1/2}$ at 128°C (min ⁻¹)	Young's modulus (MPa)	Tensile strength (MPa)	Elongation at break (%)
R1	PP ^c	0.0	50	163	0.46-0.49	641 ± 32	25.6 ± 0.9	>300
R2	PP/SiO ₂ ^d	0.0	47	162	0.51	648 ± 41	25.9 ± 1.5	>300
R3	PP/PPV1 ^e	12.0	50	158	0.19	526 ± 33	26.9 ± 0.4	>300
R4	PP/PPV2 ^e	12.0	50	162	0.23	540 ± 40	27.0 ± 0.7	>300
R5	PP/mPP- <i>g</i> -SiO ₂ ^f	0.0	53	161	1.20	816 ± 47	33.1 ± 1.3	10±1
R6	PP/PPV1/SiO ₂ ^g	12.0	51	159	0.28	563 ± 34	27.9 ± 0.8	111 ± 70
1 (6)	PP/PPV1- <i>g</i> -SiO ₂	12.0	51	159	0.27	568 ± 18	29.3 ± 0.5	106 ± 52
2 (7)	PP/PPV1- <i>g</i> -SiO ₂ (Pt)	12.0	51	158	0.27	601 ± 70	32.2 ± 0.6	18±4
3 (7)	PP/PPV1- <i>g</i> -SiO ₂ (Pt)	6.0	51	160	0.36	641 ± 43	32.3 ± 0.6	133 ± 100
4 (7)	PP/PPV1- <i>g</i> -SiO ₂ (Pt)	3.0	50	161	0.36	614 ± 8 5	30.4 ± 1.2	>300
5 (7)	PP/PPV1- <i>g</i> -SiO ₂ (Pt)	1.5	51	161	0.38	622 ± 25	30.3 ± 1.1	215 ± 61
6 (8)	PP/PPV1- <i>g</i> -inSiO ₂	12.0	51	159	0.27	587 ± 61	28.5 ± 0.6	25 ± 9
7 (9)	PP/PPV1- <i>g</i> -inSiO ₂ (Pt)	12.0	50	158	0.39	614 ± 36	33.0 ± 0.3	30 ± 10
8 (22)	PP/PPV2- <i>g</i> -SiO ₂ (Pt)	12.0	49	161	0.38	668 ± 33	32.5 ± 1.0	59 ± 10

^a All of the nanocomposites contained 5.0 wt% of SiO₂ if not specified.: ^b The numbers in parentheses correspond to the numbers of hydrosilylated PP-*t*-DB in Table 1.: ^c Pristine PP.: ^d Unmodified SiO₂ was melt mixed.: ^e 12 wt% of PP-*t*-DB was melt mixed without the hydrosilylation process.: ^f 5.0 wt% of mPP-*g*-SiO₂ (4.5 wt% of SiO₂ grafted to 0.5 wt% of metallocene-catalyzed PP) was melt mixed.: ^g 12 wt% of non-hydrosilylated PP-*t*-DB was melt mixed together with unmodified SiO₂.

The dispersion of SiO₂ nanoparticles was observed by TEM (**Figure 3**). As shown in Figure 3a, unmodified SiO₂ did not disperse well in PP to form micro-sized aggregates. The poor dispersion was readily solved when metallocene-catalyzed PP-*t*-OH was grafted to SiO₂ (Figure 3b). In contrast, the addition of PP-*t*-DB hardly improved the poor dispersion of SiO₂ nanoparticles (Figure 3c), indicating that PP-*t*-DB itself does not possess a compatibilizing ability for SiO₂. The impact of the hydrosilylation was significant: Even though PP-*t*-DB hydrosilylated in the absence of the catalyst exhibited a quite small OEt content, its addition dramatically improved the dispersion at a level similar to our best PP/mPP-*g*-SiO₂ sample (Figure 3d). This fact suggested that terminal Si(OEt)₃ groups were *in-situ* grafted to or at least interacted with SiO₂ nanoparticles. The dispersion was not anymore improved when the hydrosilylation degree was enhanced with the catalyst (Figure 3e). This is consistent with our previous finding that good dispersion of SiO₂ is relatively easily attained irrespective of the density of grafted PP chains [8]. The dispersion of PP-*g*-inSiO₂ was slightly worse but an interesting phenomenon was observed (Figure 3f): the addition of PP-*g*-inSiO₂ always accompanied fibrils, which looked to be grown from SiO₂ nanoparticles. Judging from the contrast, the fibrils must be inorganic SiO₂, plausibly formed through microwave-assisted sol-gel reaction of TES (and/or grafted Si(OEt)₃) initiated from surface hydroxyl groups of SiO₂ nanoparticles.

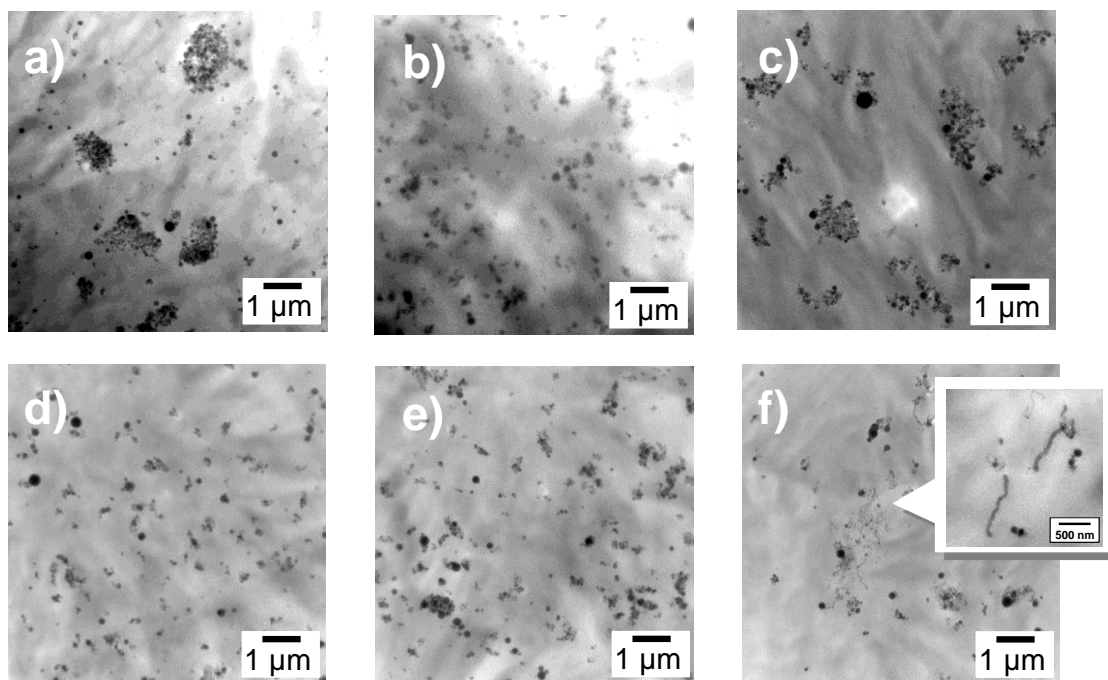


Figure 3. TEM images of nanocomposites: a) PP/SiO₂ as No. R2, b) PP/mPP-*g*-SiO₂ as No. R5, c) PP/PPV1/SiO₂ as No. R6, d) PP/PPV1-*g*-SiO₂ as No. 1, e) PP/PPV1-*g*-SiO₂ (Pt) as No. 2, f) PP/PPV1-*g*-inSiO₂ (Pt) as No. 7

The crystallinity [X_c] and the melting temperature [T_m] were acquired using DSC for each sample film (Table 2). The sample crystallinity was always around 50 wt%, being hardly affected by the composition of the samples. This fact assured that tensile properties could be fairly compared among the different samples. On the one hand, the addition of 12 wt% of PPV1 always reduced the melting temperature by 3-4°C from that of pristine PP (162°C) (see Nos. R3,R6,1,2,6,7). Since the melting temperature of PP is dependent on the lamellar thickness of the crystalline phase, it is plausible that visbroken PP has a reduced isotactic sequence length, and disturbs the growth of the lamellae. The addition of the less visbroken PPV2 did not reduce the melting temperature (Nos. R4,8).

Isothermal crystallization experiments were conducted at 128°C to measure the crystallization rate of each sample as $t^{-1/2}$. The exotherms for selected samples are shown in **Figure 4**. The pristine PP exhibited the exotherm maximum at around 4 min, while that of PP/mPP-g-SiO₂ was shortened to around 2 min. In this way, grafted PP chains with lower mobility greatly accelerate the crystallization. On the other hand, the addition of 12 wt% of non-hydrosilylated PPV1 elongated the exotherm maximum to about 8-9 min: PP-*t*-DB not only restricts the lamellar growth but also decelerates the crystallization. The addition of 5.0 wt% of SiO₂ together with 12 wt% of hydrosilylated PPV1 partially compensated the crystallization deceleration caused by PPV1. This fact suggested that hydrosilylated PP-*t*-DB was *in-situ* grafted to SiO₂ nanoparticles. The other results in Table 2 were all in line with the results explained in Figure 4. As the sole exception, PP/PPV1/SiO₂ (No. R6) showed enhanced crystallization even without the hydrosilylation, *i.e.* believed to be not grafted. It might be possible that some polar groups in original PP-*t*-DB (such as carbonyl groups and DBs) were more or less trapped onto SiO₂ surfaces to be crystallization nuclei.

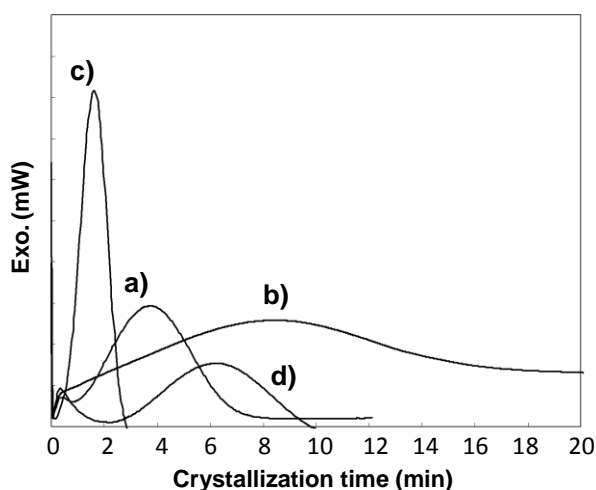


Figure 4. Exotherms during isothermal crystallization at 128°C: a) PP/SiO₂ as No. R2, b) PP/PPV1 as No. R3, c) PP/mPP-g-SiO₂ as No. R5, d) PP/PPV1-g-SiO₂ (Pt) as No. 2

In the end, the uniaxial tensile tests were implemented, where the stress-strain (SS) curves for selected samples are plotted in **Figure 5**. In general, a SS curve of PP shows a linear rise up of the stress along the initial strain (elastic behavior), whose gradient corresponds to the Young's modulus. After the elastic region, the curve once reaches the maximum stress, followed by a necking behavior and the neck development. The maximum stress corresponds to the tensile strength, whose magnitude is related to the density of tie molecules. The addition of 5.0 wt% of mPP-*g*-SiO₂ significantly enhanced both the Young's modulus and tensile strength, while the elongation at break as well as the toughness was greatly sacrificed. Such a tremendous improvement in the tensile strength has never been achieved with spherical nanoparticles, and originated from a cross-linkage effect of PP-grafted SiO₂ [8]. The addition of non-hydrosilylated PPV1 decreased the Young's modulus without affecting the tensile strength, while the necking behavior became less obvious. The latter led to an increment of the toughness. The co-addition of SiO₂ and hydrosilylated PPV1 obviously improved the tensile strength. When the hydrosilylation was conducted in the presence of the catalyst, the improvement became much more pronounced, reaching a level comparable with our best previous PP/mPP-*g*-SiO₂. Moreover, the same sample also exhibited a drastic decrease in the elongation at break. All of these facts let us conclude that a large amount of hydrosilylated PP-*t*-DB (estimated to be around 10 wt%) was successfully *in-situ* grafted to SiO₂ nanoparticles.

Thus obtained characteristic values of the SS curves are summarized in Table 2. The inclusion of non-hydrosilylated PPV2 deteriorated the Young's modulus but less compared with PPV1 (Nos. R3,R4), consistently with their DB contents. The co-addition of SiO₂ and non-hydrosilylated PPV1 only slightly recovered the Young's

modulus and increased the tensile strength, but the degree of the improvements was too small to be regarded as being grafted to SiO₂ (No. R6). By decreasing the amount of hydrosilylated PPV1 at the fixed SiO₂ content, the loss of the Young's modulus could be partially suppressed (Nos. 2-5). At 6.0 wt% of PPV1 (No. 3), the best balance between the Young's modulus and tensile strength was attained, where the Young's modulus was comparable with that of the pristine PP and the tensile strength was enhanced as much as PP/mPP-*g*-SiO₂ could do. The toughness was even better than that for PP/mPP-*g*-SiO₂. Similar properties were obtained when hydrosilylated PPV2 was employed (No. 8). Comparing the results for hydrosilylated PPV1 and PPV2 at the same 12 wt% (Nos. 2,8), it is suggested that the visbreaking strength is an important parameter for the tensile properties of the nanocomposites, and to employ less visbroken PP-*t*-DB must be a way to achieve further improvements.

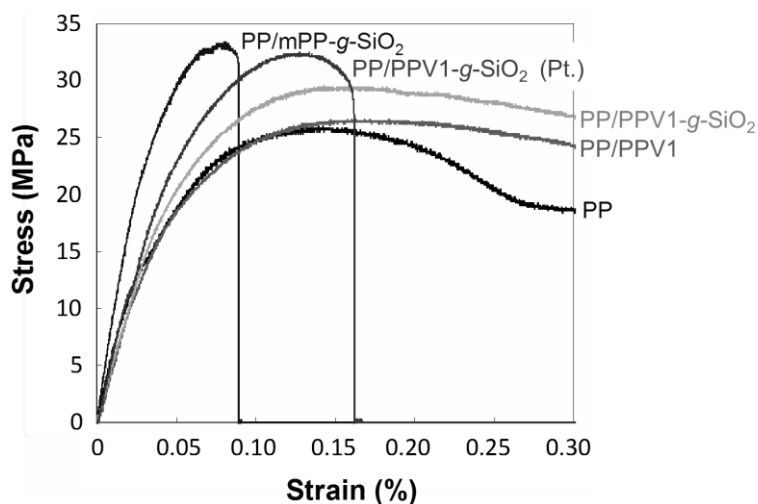


Figure 5. SS curves in tensile tests

5.5. Conclusions

In order to establish a cost- and time-efficient synthetic strategy for PP/PP-*g*-SiO₂ nanocomposites, the hydrosilylation of the terminal double bonds for visbroken PP and *in-situ* grafting of the hydrosilylated PP to SiO₂ nanoparticles were successfully achieved. The resultant nanocomposites were found to endow promising mechanical properties: the highest tensile strength and relatively better toughness. On the other hand, the addition of visbroken PP also brought some disadvantages, such as the ease of thermal degradation, the prevention of the crystallization, and reduced Young's modulus. In particular, the ease of the degradation limited the maximum temperature for the hydrosilylation, which did not allow for us to alleviate the expensive Pt-based catalyst. I suggest that to reduce the visbreaking strength must be the best solution for the said problems.

Reference:

- [1] Kawasumi, M., Hasegawa, N., Kato, M., Usuki, A., Okada, A., *Macromolecules* **1997**, *30*, 6333-6338.
- [2] Pavlidou, E., Bikiaris, D., Vassiliou, A., Chiotelli, M., Karayannidis, G., *J. Phys.* **2005**, *10*, 190-193.
- [3] Wang, Z.M., Nakajima, H., Manias, E., Chung, T.C., *Macromolecules* **2003**, *36*, 8919-8922.
- [4] Brune, D.A., Bicerano, J., *Polymer* **2002**, *43*, 369-387.
- [5] Rong, M.Z., Zhang, M.Q., Pan, S.L., Lehmann, B., Friedrich, K., *Polym. Int.* **2004**, *53*, 176-83.
- [6] Rong, M.Z., Zhang, M.Q., Zheng, Y.X., Zeng, H.M., Walter, R., Friedrich, K., *Polymer* **2001**, *42*, 167-183.
- [7] Wu, C.L., Zhang, M.Q., Rong, M.Z., Friedrich, K., *Compos. Sci. Technol.* **2002**, *62*, 1327-1340.
- [8] Taniike, T., Toyonaga, M., Terano, M., *Polymer*, **2014**, *55*, 1012-1019.

Chapter 6.

General Conclusion

6.1. General summary

In this dissertation, four approaches were explored for improvement of PP-based nanocomposites. In the **Chapter 2**, the terminally hydroxylated polypropylene grafted to SiO₂ nanoparticles (PP-*g*-SiO₂) with various chain lengths ($M_n = 5.6 \times 10^3 \sim 4.6 \times 10^4$) were melt-mixing with PP matrix to prepare a series of PP/PP-*g*-SiO₂ nanocomposites. PP/PP-*g*-SiO₂ offered several advantages over pristine PP and PP/SiO₂ such as highly uniform dispersion up to 5.0 wt%, 300-400% faster isothermal crystallization rate at 128°C, and about 30% increments for both the Young's modulus and the tensile strength without largely sacrificing the melt-viscosity of pristine PP. Chapter 2 concluded that grafted chains act as crystallization nuclei and co-crystallize with matrix chains to make PP-*g*-SiO₂ as a physical cross-linker between lamellae, while the linkage disappears in melt and grafted chains minimize the cohesive attraction between nanoparticles. In the **Chapter 3** reported that the effects of relationship between the number of grafted PP chains and the mechanical properties investigated. Tensile test indicated that the reinforcement of PP-*g*-SiO₂ nanoparticles was more effective than that in conventional unmodified SiO₂ nanoparticles. The result concluded that improvement of tensile strength strongly correlate with the number of grafted PP chains. On the other hand, Young's modulus was strongly related to the dispersion of nanoparticles than the grafted PP chains.

As application of the grafting technology, the **Chapter 4** of polyethylene (PE)-based nanocomposites were developed by adding PE-grafted SiO₂ (PE-*g*-SiO₂) nanoparticles, which were prepared by grafting terminally hydroxylated PE with chain length via M_n value of $3.0 \times 10^3 \sim 8.0 \times 10^3$. The obtained PE/PE-*g*-SiO₂ nanocomposites were

characterized in terms of the nanoparticle dispersion, the crystallization, and the tensile properties in a comparative way to pristine PE, PE/SiO₂ nanocomposites, and Chapter 2 reported PP/PP-*g*-SiO₂ nanocomposites. Similarly to the PP grafting, the PE grafting markedly improved the dispersion of the nanoparticles in the corresponding matrix and accelerated the crystallization. The addition of 5.0 wt% of PE-*g*-SiO₂ led to increments of the Young's modulus and tensile strength over pristine PE by 23% and 11%, respectively, while the addition of SiO₂ hardly improved these tensile properties. The reinforcing mechanism in the PE/PE-*g*-SiO₂ nanocomposites was also discussed. In the **Chapter 5**, in order to establish a cost- and time-efficient synthetic strategy for PP/PP-*g*-SiO₂ nanocomposites, the hydrosilylation of the terminally unsaturated for visbroken PP and *in-situ* grafting of the hydrosilylated PP to SiO₂ nanoparticles were successfully achieved. The resultant nanocomposites were found to endow promising mechanical properties: the highest tensile strength and relatively better toughness. On the other hand, the addition of visbroken PP also brought some disadvantages, such as the ease of thermal degradation, the prevention of the crystallization, and reduced Young's modulus. Especially, the ease of the degradation limited the maximum temperature for the hydrosilylation, which did not allow for us to alleviate the expensive Pt-based catalyst. The Chapter 5 suggests that to reduce the visbreaking strength must be the best solution for the said problems.

The general conclusion is shown in next section (**6.2.**).

6.2. General conclusion

In general conclusion, 4 approaches via the two kinds of studies (**Chapter 2** and **3**) and the two kinds of applications (**Chapter 4** and **5**) succeeded using the polymer-grafting technology.

In recent years, the amount of annual worldwide production of PP as a one of the general plastics has exceeded 60 million tons because of its versatile properties and wide range of applications. Therefore, further expansions of use application are necessary with the objective of substitute and recycle. The nanocomposite technique is the most promising methods for the demand. However, poor adhesion between apolar PP and polar nanofiller causes severe agglomeration of fillers, and results in only marginal improvements. In order to overcome this difficulty, one of the best strategy is to graft PP chains onto the nanoparticle. Grafted PP chains can reinforce the matrix/filler interface through the physical-cross linkage.

In this research, various PP-*g*-SiO₂ nanoparticles on PP-based nanocomposites were prepared by accurate controls from the functionalization condition, grafting reaction condition, and other preparation conditions. The experimental results of PP/PP-*g*-SiO₂ nanocomposites using various PP-*g*-SiO₂ were measured by some instrument such as ¹H- and ¹³C-nuclear magnetic resonance (NMR) analyzer, Thermogravimetric (TG) analyzer, transmission electron microscope (TEM) and scanning electron microscope (SEM) observations, differential scanning calorimetry (DSC) measurement, tensile test, and rheometer instrument.

The details are shown below.

- The synthesis and functionalization of PP-*t*-OH and PE-*t*-OH succeeded using isotactic specific metallocene catalyst and TEA as a chain transfer agent, which could control the M_n between minimum 3.0×10^3 and maximum 4.6×10^4 via TEA concentration. The functionalization rate on chain end was 60-80% approximately by ^{13}C -NMR analysis. In PP-*t*-OH, high M_n more than 4.6×10^4 could not keep the functionalization rate of over 60%.
- PP-*g*-SiO₂ and PE-*g*-SiO₂ using PP(or PE)-*t*-OH and spherical SiO₂ succeeded by grafting-reaction at 200C of 6 h in tetradecane solvent, which could control the grafted amount between 21-120 chain/particle via different *t*-OH amounts.
- The crystallization rate of PP/PP-*g*-SiO₂ nanocomposites improved by 300-400% compared with pristine PP, which depends on the chain length and chain number. In grafted chain effect, crystallization rate of grafted amount 10 wt% improved by short length more than long chain. However, crystallization rate of grafted chain number was same value by excess grafted chain number.
- The tensile properties of PP/PP-*g*-SiO₂ nanocomposites improved the Young's modulus and tensile strength compared with pristine PP and PP/SiO₂ nanocomposites without changing crystallinity degree, melting point, and crystal form. Young's modulus and tensile strength indicated totally different dependence. It was suggested that the dispersion of SiO₂ nanoparticles dominated the Young's modulus. On the other hand, the tensile strength was almost linearly improved by increasing the number of grafted PP chains. In particular, the tensile strength of sample greatly

improved more than M_n of 1.2×10^4 . This tendency indicates that grafted chain length is over the critical molecular weight, which can tangle to matrix chain. Therefore, this chain and matrix chain can form the physical cross-linkage structure. As a result, the maximum improvements of PP/PP-*g*-SiO₂ were obtained by PP/PP460-*g*-SiO₂ using longest grafted chain in Chapter 2, which is 29% for the Young's modulus and 26% for the tensile strength respectively.

However, the reinforcement mechanism in PE/PE-*g*-SiO₂ nanocomposites was suggested that the physical cross-linkage effect on the tensile reinforcements was less pronounced for PE/PE-*g*-SiO₂ compared with PP/PP-*g*-SiO₂, which is 23% for the Young's modulus and 11% for the tensile strength respectively. In particular, the decisive difference between the PP/PP-*g*-SiO₂ and PE/PE-*g*-SiO₂ is the elongation at break. In PE-*g*-SiO₂ can lengthen over 300% of elongation at break. Thus, improvement of tensile strength is limited to 11% compared with pristine PE. Moreover, the toughness of PP-based nanocomposites using visbreak PP-terminal vinylidene group (*t*-VD) indicated 200% compared with PP-based nanocomposites using PP-*t*-OH.

- The melt viscoelasticity of PP/PP-*g*-SiO₂ nanocomposites can support the results of mechanical properties and physical cross-linkage effect. The melt properties of PP/PP-*g*-SiO₂ was same similar compared with pristine PP. This result indicated not only the presence of physical cross-linkage but also the improvement of melt processability more than PP/SiO₂.

These results consider that grafting technologies assist to development of novel nanocomposite materials.

Achievements

Original Articles

1. “Polypropylene-grafted nanoparticles as a promising strategy for boosting physical properties of polypropylene-based nanocomposites.” by Taniike, T., Toyonaga, M., Terano, M. *Polymer* **2014**, 55, 1012-1019.
2. “Fabrication of polyethylene-grafted SiO₂ nanoparticles and their application to polyethylene-based nanocomposites” by Toyonaga, M., Ono, K., Arai, M., Taniike, T., Terano, M., *J. Mater. Life Soc.* **2014**, submitted.

Domestic Conference

1. 豊永 匡仁、梅森 昌樹、谷池 俊明、寺野 稔、末端変性ポリプロピレンによるシリカナノ粒子の修飾とナノコンポジットへの応用、マテリアルライフ学会第 21 回研究発表会、東京、2010 Jul.
2. 豊永 匡仁、梅森 昌樹、谷池 俊明、寺野 稔、ポリプロピレン修飾ナノシリカを用いたポリプロピレン系ナノコンポジットの特性改良、マテリアルライフ学会第 15 回春季研究発表会、東京、2011 Mar.
3. 豊永 匡仁、梅森 昌樹、谷池 俊明、寺野 稔、ポリプロピレン/シリカナノコンポジットにおけるシリカへのポリプロピレングラフト鎖の一次構造設計、第 60 回高分子学会年次大会、東京、2011 May

4. 豊永 匡仁、梅森 昌樹、谷池 俊明、寺野 稔、ポリプロピレン系ナノコンポジットの特性改良を目的としたポリプロピレングラフト鎖の一時構造設計、マテリアルライフ学会第 22 回研究発表会、東京、2011 Jul.
5. 豊永 匡仁、梅森 昌樹、谷池 俊明、寺野 稔、ポリプロピレングラフトシリカを用いたナノコンポジットにおけるグラフト鎖長の影響、第 60 回高分子討論会、岡山、2011 Sep.
6. 豊永 匡仁、梅森 昌樹、谷池 俊明、寺野 稔、分子鎖長を制御したポリプロピレン修飾ナノシリカによるポリプロピレン系ナノコンポジットの補強効果、マテリアルライフ学会第 16 回春季研究発表会、東京、2012 Feb.
7. 豊永 匡仁、梅森 昌樹、谷池 俊明、寺野 稔、ポリプロピレン修飾シリカを含有したナノコンポジットにおけるグラフト鎖長と補強効果の相関、第 61 回高分子学会年次大会、神奈川、2012 May
8. 豊永 匡仁、梅森 昌樹、谷池 俊明、寺野 稔、ポリマー量を制御したポリプロピレン修飾ナノシリカによるポリプロピレン系ナノコンポジットの補強効果、マテリアルライフ学会第 23 回研究発表会、群馬、2012 Jul.
9. 豊永 匡仁、梅森 昌樹、谷池 俊明、寺野 稔、ポリマー修飾ナノシリカによる物理架橋型ポリプロピレン系ナノコンポジット、第 61 回高分子討論会、愛知、2012 Sep.
10. 豊永 匡仁、谷池 俊明、寺野 稔、小野 和也、物理架橋型ポリオレフィンナノコンポジットの調製条件の力学的性質と機能性への影響、マテリアルライフ学会第 17 回春季研究発表会、

東京、2013 Mar.

11. 豊永 匡仁、谷池 俊明、寺野 稔、物理架橋によるポリオレフィン系ナノコンポジットの特性改良を目的としたフィラーの添加量と表面修飾量の検討、第 62 回高分子学会年次大会、京都、

2013 May

12. 豊永 匡仁、谷池 俊明、寺野 稔、物理架橋ポリプロピレン系ナノコンポジットにおいて力学的性質や機能性に与えるフィラー粒径の影響、第 62 回高分子討論会、石川、2013 Sep.

13. 豊永 匡仁、谷池 俊明、寺野 稔、粒径の異なるポリプロピレン修飾ナノシリカを用いたポリマーナノコンポジットの界面強化メカニズムの解明、平成 25 年度北陸地区講演会と研究発表会、石川、2013 Nov.

14. 豊永 匡仁、谷池 俊明、寺野 稔、ポリプロピレン修飾ナノシリカに起因するポリプロピレンマトリックスの結晶化挙動、第 63 回高分子学会年次大会、愛知、2014 May

International Conferences

1. Masahito Toyonaga, Masaki Umemori, Toshiaki Taniike, Minoru Terano, Influences of Molecular Weight of Grafted Polypropylene on Mechanical Properties of Polypropylene / Silica Nanocomposites, 8th International Colloquium on Heterogeneous Ziegler-Natta Catalysts, Ishikawa, Japan, 2012 Mar.

2. Masahito Toyonaga, Toshiaki Taniike, Minoru Terano, Physical Cross-Linking Effects of Polypropylene-Graft Silica on Mechanical Properties of Nanocomposites, 9th International Symposium on Weatherability, Tokyo, Japan, 2013 Mar.
3. Masahito Toyonaga, Toshiaki Taniike, Minoru Terano, A novel approach for improved mechanical properties of polypropylene-based nanocomposites using precisely designed polypropylene-grafted nanosilica, Asian Polyolefin Workshop 2013, Beijing, China, 2013 Oct.
4. Masahito Toyonaga, Toshiaki Taniike, Minoru Terano, Study on Strain-Stress Curve of Polypropylene Nanocomposites Including Polypropylene-Grafted Nanosilica, International Symposium for Green-Innovation Polymers 2014, Kanazawa, Japan, 2014 Mar.

Awards

1. “ポリプロピレン修飾ナノシリカを用いたポリプロピレン系ナノコンポジットの特性改良”、第15回春季マテリアルライフ学会 研究奨励賞 2011
2. “物理架橋型ポリオレフィンナノコンポジットの調製条件の力学的性質と機能性への影響”、第17回春季マテリアルライフ学会 研究奨励賞 2013

Acknowledgements

The author deeply appreciates Professor Minoru Terano for his continually guidance and warm encouragement.

The author is grateful to Associate Professor Toshiaki Taniike, JAIST for many helpful and useful advices and warm encouragement.

The author would like to thank Professor Hisayuki Nakatani, KITAMI Institute of Technology for review and fine suggestions.

The author would like to thanks to Associate Professor Tatsuo Kaneko and Associate Professor Kazuaki Matsumura, JAIST for many for review and fine suggestions.

The author would like to thank to Mr. Ikki Katada, Mr. Kengo Takeuchi, and other members of nanocomposite group in Terano laboratory.

The author is also grateful heartily to Masaki Umemori, graduated student of Terano laboratory for his kind help in supporting the research.

The author greatly appreciates to Managing director Rie Yamada, Branch office manager Tetsu Sato, and other members in TEI Co., Ltd. for many helps, advice and kind cooperation for both the experiments and daily lives. Details are shown in acknowledgements of minor research.

Minor Research

**Characterization of Isotactic Polypropylene/
Stabilizer Using
Imaging Chemiluminescence Analysis**

Masahito Toyonaga

School of Material Science

Japan Advanced Institute of Science and Technology

1. Introduction

Science of polymer materials has advanced rapidly because of the major breakthroughs on polymer structure, properties and usage during the last 50 years. Especially, polypropylene (PP)-based materials are one of the most widely used plastics (6080×10^4 tons/year), characterized by various advantages such as low cost, light weight (0.90 g/cm^3), balanced mechanical properties, high melting temperature ($T_m = 155\text{-}165^\circ\text{C}$), good processability, low environmental load and so on [1]. In mechanical properties and cost, PP is gaining attention as a possible construction material. However, PP easily undergoes oxidative degradation, which is initiated by oxygen, shear, heat, ultraviolet rays, catalyst residues and so on [2,3]. Oxidative degradation is one of the most serious problems of polymer materials. This problem causes deterioration of various mechanical properties and appearance [4,5]. Therefore,

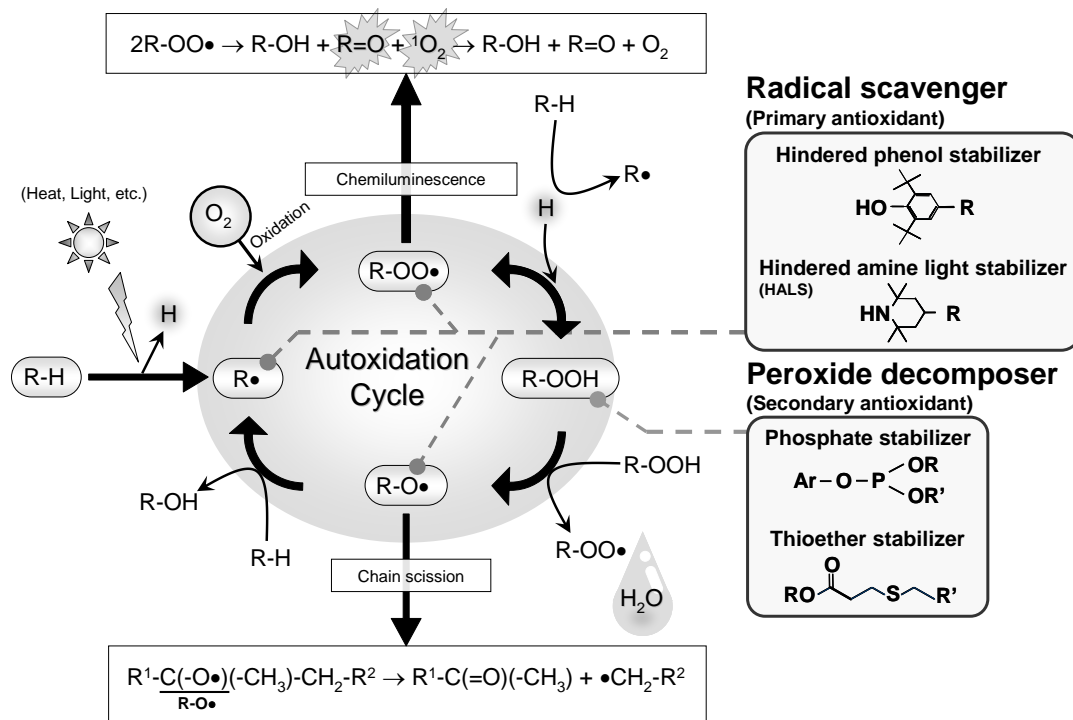


Figure 1. Autoxidation cycle

addition of stabilizers is essential to keep the properties. In **Figure 1**, oxidative degradation of PP has been explained by the autoxidation cycle which basically consists of initiation, propagation, chain scission and branching [6-9]. Stabilizers effectively trap radicals and decompose peroxide products [10-12]. These two effects of stabilizers are categorized as "primary antioxidant" and "secondary antioxidant" respectively. In Figure 1 and **Figure 2**, primary antioxidants scavenge for alkyl ($R\bullet$), alkoxy ($R-O\bullet$), and peroxy ($R-OO\bullet$) radicals by donating hydrogen atoms. Thus

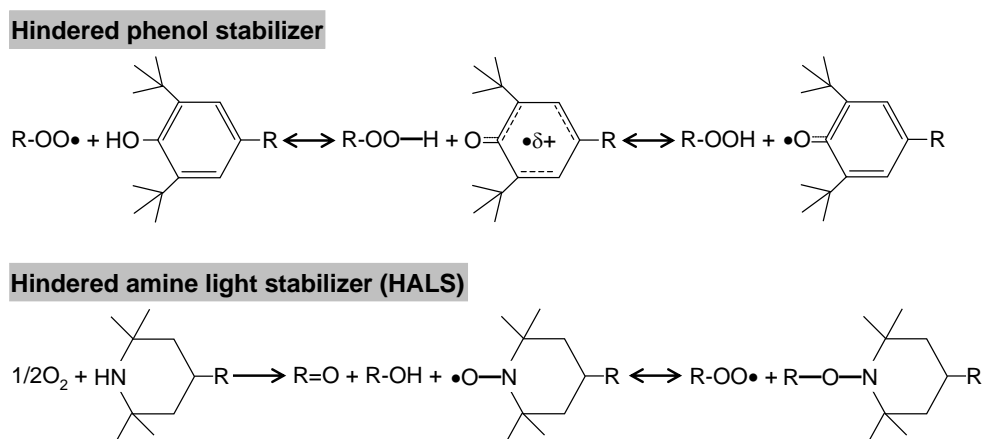
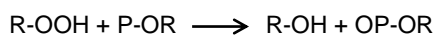


Figure 2. Reactions of primary antioxidants

these stabilizers stop the free-radical chain reaction of oxidation. On the other hand, secondary antioxidants decompose the hydroperoxides ($R-OOH$) and stop the propagation of radicals in Figure 1 and **Figure 3**. Their reactions alter hydroperoxides to more stable products. Especially, phosphates-based stabilizers show strong synergistic effects in combination with hindered phenol-based stabilizers [10]. Furthermore, stabilizer effects in PP depend on chemical structure (antioxidant ability), molecular weight (mobility, melting and boiling temperature), solubility (mobility and diffusion), and combination of stabilizers [13,14]. Hence, evaluation of stability is

most important factor on the lifetime of polymer products.

Phosphate stabilizer



Thioether stabilizer

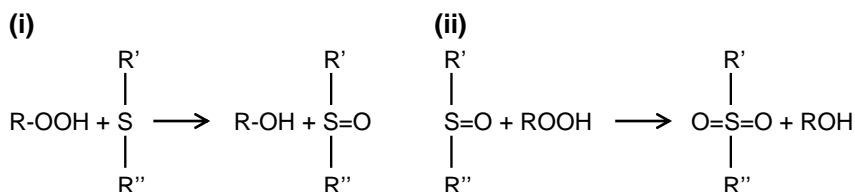


Figure 3. Reactions of secondary antioxidants

Stability and mechanism on the oxidative degradation of PP were investigated by various instruments such as thermo gravimetry analyzer (TGA), high-temperature gel permeation chromatography (HT-GPC), infrared spectroscopy (IR), ultraviolet visible absorption spectroscopy (UV-vis), nuclear magnetic resonance (NMR), electron spin resonance (ESR), gas chromatograph mass spectrometer (GC/MS), chemiluminescence analyzer (CLA) and so on [15-21]. Especially, CLA have some advantages compared with other instruments. In **Figure 4** this instrument can detect the ultra-weak chemiluminescence (CL) of initial stage before oxidative degradation.

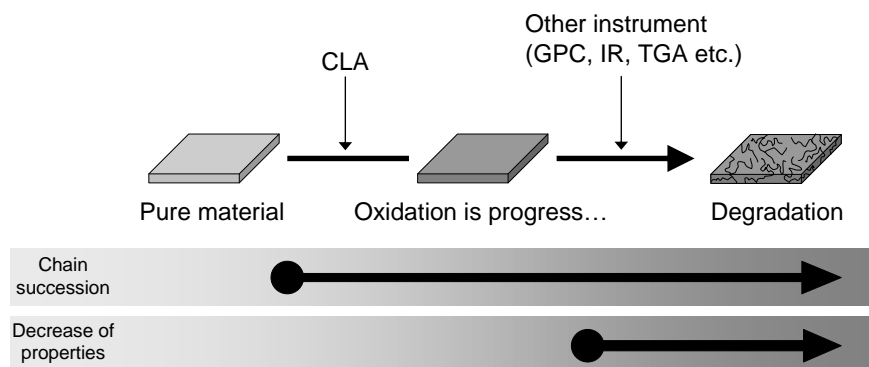


Figure 4. The advantage of CLA measurements

Furthermore, CLA not need oven, because this instrument can perform both the detection and the heating in sample space (**Figure 5**). Therefore, CLA can obtain the detailed information more than other instruments. For instance, George et al. reported that model PP is able to explain the observations of volatile formation in the earliest stages of oxidation and the rapid crack formation at the end of the induction period as well as other anomalies which cannot be rationalized in a homogeneous kinetic model by CLA [21]. The aim of this work is to enlarge the performance and application of the CLA instrument on the various characterizations. In this report, degradation behavior of stabilized PP was observed by imaging CLA measurements.

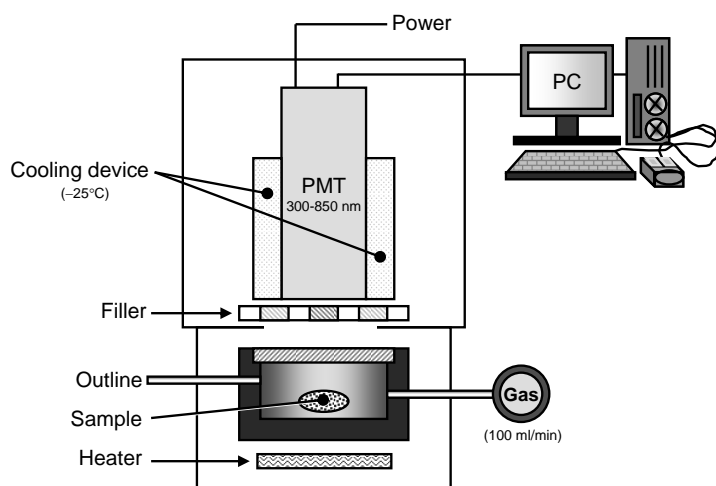


Figure 5. Model of CLA instruments

2. Experimental

2.1. Materials

PP pellet (**Figure 6**, Novatec® PP MA 3, $M_n = 1.11 \times 10^5$, $M_w = 3.97 \times 10^5$, MWD = 3.58, MFR = 11 g/10min, $mmmm = 98$ mol%, $T_m = 165^\circ\text{C}$, density = 0.90 g/cm^3 , Japan Polypropylene Co., Ltd.) was donated by the company. Irganox 1010 (**Figure 7(a)**, pentaerythritol-tetrakis(3-(3,5-di-*tert*-butyl-4-hydroxyphenyl)propionate), hindered phenol-based primary antioxidant, MW = 1178 g/mol, $T_m = 110\text{-}125^\circ\text{C}$, BASF Japan Co., Ltd.) stabilizer and Irgafos 168 (**Figure 6(b)**, Tris(2,4-di-*tert*-butylphenyl) phosphate, hydrolytically stable phosphate-based secondary antioxidant, MW = 646.9 g/mol, $T_m = 183\text{-}186^\circ\text{C}$, BASF Japan Co., Ltd.) stabilizer were used as a stabilizer. These materials were used for a sample preparation.

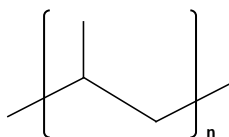


Figure 6. Molecular structures of PP

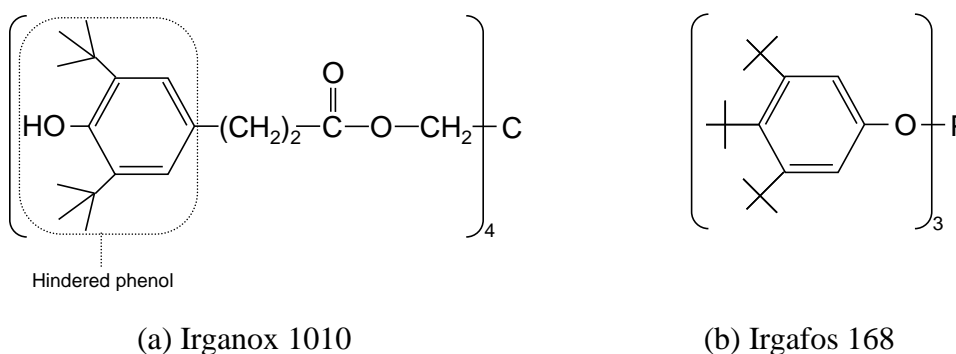


Figure 7. Molecular structures of Irganox 1010 stabilizer and Irgafos 168 stabilizer

2.2. Sample preparations

Pristine PP (PP) was donated by the company. In **Table 1**, rPP, rPP/Irganox 1010, rPP/Irgafos 168, and rPP/Irganox 1010/Irgafos 168 were prepared by injection molding at 230°C. This rPP gave the thermal loading same as other samples in order for accurate evaluation.

Table 1. PP and PP/stabilizer samples

Sample ^a	Irganox 1010 amount (ppm)	Irgafos 168 amounts (ppm)
PP	0	0
rPP	0	0
rPP/Irganox 1010	2000	0
rPP/Irgafos 168	0	4000
rPP/Irganox 1010/Irgafos 168	2000	4000

^a PP: Pristine PP, rPP: PP without stabilizer in injection molding at 230°C, rPP/iox1010

2.3. Characterization of imaging CLA

Imaging CLA of TOHOKU ELECTRONIC INDUSTRIAL (TEI) Co., Ltd. is shown in **Figure 8**. Measurement samples of about 20-40 mg are set into the sample dish in the chamber. CCD camera can detect the CL from the sample and monitor the data by personal computer. This camera is cooled down to under -25°C by cooling device to decrease the noise level. Samples can be heated up to 300°C and O_2 gas (100 ml/min) can be introduced into the sample chamber. Measurement range is $150\text{-}300^{\circ}\text{C}$ (0.2 $^{\circ}\text{C}/\text{min}$). Incidentally sample position in chamber is shown in **Figure 9**.

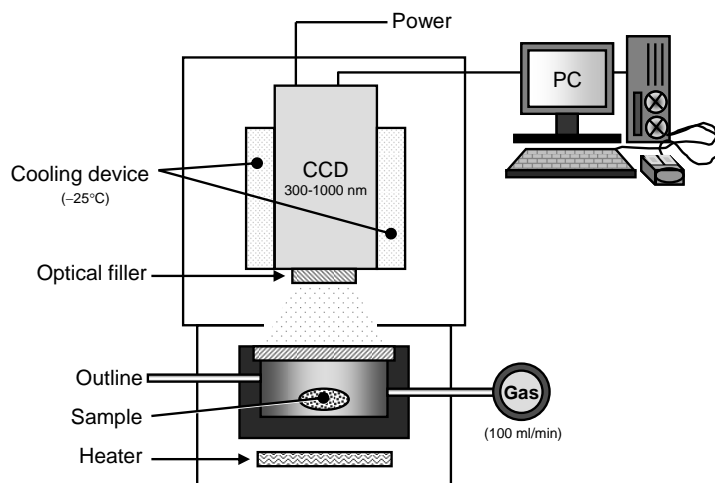


Figure 8. Model of CCD imaging type CLA-IMG instrument

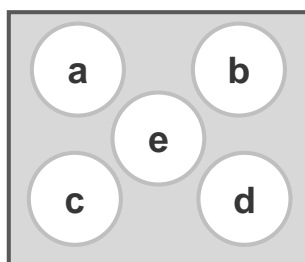


Figure 9. Sample positions of (a) Pristine PP, (b) rPP, (c) rPP/Irganox 1010, (d) rPP/Irgafos 168 and (e) rPP/Irganox 1010/Irgafos 168

3. Results and discussion

Figure 10 shows the raw data of all samples on imaging CLA.

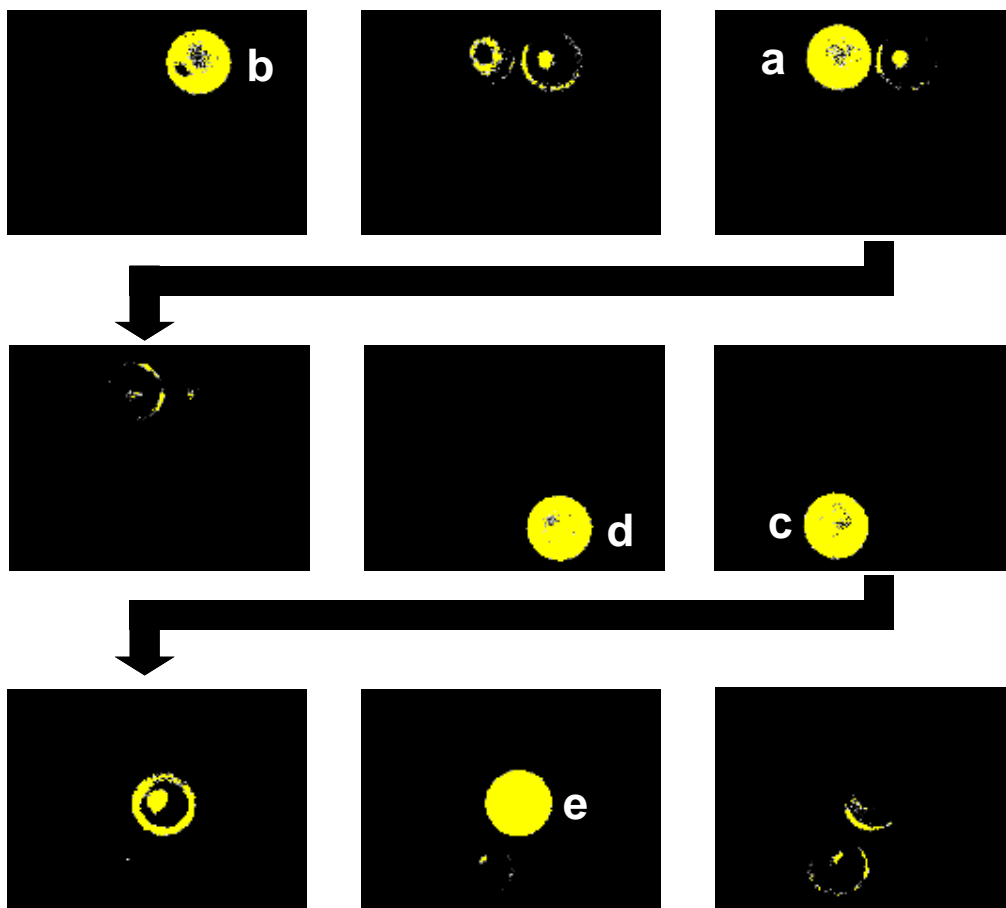


Figure 10. Result of imaging CLA observation from (a) Pristine PP, (b) rPP, (c) rPP/Irganox 1010, (d) rPP/Irgafos 168 and (e) rPP/Irganox 1010/Irgafos 168

Yellow regions of photographs show CL by the decomposing R-OOH groups and/or deactivating stabilizer. Figure 10 can see the oxidation degradation very visually. This raw data change it to spectrum data in **Figure 11**. It shows time dependence of imaging CLA during oxidative degradation. The CL intensity of the vertical axis includes not only the luminescence intensity but also the total luminous region

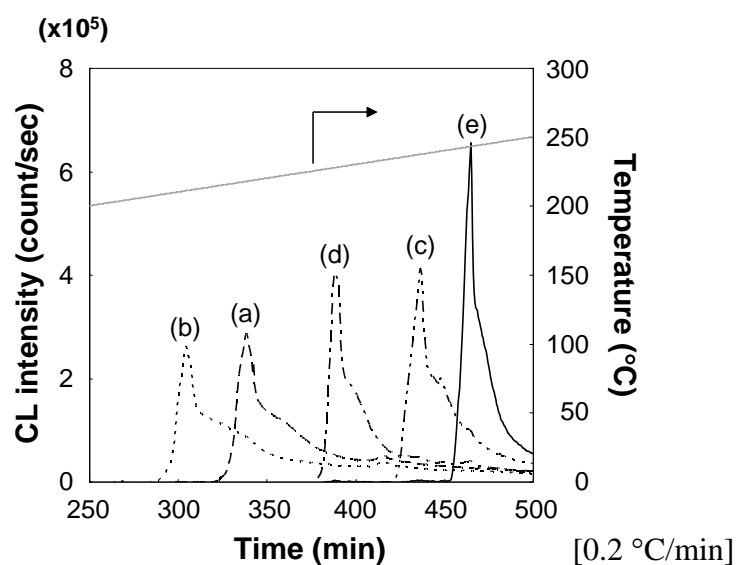


Figure 11. Result of imaging CLA measurements of (a) Pristine PP, (b) rPP, (c) rPP/Irganox 1010, (d) rPP/Irgafos 168 and (e) rPP/Irganox 1010/Irgafos 168

on sample cell. The CL in induction period is very weak and could not get the spectrum before 290 min (208°C). CL of samples was detected in order of rPP, PP, rPP/Irganox 168, rPP/Irganox 1010, and rPP/Irganox 1010/Irganox 168 after 290 min. The rPP is fastest detection by thermal loading, next is pristine PP without thermal loading, and next is 3 types of stabilized PP. On stabilized PP, rPP/Irgafos 168 showed the stability that was lower than rPP/Irganox 1010 containing hindered phenol structure. This reason depends on effective site of stabilizer in autoxidation cycle of Figure 1. The synergy effect of two types of stabilizers between the primary antioxidant and secondary antioxidant was seen in rPP/Irganox 1010/Irgafos 168. CL peak of this sample is only one place despite using two stabilizers. Furthermore, this CL peak was not same on rPP/Irganox 1010 and rPP/Irgafos 168. These results definitely suggest that CL of PP is not the thing by boiling point and decomposition point of stabilizer merely.

4. Conclusion

PP materials are deteriorated by heat, light, or other stimulators. Degradation behaviors of various PP/stabilizer samples were observed by imaging CLA. As a result, samples deteriorated according to general knowledge in order of rPP, PP, rPP/Irganox 168, rPP/Irganox 1010, and rPP/Irganox 1010/Irganox 168. Stability of rPP/Irganox 1010/Irgafos 168 was able to observe the synergistic effect by two types of stabilizers of the primary antioxidant and secondary antioxidant. These results will support the performance of CLA instruments. In future, CLA instruments shall be used in various fields such as high throughput technology, lifetime prediction [22], and so on.

Acknowledgement for minor research

The author greatly appreciates to managing director Yamada and branch office manager Sato in TEI Co., Ltd. for many helps, advice and kind cooperation for both the experiments and daily lives. Measurements of imaging CLA were supported by Mr. Sekine, Mr. Nakagawa, Mr. Saito, and Mr. Kumagai. This work was kindly supported by all the members in TEI Co., Ltd. The author is deeply grateful for kind suggestion of Prof. Matsumi and Prof. Taniike. Finally, the author deeply appreciates to Prof. Terano for giving me a precious chance to work at TEI Co., Ltd.

References:

- [1] "Next generation polyolefins" **2013**, 7.
- [2] Reich, L., Stivala, S. S., "Elements of Polymer Degradation", McGraw hill **1971**.
- [3] Schabel, W., "Polymer Degradation – Principles and Practical Applications", Hanser **1981**.
- [4] Ricardo, B.N., Marco, D.P., *Polym. Deg. Stab.* **1993**, 40, 59-64.
- [5] Fayolle, B., Audouin, L., Verdu, J. , *Polym. Deg. Stab.* **2002**, 75, 123-129.
- [6] Osawa, Z., Suzuki, M., Ogiwara, Y., Matsuzaki K., "Catalytic Action of Metallic Salts in Autoxidation and Polymerization: Cobalt (II, III) acetylacetonate-catalyzed thermal oxidative degradation of polypropylene. II", **1970**.
- [7] Carlsson, D. J., Wiles, D. M., *Macromol.* **1969**, 6, 587-597.
- [8] Billingham, N. C., *Makromol. Chem., Makromol. Symp.* **1989**, 28, 145-152.
- [9] Alam, M. S., Nakatani, H., Ichiki, T., Goss, G. S. B., Liu, B., Terano, M., *J. Appl. Polym. Sci.* **2002**, 86, 1863-1867.
- [10] Naskar, K., Kokot, D., Noordermeer, J. W. M., *Polym. Degrad. Stab.* **2004**, 85(2), 831-839.
- [11] Gugumus, F., *Polym. Degrad. Stab.* **1989**, 24, 289-301.
- [12] Malik, J., Hrivik, A., Tomova, E., *Polym. Degrad. Stab.* **1992**, 35(1), 61-66.
- [13] Ohaktsu, Y., Suzuki, F., *J. Jpn. Petrol. Inst.* **2011**, 54(1), 22-29.
- [14] Ohaktsu, Y., Takenaka, H., *J. Jpn. Petrol. Inst.* **2008**, 51(2), 88-94.
- [15] Carlson, D. J., Wiles, D. M., *Macromol.* **1971**, 4, 174-179.
- [16] Bovey, F. A., Schilling, F. O., *ACS Adv. Chem. Ser.* 1977, 169, 133-141.
- [17] Daniel, M. M., Roger, A. A., Dora, K. D., Sara, B. K., Roger, L. C., Robert, B., *Macromol.* **2005**, 38(12), 5035-5046.

- [18] Kuroda, H., Ozawa, Z., *Macromol. Chem., Macromol. Symp.* **1989**, 27(1), 97-119.
- [19] Bockhorn, H., Hornung, A., Hornung, U., Schawaller, D., *J. Anal. Appl. Pyrol.* **1999**, 48(2), 93-109.
- [20] Osawa, Z., Wu, S., Knorowa, F., *Polym. Degrad. Stab.* **1988**, 22, 97.
- [21] Celina, M., George, G. A., *Polym. Degrad. Stab.* **1993**, 40(3), 323-335.
- [22] Käser, F., Roduit, B., *J. Therm. Anal. Calorim.* **2008**, 93(1), 231-237.